REPUBLIC OF TÜRKİYE
KIRŞEHİR AHİ EVRAN UNIVERSITY
INSTITUTE OF NATURAL AND APPLIED SCIENCES
DEPARTMENT OF MECHANICAL ENGINEERING

THEORETICAL AND EXPERIMENTAL INVESTIGATION TO CALCULATE HEAT GAIN OF MULTILAYERED WALLS BY USING RTS METHOD

KHALIL HASSAN KHALIL KHALIL

MSc THESIS

KIRŞEHİR
2024

REPUBLIC OF TÜRKİYE
KIRŞEHİR AHİ EVRAN UNIVERSITY
INSTITUTE OF NATURAL AND APPLIED SCIENCES
DEPARTMENT OF MECHANICAL ENGINEERING

THEORETICAL AND EXPERIMENTAL INVESTIGATION TO CALCULATE HEAT GAIN OF MULTILAYERED WALLS BY USING RTS METHOD

KHALIL HASSAN KHALIL KHALIL

MSc THESIS

SUPERVISOR
ASST. PROF. DR. Merdin DANIŞMAZ

II. SUPERVISOR
ASST. PROF. DR. Omer Adil ZAINAL

KIRŞEHİR
2024

KIRŞEHİR AHİ EVRAN UNIVERSITY

INSTITUTE OF NATURAL AND APPLIED SCIENCES

MSc THESIS

ETHICS DECLARATION

In this thesis study, which I have read and understood the Kırşehir Ahi Evran University Scientific Research and Publication Ethics Directive and which I have prepared in accordance with the Kırşehir Ahi Evran University Institute of Natural and Applied Science Thesis Writing Rules;

- I have obtained the data, information and documents I have presented in the thesis within the framework of academic and ethical rules,
- I present all information, documents, evaluations and results in accordance with scientific ethical rules,
- I have cited all the works I have benefited from in the thesis by making appropriate references,
- I have not made any changes in the data used and the results,
- This study, which I have presented as a thesis, is original,

Otherwise, I declare that I accept all legal actions to be taken against me in this regard and all loss of rights that may arise against me 02 /February/2024.

Student

KHALIL HASSAN KHALIL KHALIL

LIST OF CONTENTS

Page No

LIST OF CONTENTS ..... **I**

ACKNOWLEDGEMENTS ..... **III**

GENİŞLETİLMİŞ ÖZET ..... **V**

ABSTRACT ..... **VII**

LIST OF TABLES ..... **IX**

LIST OF FIGURES ..... **X**

LIST OF ICONS AND ABBREVIATIONS ..... **XII**

1. INTRODUCTION **1**

1.1. Cooling Load 1

1.2. Energy Consumption and CO2 Emissions 3

1.3. Radiant Time Series (RTS) 5

1.4. Objective 6

1.5. Importance 7

1.6. Thesis Outline 7

2. LITERATURE REVIEW **9**

2.1. Energy Consumption and CO_2 Emissions 9

2.2. Effect of Buildings Walls and Roofs Design and Materials 11

2.3. Cooling Load Calculations 14

2.4. Summary 20

2.5. Present Work Scope 21

3. MATERIAL AND METHOD **23**

3.1. Methodology 23

3.2. Materials 24

3.3. Measurement Equipment 29

3.4. Case Study 32

3.5. Implementing RTS Method to Calculate the Heat Gains 38

3.5.1. Data collection 38

3.5.1.1. Sol-air temperature 39
3.5.1.2. Conductive heat gains calculation 40
3.5.1.3. Convective heat gains calculation 40
3.5.1.4. Changing the radiation heat gains to cooling loads 41
3.5.1.5. Wall and roof response factor generation procedure 42
3.5.2. Applying RTS method 44
3.5.3. RTS method MATLAB code modelling 47
3.6. ASHRAE RTS Procedure Spreadsheet 48

4. RESULTS AND DISCUSSION 51
4.1. Results of ASHRAE RTS Procedure Spreadsheet 51
4.1.1. Incident solar flux 53
4.1.2. Air temperature and sol-air temperatures 55
4.1.3. Conduction heat gains 57
4.1.4. Window solar heat gain 58
4.2. Results of the Developed MATLAB Code 59
4.3. Walls Results in Comparison 65
4.4. Results Validation 66
4.5. Orientation Effect 66
4.6. Cost Analysis Results 69
4.7. Monthly Energy Cost 70

5. CONCLUSIONS AND RECOMMENDATIONS 73
5.1. Conclusions 73
5.2. Recommendations 74

REFERENCES 77
APPENDIX A 81
APPENDIX B 87
APPENDIX C 89
CURRICULUM VITAE 91

ACKNOWLEDGEMENTS

I extend my deepest gratitude to my supervisor, Assist. Prof. Dr. Merdin DANIŞMAZ, for his unwavering guidance, support, and invaluable insights throughout the entire research process. I also appreciate the dedicated supervision provided by Assist. Prof. Dr. Omer Adil Zainal Al-Bayati, who spared no effort in offering onsite and day-to-day assistance. Their expertise and encouragement have played a leading role in shaping the direction of this thesis.

I am thankful to the Engineering and Architecture Faculty at Kırşehir Ahi Evran University for providing supportive and friendly academic environment and access to essential resources, crucial for the successful completion of this thesis. The Mechanical Engineering Department has been both a source of inspiration and a platform for intellectual growth.

I express my appreciation to my friends and colleagues who provided encouragement, shared ideas, and offered assistance whenever needed -specifically Mohammed Oral-. This thesis is the culmination of the collective efforts of many, and I sincerely thank everyone for their support and encouragement.

Finally, my heartfelt thanks go to my family for their unwavering support and understanding during this challenging academic journey. Their love and encouragement have served as my anchor, motivating me to strive for excellence.

02, February, 2024 KHALIL HASSAN KHALIL KHALIL

GENİŞLETİLMİŞ ÖZET

YÜKSEK LİSANS TEZİ

RTS METHOD KULLANARAK ÇOK KATMANLI DUVARLARIN ISI KAZANCINI HESAPLAMAK İÇİN TEORIK VE DENEYSEL İNCELEME

KHALIL HASSAN KHALIL KHALIL

KIRŞEHİR AHİ EVRAN ÜNİVERSİTESİ
FEN BİLİMLERİ ENSTİTÜSÜ
MOLEKÜLER BİYOLOJİ VE GENETİK ANABİLİM DALI

Danışman: **Dr. Öğr. Üyesi Merdin DANIŞMAZ**
Yıl: 2024 Sayfa: 91

Jüri: **Dr. Öğr. Üyesi Merdin DANIŞMAZ**
Dr. Öğr. Levent URTEKİN
Dr. Öğr. Ali Osman KURBAN
Dr. Öğr. Tahseen Ahmad TAHSEEN
Dr. Öğr. Üyesi Omer Adil ZAINAL

İkinci Danışman **Dr. Öğr. Üyesi Omer Adil Zainal**

Bu çalışma, çok katmanlı duvarlar ve çatılardaki ısı kazanımını hesaplamak için ASHRAE Radyant Zaman Serisi (RTS) yönteminin uygulanmasına derinlemesine odaklanmaktadır. Temel amacı, yaygın olarak kullanılan duvar yapılarının termal performansını değerlendirmek ve binalarda enerji verimliliğini ve termal konforu artırmak için içgörüler sunmaktadır. Çalışma, RTS yönteminin genel bir bakışla başlamakta ve etkili soğutma sistemlerini ve enerji yönetimi stratejilerini değerlendirmedeki önemini vurgulamaktadır. Eleştirel bir literatür taraması, ısı kazanımı hesaplamaları ve çok katmanlı duvar performansı üzerine önceki araştırmaları değerlendirerek, Irak'ın özgün bağlamında daha fazla araştırma ihtiyacını vurgulamaktadır. Bu aşamayı takiben, enerji tasarrufu yoluyla ısı kazancı azaltımına yönelik önemli makalelerin toplandığı, özetlendiği ve seçildiği bulgulara dayanarak bir test düzeneği tasarlanmıştır. Maliyet, etkinlik ve malzeme maliyetleri göz önüne alınarak tasarlanan test düzeneği, boyutları 115 x 100 x 100 cm olan küçük bir odadan oluşmaktadır ve her biri üç katmana sahip üç duvar (A, B ve C), iki katmanlı beton çatı ve çift camlı pencere/kapı içermektedir. Sıcaklık ölçümleri için K-tipi termokupl, veri kaydedici, sensörler, güç kaynağı ve SD-hafıza gibi araçlar kullanılmıştır. Sonraki aşama, çeşitli bina ve yalıtım malzemelerinin ısı kazanımı ve soğutma ihtiyaçlarının analizi, nicelendirilmesi ve test edilmesini içermektedir. Bu testlerden elde edilen sonuçlar derlenmiş, tartışılmış ve anahtar sonuçlar, avantajlar, dezavantajlar ve önleyici tedbirler belirlenmiştir. Yöntem bölümü, teorik çerçeve ve deneysel yaklaşımı detaylandırmış, RTS yöntemini kullanarak ısı kazanımını hesaplamak için MATLAB kodunun geliştirilmesini ve veri toplama için deneysel kurulumu açıklamıştır. Karşılaştırmalı analiz için ASHRAE RTS Prosedürü elektronik tablosu referans olarak kullanılmıştır. Çalışmadan çıkarılan temel sonuçlar şunlardır: Araştırma, güneş enerjisi faktörlerini, olay güneş akısı, güneş-hava sıcaklıkları, iletkenlik ısı kazançları, pencere güneş ısı kazancı ve duvarların genel bina termal verimliliği üzerindeki etkilerini analiz etmiştir. Bulgular, duvar katmanları arasında ısı kazanımı ölçümlerinde önemli farklılıklar olduğunu, güneş radyasyonu maruziyetinin etkilerini ve yalıtımın ısı kazanımını hafifletmedeki önemini vurgulamaktadır. RTS yönteminin çok katmanlı duvarlardaki ısı kazanımını tahmin etmek için güvenilir ve kesin

bir yöntem olduğu kanıtlanmıştır. Çalışmada kullanılan malzemelerin termal özellikleri, ısı kazanımı üzerinde önemli bir etkiye sahiptir. İletkenlik, yoğunluk ve özgül ısı, hesaplamalarda hesaba katılmalıdır. Duvarlara düşen güneş radyasyonu, ısı kazanımındaki önemli bir rol oynamaktadır. Bu bilgilerin RTS yöntemine entegre edilmesi, ısı kazanımı tahminlerinin hassasiyetini artırır. Isı kazanımı, çok katmanlı duvarlardaki katmanların düzeni ve kompozisyonu tarafından önemli ölçüde etkilenir. Farklı duvar konfigürasyonları, farklı ısı transfer karakteristiklerine neden olabilir. Ayrıca, çok katmanlı duvarlardaki olay güneş akısının detaylı analizi, termal performansı optimize etmek için anahtar gözlemler sunar. Duvar B, sürekli olarak en yüksek olay akı alır, bu da doğrudan güneşe maruz kalma açısından belirgin bir maruziyeti gösterir. Duvarlar A ve C, olay akı seviyelerini orta seviyede alırlar, benzer güneş radyasyonu maruziyeti anlamına gelir. Çatı, en yüksek olay akısını kaydeder, bu da önemli güneş radyasyonu maruziyetini gösterir. Duvar B, doğuya (güneş doğuşu) baktığı için gün boyunca sürekli olarak en yüksek olay güneş akısını alır, bu da Duvarlar A ve C'ye göre daha yüksek bir güneş radyasyonu ve termal emilim derecesini ima eder. Solar akıdaki değişimler, Duvar B'nin pik saatlerde en yüksek dalgalanmaları yaşadığını, Duvar C'nin ise en az dalgalanmayı gösterdiğini gösterir. Pik güneş akısı zamanı, her duvar için farklıdır, bu da duvarların konumları ve güneş ışınlarının maruziyetindeki farklılıkları vurgular. Çalışma, MATLAB kodu ve ASHRAE elektronik tablosu ile duvar yönlendirmesinin etkisini inceleyerek duvar A'nın güneye baktığında en yüksek ısı kazancının elde edildiğini göstermektedir, bu da öğle saat 12:00 civarında 65 W'a kadar ulaşmaktadır. Bunun aksine, diğer üç yönde daha düşük ısı kazancı elde edilir, en fazla 52 W'a 14:30 civarında ulaşılır. Bu bulgular, olay güneş akısının varyasyonlarının ve duvar yönlendirmesinin ısı kazancı üzerindeki etkilerini dikkate alarak bina tasarımını optimize etme konusunda değerli içgörüler sunar. Çalışma, termal dinamiklerin anlayışımızı artırarak enerji verimli ve konforlu bina ortamlarının geliştirilmesine katkıda bulunmaktadır. Çalışmadan elde edilen bulgulara dayanarak çeşitli öneriler ortaya çıkmaktadır. İlk olarak, duvar bileşenlerinin genel oda termal performansındaki önemi, güneş radyasyonu maruziyetini optimize etmek ve ısı kazancını en aza indirmek için yalıtım ve dikkatli yönlendirmenin gerekliliğini vurgular. Pencere tasarımı, hem güneş ısı kazanımı sınırlamalarını hem de yeterli gün ışığı alımını dikkate alarak ele alınmalıdır. Soğutma ihtiyaçlarının analizi, enerji verimli soğutma sistemlerinin uygulanması gerektiğini göstermektedir. Gece boyunca soğutma yükündeki azalış, serin saatlerde doğal soğutmanın kullanımının potansiyelini gösterir, bu da mekanik sistemlere ve enerji tüketimine olan bağımlılığı azaltabilir. Gelecekteki araştırmalar, güneşlik cihazlar, termal kütle ve HVAC sistem verimliliği gibi ısı kazancını etkileyen ek parametreleri ve değişkenleri inceleyerek çok katmanlı duvarların termal performansını daha kapsamlı bir şekilde anlamak için yapılmalıdır. Sonuç olarak, bu çalışma, ASHRAE RTS yönteminin çok katmanlı duvarlardaki ısı kazanımını değerlendirmedeki etkinliğini kapsamlı bir şekilde inceleyerek, Irak'taki binalarda termal performansı optimize etme konusunda pratik sonuçlar sunmaktadır.

Anahtar Kelimeler: Isı kazanımı, Çok Katmanlı Duvarlar, RTS, ASHRAE, MATLAB.

ABSTRACT

MASTER'S THESIS

THEORETICAL AND EXPERIMENTAL INVESTIGATION TO CALCULATE HEAT GAIN OF MULTILAYERED WALLS BY USING RTS METHOD

KHALIL HASSAN KHALIL KHALIL

KIRŞEHİR AHİ EVRAN UNIVERSITY
INSTITUTE OF NATURAL AND APPLIED SCIENCES
DEPARTMENT OF MECHANICAL ENGINEERING

Supervisor:	**Assist. Prof. Dr. Merdin DANIŞMAZ**
	Year: 2024 Page: 91
Jury:	**Assist. Prof. Dr. Merdin DANIŞMAZ**
	Prof. Dr. Levent URTEKİN
	Prof. Dr. Tahseen Ahmed TAHSEEN
	Prof. Dr. Ali Osman KURBAN
	Assist. Prof. Dr. Omer Adil ZAINAL
Co-Supervisor	**Assist. Prof. Dr. Omer Adil ZAINAL**

This study delves into the application of the ASHRAE Radiant Time Series (RTS) method for calculating heat gain in multilayered walls within the context of Iraq. The primary objective is to assess the thermal performance of commonly used wall constructions, offering insights to enhance energy efficiency and thermal comfort in buildings. Commencing with an overview of the RTS method, the study highlights its significance in evaluating heat gain for effective cooling systems and energy management strategies. A critical literature review evaluates prior research on heat gain calculations and multilayered wall performance, emphasizing the necessity for tailored investigation in Iraq.

This was followed by the collection, summarization, and selection of key papers related to energy savings through heat gain reduction. Based on these findings, a test rig was designed, considering cost, effectiveness, and material costs. The test rig, a small room of dimensions 115 x 100 x 100 cm, incorporated three walls (A, B, and C), each with three layers, a concrete roof of two layers, and a double-glazed window/door. Instruments such as K-type thermocouples, a data logger, sensors, a power supply, and SD memory were utilized for temperature measurements. The subsequent stage involved the analysis, quantification, and testing of heat gain and cooling requirements for various building and insulation materials.

Results from these tests were compiled, and discussed, and key conclusions, benefits, drawbacks, and preventative measures were defined. The methodology section also detailed the theoretical framework and experimental approach. It introduced the development of a MATLAB code for computing heat gain using the RTS method and explained the experimental setup for data collection. The ASHRAE RTS Procedure spreadsheet served as a reference for comparative analysis.

Detailed analysis of incident solar flux on multilayered walls offers key observations for optimizing thermal performance. Wall B consistently receives the highest incident flux, indicating pronounced exposure to direct sunlight. Walls A and C receive moderate levels of

incident flux, suggesting comparable solar radiation exposure. The roof records the highest incident flux, signifying substantial solar radiation exposure.

Wall B, facing east (sunrise), consistently garners the highest incident solar flux throughout the day, reflecting a higher degree of solar radiation and thermal absorption than Walls A and C. Variations in solar flux reveal Wall B experiences the highest fluctuations during peak hours, while Wall C exhibits the least variation. The time of peak solar flux varies for each wall, highlighting differences in positioning and solar irradiation levels. Further investigation into wall orientation using MATLAB code and ASHRAE spreadsheet indicates that when Wall A faces south, the highest heat gain is achieved, peaking at approximately 65 W around 12:00. In contrast, the other three orientations result in lower heat gain, with a maximum of 52 W at 14:30.

These findings provide valuable insights for optimizing building design, considering the impact of incident solar flux variations and wall orientation on heat gain. The study enhances our understanding of thermal dynamics, contributing to the development of energy-efficient and comfortable building environments.

The main conclusions drawn from the study are as follows; The research analyzed solar energy factors, including incident solar flux, sol-air temperatures, conduction heat gains, window solar heat gain, and sensible cooling load. The data underwent analysis to understand heat gain patterns in various wall layers and their impact on overall building thermal efficiency. The findings indicated significant differences in heat gain measurements across wall layers, emphasizing the effects of solar radiation exposure and the crucial role of insulation in mitigating heat gain. The RTS method was proven to be a dependable and precise method for estimating heat gain in multilayered walls. The thermal properties of the materials used in multilayered walls significantly impact heat gain. Conductivity, density, and specific heat must be accounted for in calculations. Solar radiation incident on walls plays a substantial role in heat gain. Incorporating solar exposure patterns into the RTS method enhances heat gain forecast precision. Heat gain is significantly influenced by the arrangement and composition of layers in multilayered walls. Different configurations result in varying heat transfer characteristics.

There are several recommendations arising from the study. First, the importance of wall components to overall room thermal performance underscores the need for insulation and careful orientation to optimize solar radiation exposure and minimize heat gain. Window design should be approached with caution, considering both solar heat gain limitations and the need for adequate daylighting. The analysis of cooling requirements suggests implementing energy-efficient cooling systems. The decreasing trend of the cooling load throughout the night suggests the potential for utilizing natural cooling during cooler hours, reducing reliance on mechanical systems and energy consumption. Future research should explore additional parameters such as external shading devices, thermal mass, and HVAC system efficiency to gain a more complete understanding of multilayered wall thermal performance. In conclusion, this study provides a thorough examination of the ASHRAE RTS method's efficacy in assessing heat gain in multilayered walls, with practical implications for optimizing thermal performance in Iraqi buildings.

Key Words: Heat gain, Multilayered Walls, RTS, ASHRAE, MATLAB, Cooling load

LIST OF TABLES

Page No

Table 3.1. Dimensions of the material used in model construction **28**
Table 3.2. Thermophysical properties of walls and roof materials used in Iraq (Yang et al., 2014)..... **38**
Table 4.1. Error Percentages Results of Heat gain. **66**
Table 4.2. Costs of the wall's material **69**

LIST OF FIGURES

Page No

Figure 1.1. 2019 Energy Consumption and CO2 Emissions (Global, 2020) **4**
Figure 1.2. Concentrations of carbon dioxide in the atmosphere (Skelly, 2021) **4**
Figure 3.1. Room model **24**
Figure 3.2. Gypsum (Egypt, 2022) **25**
Figure 3.3. The inside walls are covered with Gypsum plastering. **25**
Figure 3.4. Cement powder used as mortar and for plastering **26**
Figure 3.5. The exterior walls are covered with Cement plastering **26**
Figure 3.6 (a) Solid Bricks (*Bricks PNG 7 - PNG All*) . (**b)** White and Yellow Hollow Bricks.(Ltd, 2024) **27**
Figure 3.7. Concrete Blocks **28**
Figure 3.8. Room schematic showing each wall components **29**
Figure 3.9. K-Type Thermocouple **30**
Figure 3.10. Temperature Sensor. **30**
Figure 3.11. Data Logger **31**
Figure 3.12. UPS power supply **32**
Figure 3.13. Wall A: (a) section in the wall, (b) wall under construction **33**
Figure 3.14. Wall B: (a) section in the wall, (b) wall under construction **34**
Figure 3.15. Wall C: (a) section in the wall, (b) wall under construction **35**
Figure 3.16. Double-glazed door. (*Ecosafe - TPRS*) **35**
Figure 3.17. Concrete roof: (a) section showing the layers (14, 15 are thermocouples), (b) roof under construction. **36**
Figure 3.18. Section in the floor layers. **36**
Figure 3.19. Model Construction Steps. **38**
Figure 3.20. The flow diagram for the original RTSM cooling load calculation technique (Rees et al., 2000) **39**
Figure 3.21. Pseudo-Code for Determine Conductive Heat Gains per hour using response variables. **45**
Figure 3.22. Pseudo-Code of Converting Heat gains to cooling loads. **46**
Figure 3.23. Pseudo code of generating hourly fractional cooling loads. **46**
Figure 3.24. Pseudo Code for Summing all Portions. **47**
Figure 3.25. ASHRAE RTS Procedure Spreadsheet (Spitler et al., 1997). **49**
Figure 4.1. Program interface to generate PRF/RTFs. **52**
Figure 4.2. Periodic Response Factors. **52**
Figure 4.3. Incident Solar Irradiation. **53**
Figure 4.4. Air and Sol-Air Temperatures. **55**
Figure 4.5. Conduction Heat Gains **57**
Figure 4.6. Solar Heat Gain **59**
Figure 4.7. Sol-air Temperature Results for Wall A. **60**
Figure 4.8. Heat gain results for wall A layers. **61**
Figure 4.9. Sol-air Temperature Results for Wall B. **62**
Figure 4.10. Heat Gain Results of Wall B Layers. **62**
Figure 4.11. Sol-air Temperature Results for Wall C **63**
Figure 4.12. Heat Gain Results of Wall C Layers. **64**
Figure 4.13.. Heat Gain Results for Roof. **64**
Figure 4.14. Total Heat Gain Results. **65**
Figure 4.15. Heat gain for each orientation of wall A. **67**
Figure 4.16. Heat gain for each orientation of wall B. **67**

Figure 4.17. Heat gain for each orientation of wall C. **68**
Figure 4.18. Walls and Roof Cost. **70**
Figure 4.19. Cooling Loads for each room. **71**
Figure 4.20. Monthly Energy Cost for each room **71**

LIST OF ICONS AND ABBREVIATIONS

Icons		Described
q_θ	:	Hourly conductive heat gain, Btu/h (W), for the surface;
A	:	Surface area, ft^2 (m^2);
Y_{Pj}	:	Response factor;
$t_{e,\theta-j\delta}$	:	Sol-air temperature, °F (°C), j hours ago;
t_{rc}	:	Presumed constant room air temperature, °F (°C).
Q_θ	:	Cooling load for the hour θ
q_θ	:	Heat gain for the current hour
$q_{\theta-n\delta}$	:	Heat gain n hours ago
r_0, r_1, etc.	:	Radiant time factors
q''_θ	:	Heat flux at the inside surface of the wall at the current hour,
n	:	Large number dependent on the construction of the wall,
Z_j, Y_j	:	Response factors,
$T_{i,t-j\delta}$	:	Inside surface temperature j hour's ago,
$T_{o,t-j\delta}$	:	Outside surface temperature j hours ago.

Abbreviations		Described
ASHRAE	:	American Society of Heating, Refrigerating and Air-Conditioning Engineers.
CO_2	:	Carbon dioxide
EIU	:	Economist Intelligence Unit
HVAC	:	Heating, ventilation, and air conditioning
OPEC	:	Organization of the Petroleum Exporting Countries
E.U.	:	European Union
U.S.	:	United States
NZEB	:	Net-Zero Energy Building
HRV	:	Heat Recovery Ventilator
ERV	:	Energy Recovery Ventilator
ASHP	:	Air-Source Heat Pump
GSHP	:	Ground-Source Heat Pump
MDH	:	Mälardalen University
RTNYS	:	Residential Energy Consumption Survey
TS	:	Thermal Insulation Standard

CFFT	**:**	Complex Finite Fourier Transform
CFL	**:**	Compact Fluorescent Lamp
RTS	**:**	Radiant Time Series
CLTD	**:**	Cooling Load Temperature Difference
PRF	**:**	Periodic Radiant Fraction
RTF	**:**	Radiant Time Factor
HVAC	**:**	Heating, Ventilation, and Air Conditioning
HBM	**:**	Heat Balance Method
RTSM	**:**	Radiant Time Series Method
TETD/TA	**:**	Total Equivalent Temperature Differential/Time-Averaging
TFM	**:**	Transfer Function Method
TETD	**:**	Total Equivalent Temperature Difference
TA	**:**	Time Averaging
SCL	**:**	Solar Cooling Load
CLF	**:**	Cooling Load Factor

1. INTRODUCTION

Over 30 % of the world's carbon dioxide emissions and 40 % of its energy consumption come from buildings. Most of this energy is used to maintain a comfortable indoor temperature.

Energy use in buildings accounts for a disproportionate share of total energy use, leading to a host of environmental issues that threaten human civilization. Predicting a building's energy use is promoted as a means of energy conservation and better decision-making to cut down on consumption. In addition, cutting down on the overall energy used by new buildings is facilitated by the development of energy-efficient structures (Olu-Ajayi et al., 2022).

Residential building energy consumption is the world's greatest energy demand source. The recent expansion of urban sectors, economic growth, and elevated living standards has led to a doubling of energy consumption. Additionally, it has been discovered that places with a lower population density have reported an increase in energy usage. Since the current goal for sustainable urban growth is apartment-based living, it is expected that energy consumption will rise here as well. Residential energy consumption is influenced by both foreign and domestic influences, as well as geographical, complexity, and temporal variations (Almalki, 2020).

The study focuses on analyzing heat gain in multilayered walls using both theoretical models and experimental methods, employing the RTS technique. This research contributes to insights on energy-efficient designs by selecting the most appropriate wall types and layers by looking into their thermal behaviour and properties.

1.1. Cooling Load

Cooling load is the rate at which sensible and latent heat must be evacuated from the space to maintain a constant space dry-bulb air temperature and humidity (Handbook, 2013; Reddy et al., 2016). The addition of sensible heat to a room causes its air temperature to rise, whereas the addition of latent heat is connected with an increase in the space's relative humidity. Different heat transmission techniques may be affected by the building's architecture, its interior equipment, its inhabitants, and the weather conditions outside (Bhatia, 2001).

The overall cooling load of a building is made up of heat conveyed via the building envelope (walls, roof, floor, windows, doors, etc.) and heat created by inhabitants, equipment, and lighting. External load refers to the load caused by heat transfer through the envelope, while internal load refers to all other loads. The ratio of exterior to interior load varies based on building type, site climate, and architectural design. A building's overall cooling load comprises both sensible and latent load components. The sensible load influences the dry bulb temperature, while the latent load affects the relative humidity of the room being conditioned (Handbook, 1997). Buildings may be categorized as either internally or externally loaded. The main factor contributing to the cooling demand in buildings impacted by external loads is heat transmission from the surrounding environment to the conditioned interior space. The cooling demand of an externally exposed structure experiences substantial fluctuations throughout the day as a result of the considerable variety in the surrounding environment. Interior heat sources such as occupants, lighting, and appliances are the main contributors to the cooling load in buildings with internal heat generation. The cooling load of an internally loaded structure remains relatively constant due to the substantially smaller heat transfer from its fluctuating surroundings compared to the internal heat sources. Typically, the generation of heat due to internal heat sources tends to remain rather stable. The overall approach to design for externally loaded structures should inherently differ from that of an internally loaded building in terms of energy conservation and economics. In order to achieve efficient system design, it is essential to possess previous knowledge of whether the building's framework is subjected to internal or external loading (Bhatia, 2001).

For a precise estimate of the zone and building-wide loads, one of the following three approaches should be utilized (Handbook, 2013).

1. Transfer Function Method (TFM): This is the most complicated of the ASHRAE-proposed procedures and involves utilizing a computing application or an advanced worksheet.

2. The 'Cooling Load Temperature Difference (CLTD)/Cooling Load Factors (CLF)' approach is a simplified version of the TFM method that utilizes tabular data for calculating purposes. The method can be used in simple spreadsheet programs but it has some limits because it uses tabulated data.

3. Total Equivalent Temperature Different /Time-Averaging (TETD/TA): Before the advent of the CLTD/CLF technique, this was the most efficient approach for manual or basic spreadsheet computation.

1.2. Energy Consumption and CO2 Emissions

The energy systems of nations will suffer if severe weather events like droughts, heat waves, and storms occur more often. Drought conditions in significant river systems like the Yangtze (China), the Danube and the Rhine (Europe), and the Colorado River (US) in 2022 were caused by a large portion of the northern hemisphere's dry weather. This had a detrimental effect on hydropower generation, which accounts for nearly half of the world's low-carbon electricity generation. Blackouts may result from heat waves since they increase peak power demand and reduce power plant production; storms may also harm energy infrastructure (Rivers Are Running Dry Today - China Water Risk, 2022).

The entire final energy consumption of the worldwide buildings industry remained unchanged in 2019 compared to the previous year (Figure 1.1). However, the release of carbon dioxide caused by building-related activities have reached an unprecedented level, around 10 gigatons (Gt) of CO2, accounting for 28 percent of the overall world CO2 emissions connected to energy. When accounting for emissions from the building construction sector, the proportion increases to 38% of global energy-associated carbon dioxide emissions. The decrease in the proportion of emissions from buildings, compared to 39 percent in 2018, can be attributed to the rise in transportation and other economic emissions from buildings. (Global, 2020).

In 2023, the energy usage in the sixty-nine countries considered by the industrial division of the EIU is projected to grow by a mere 1.3 percent, despite the global economy's decline and the escalating energy expenses. For the second consecutive year, there was a modest increase in consumption. The specialists predict that consumption will only grow by 0.9% in 2022 due to record-high prices and a decrease in the Russian gas and oil supply (Risk, 2022).

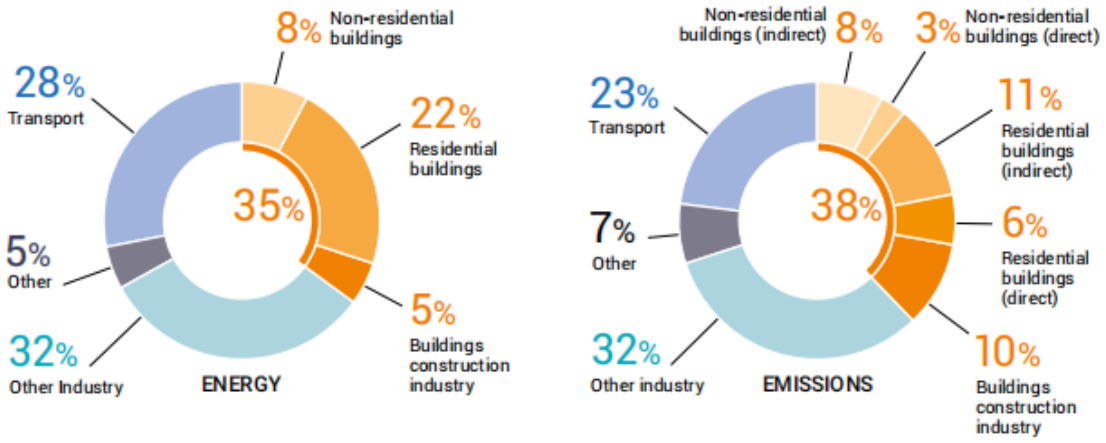

Figure 1.1. 2019 Energy Consumption and CO2 Emissions (Global, 2020)

Energy supplies were predicted to decrease in 2023, as OPEC+ members are ready to reduce output to prevent oil prices from falling too much. With the complete implementation of EU oil sanctions by the end of 2022, it was anticipated that Russia's oil and gas production will decline further. Despite pricing pressures from supply-side difficulties, oil prices are falling due to worries about a worldwide recession. In 2023, it was anticipated an average price for Brent oil of $89,6 per barrel, a decrease from the prior projection of $91 per barrel (Risk, 2022).

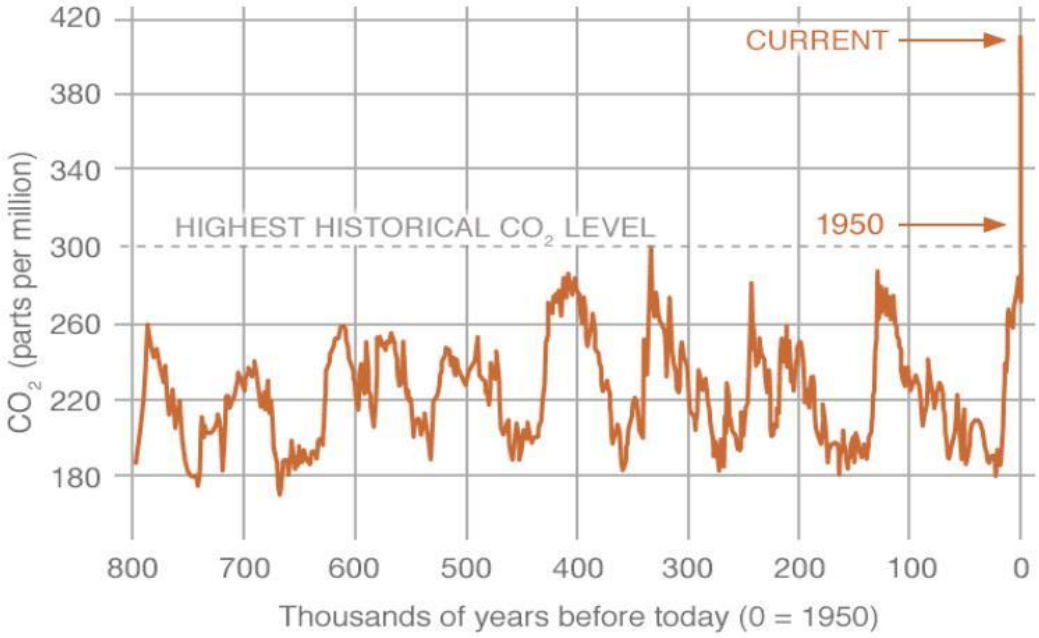

Figure 1.2. Concentrations of carbon dioxide in the atmosphere (Skelly, 2021)

According to NASA's webpage on climate change and factors influencing global warming, carbon dioxide is the primary driver of greenhouse effects in the atmosphere. This gas, largely absorbed by the seas, contributes to the global warming. Prehistoric CO2 levels are shown in the graph (Figure 1.2.) which was derived from data collected from ice sheets (Skelly, 2021).

1.3. Radiant Time Series (RTS)

Radiant time series is a two-step technique. Compute the whole zone convective and radiant heat gains first. Next step converts these improvements into zone air cooling load contributions (Costa, 2010). A novel technique for calculating design cooling loads that were developed from the heat balance approach is the radiant time series method. The techniques used for calculating cooling load include the 'Cooling Load Factor methodology' (CLF), 'Solar Cooling Load' (SCL), 'Total Equivalent Temperature Difference' (TETD), 'Time Averaging method' (TA), 'Transfer Function method' (TFM), and 'Cooling Load Temperature Difference' (CLTD) are all substantially replaced by the RTS (Costa, 2010).

To eliminate the repetitive stages in this procedure and make the RTS technique appropriate for spreadsheet implementation, certain essential approximations have been used to simplify the approach.

As a first simplification, the radiant time series method takes into account internior as well as exterior radiation and convection coefficients by employing the combined constant conductance. It suggests that nodes in the air and on surfaces transmit long-wavelength radiation. This presumption represents every wall as a simplified node network and allows for the insertion of individual surface heat balances (Nigusse, 2007), as seen in Figure 1.3.

The second assumption refers to the periodicity of the outside circumstances provided in the layout. In this assumption, RTS technique calculates the periodic response factor by using consistent patterns in sol-air temperature of the selected date layout and the continuously maintained temperature of the tested building. The conductive portion of the heat gains is computed using Periodic Response Factors (PRF) or Conduction Time Series Factors (CTSF) which are influenced by the variation between the room air temperature T_a and the anticipated constant design day periodic Sol-air temperature T_{SA}. The PRFs replace the conduction time series factors (CTSF) in the heat balancing

approach and eliminate the inherent repetitive computation of heat gain by conduction, which is present in load calculation techniques based on transfer functions. This crucial assumption eliminates the iteration phase, making the RTSM appropriate for spreadsheet implementation. The CTSF is calculated by dividing the periodic response factors by the total U-value of the structure (Spitler et al., 1997).

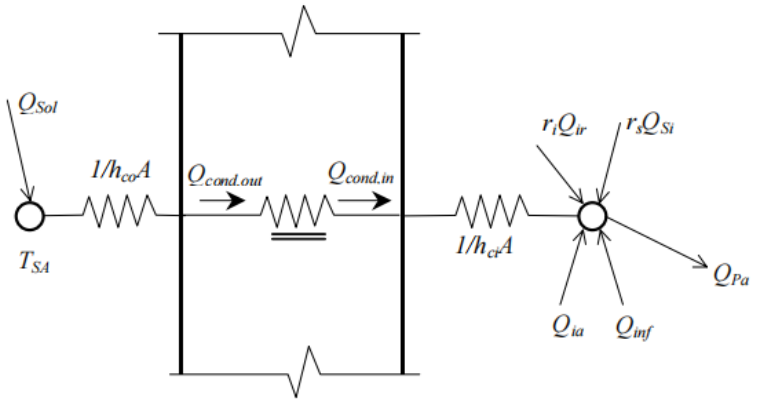

Figure 1.3. The Radiant Time Series Method shown using a Nodal Network Presentation (Nigusse, 2007)

In the third simplification of the RTSM, the radiant elements the heat gains are transformed into a cooling load using the RTF, which takes the role of the air heat balance. On an hourly basis, the radiant gains are transformed by a set of a total of twenty-four space response factors called radiant time factors (RTF). At the room air node, the load is increased by the radiant time factors r_i and r_s, respectively, from the internal heat gains Q_{ir} and transmitted solar heat gains Q_S, as illustrated in the nodal network diagram (Figure 1.3.). To determine the total hourly burden, these contributions are combined together. In Figure 1.3., Q_{Pa} represents cooling load, which is the amount of heat removal required to keep the temperatures of the air in a space constant (Nigusse, 2007). The convective and radiative components of solar and interior heat gains are separated using convection and radiation factors in the fourth approximation of the RTSM (Spitler et al., 1997).

1.4. Objective

The objective of the thesis can be summerized as follows:

1. Evaluate the efficiency of thermal characteristics of commonly used wall constructions in Iraq.

2. Employ the ‘ASHRAE Radiant Time Series’ (RTS) method for calculating heat gain in multilayered walls.
3. Provide insights into improving energy efficiency and thermal comfort in buildings.
4. Understand heat gain patterns across different wall layers.
5. Analyze the impact of solar radiation exposure on thermal performance.
6. Emphasize the importance of insulation in mitigating heat gain.
7. Contribute to optimizing building materials and design for enhanced energy efficiency and thermal comfort in Iraq.

1.5. Importance

The Importance of this work can be summarized by the following:

a. Reducing the building’s energy consumption by using the most appropriate walls and roof materials that achieve the minimum heat gain.

b. Show the effect of walls directions on the heat gain by using different rooms orientation.

c. Producing energy annual cost with construction cost analysis for the different walls and construction materials.

1.6. Thesis Outline

The following list might serve as a summary of this thesis' sections:

1. Introduction: Provides an introduction to the energy-saving methods, gas emissions as well as the study's methods and goals.
2. Literature Review: This chapter is an extrapolation or synthesis of the existing scientific studies and research publications that apply exclusively to energy consumption and cooling load calculations.

3. Materials and Methods: This chapter focuses on the analytically organized construction of the study's topic, as well as the methodology for investigating the subject of research using numerical analyses.

4. Results and Discussion: This component of the thesis discusses the experimental part of the practical procedures used to create the test rig, as well as the materials utilized in its production and the tests that are undertaken to analyze in several ways.

5. Conclusion and Recommendation: It provides practical assessment results, analytical and numerical analyses, and an examination of these results are presented. Additionally, the section summarizes key insights and provides recommendations for future procedures or techniques

2. LITERATURE REVIEW

Many previous studies and investigations have dealt with the subject of global energy consumption as well as the effects of walls and roofs of buildings on the mechanisms for calculating cooling and heating loads in buildings and carbon dioxide emissions.

This chapter of the thesis will include a brief presentation of previous studies and investigations on the global energy consumption of buildings and the most important solutions necessary to reduce this consumption. The review encompassed research studies spanning various subjects, ranging from the oldest to the most recent.

2.1. Energy Consumption and CO_2 Emissions

Emissions Pérez-Lombard et al. (2008) conducted a study examining energy consumption in buildings, focusing on HVAC systems. The study raised questions about data accessibility, building types, and end-use breakdowns. For commercial structures, international comparisons were provided, with offices being investigated more deeply. The research highlighted that building energy consumption in developed nations constitutes 20–40% of overall energy use, surpassing estimates for industry and transportation. However, the information was insufficient, hindering a comprehensive understanding of sector-specific changes. Accessible building energy data is crucial for effective analysis and future energy planning. Notably, HVAC systems, vital for thermal comfort, contribute 10–20% of total energy consumption in industrialized nations and nearly half in buildings (Pérez-Lombard et al., 2008). A study by Kusiak (Kusiak et al., 2010) provided a data-driven method for minimizing the energy required for air cooling, in which a typical office building was shown. The nonlinear link between energy usage, control settings (supply air temperature and supply air static pressure), and a collection of uncontrolled characteristics modelled using eight data-mining techniques. The ensemble of multiple-linear perceptron (MLP) outperforms other models evaluated in this study and was thus chosen to represent a chiller, a pump, a fan, and a reheating device. These four models were included in an energy optimization model with two decision variables: the supply air temperature set point and the air handling unit's static pressure. The model was resolved using a particle swarm optimization strategy. The optimization findings indicate that the HVAC system consumes almost 7 % less energy.

Thummakul (Ali & Thummakul, 2011) presented a study that investigates the ventilation system's existing condition in two computer rooms of the MDU university building. They monitored the concentration of carbon dioxide and temperature fluctuations inside these rooms. They determined whether or not this kind of control was successful. They also take into consideration the various types of heating sources accessible in the space, as well as their location and climate. In this project, they used a thermocouple and a carbon dioxide transmitter to monitor the room's temperature and carbon dioxide levels. This information was gathered and stored using a data logger and easy display software. The next stage was to create graphs for the room measurements in order to see the fluctuations in various areas of the room and then to evaluate them in order to offer suggestions for the operating circumstances. The CO_2 graphs for computer room 1 reveal that, under identical circumstances, the concentrations were higher near the room's entry than in other areas.

For a residential net-zero energy building (NZEB), Wu (Wu et al., 2018) published research examining the cost-effectiveness, comfort, and energy of commercially available HVAC devices. The ventilation, dehumidification, and heat pump solutions for the NZEB in the mixed-humid climatic zone were assessed using an experimentally verified model. Energy recovery ventilators (ERVs) and heat recovery ventilators (HRVs) reduced HVAC energy consumption by 13.5% and 17.4%, respectively, and the building energy by 7.5% and 9.7% when compared to mechanical ventilation without recovery. The thermal comfort levels of the various ventilation methods were similar. An air-source heat pump (ASHP) with a dedicated dehumidifier consumed 3.9% less energy for the building and 7.3% less energy for the HVAC system as compared to other dehumidification options. The initial investment was lower with the ASHP-only option (without specific dehumidification), but the degree of comfort was worse owing to excessive humidity. Finally, alternatives to the ASHP, such as ground-source heat pumps (GSHP), were examined. Energy consumption in the HVAC system was reduced by 26 percent and 29.2 percent for the GSHP using two holes in the ground, and by 13.1 percent and 14.7 percent for the building, respectively. Two power pricing structures and installation cost information was used to examine each HVAC arrangement's economics. The biggest energy savings and best comfort were offered by the GSHPs with the ERV and specialized dehumidification, but they were also the costliest. Reasonable payback periods were offered by the ERV (or HRV) and the ASHP with specialized dehumidification.

Šujanová (Šujanová et al., 2019) introduced a review that examines the relationships between (1) building design, (2) indoor environmental quality, and (3) tenant behaviour in their work. The emphasis of this study is on defining the limitations of adaptation on the three aforementioned levels in order to guarantee the energy efficiency of the whole system and the health of the environment. The adaptation limitations for observable physical parameters and the corresponding human sensory systems responsible for thermal comfort, visual comfort, indoor air quality, and sound quality are explained. The objective was to characterize the interactions between the three layers, each of which was an active agent of a larger human-built environment system. The conclusions were reached on the occupant's comfort. The research evaluates over 300 sources, including journals, books, conference proceedings, and reports, as well as standards and directions.

2.2. Effect of Buildings Walls and Roofs Design and Materials

The research the Ganja presented used analytical methods to investigate the influence of the outside colours on the nature of heat transfer over a flat, rigid roofing with varying thermal resistance (Granja & Labaki, 2003). Periodic approaches to the heat transfer formula and Fourier analysis were used to investigate the colour effect on the amount of heat transfer through the roof. The simulation, which took place over the course of 24 hours during Campinas' summer design day in Brazil's State of Sao Paulo, used a composite climate. An analysis of external surfaces, one grey and the other white, has revealed a roughly linear relationship between the amplitudes of heat flow (Δqi) and the thickness of a concrete roof. This relationship was observed within the range of 5 to 14 cm. On the other hand, this connection begins to flatten around 15 cm and above. The impact of the external surface colour on the periodic heat transfer through the roof decreases as the thermal resistance of the concrete roof increases to a thickness of over 15 cm. Hence, by appropriately leveraging thermal inertia, the conflict between selecting a colour for aesthetic appeal and ensuring the energy efficiency of opaque building components in warm climates could be minimized.

Eumorfopoulou (Eumorfopoulou & Kontoleon, 2009) published a study in which they discuss the thermal analysis of two equal building levels; plant-covered wall sections and non-covered wall surfaces. The research was conducted during a time of cooling in the Greek area. The bare and plant-covered surface parts of the walls were compared

using an experimental set-up (stationary method). For both situations under consideration, the results focused on the temperature changes and dynamic thermal features of the wall surfaces. As shown, the contribution of plant-covered wall sections is essential for enhancing the thermal performance of the building envelope.

Bektas Ekici (Ekici et al., 2012) provided a study to indicate the ideal insulation thicknesses for the various wall kinds; stone, brick, and concrete, which were frequently used in building construction in Turkey. Four cities from different climate zones, as determined by the Turkish "Thermal Insulation Standard" (TS 825), were selected for analysis: Antalya is located in the first zone, followed by Istanbul in the second zone, Elazığ in the third zone, and Kayseri in the fourth zone. For each city, the ideal insulating thicknesses, energy savings, and payback times were identified. The selected insulating materials included fiberglass, extruded polystyrene, expanded polystyrene, and foamed polyurethane. Five distinct energy sources were used in the calculations: coal, LPG, electricity, fuel oil, and natural gas. Consequently, the optimal insulation thickness ranges from 0.2 cm to 18.6 cm, energy savings range from 0.038 $/m^2 to 250.415 $/m^2, and payback periods range from 0.714 to 9.104 years, depending on the city, the type of wall, the type of insulation, and the price of fuel.

Shaik (Shaik & Talanki, 2016) conducted an examination of the impact of insulation placement within a flat roof that was directly exposed to solar radiation in order to lessen heat gain in buildings. By resolving a one-dimensional diffusion equation with convective periodic boundary conditions, it was possible to explore the unsteady thermal response characteristics of the building roof, including admittance, transmittance, decrement factor, and time delays. Four different kinds of walls' theoretical conclusions were contrasted with published experimental findings. The findings show that among the seven studied configurations, the roof with insulation positioned at the middle plane and inner side of the roof demonstrated the highest time lag. The roof, with insulation installed both in the central plane and on the outside side, had the highest energy efficiency when considering the decrease in factor. Out of the seven configurations using five distinct insulating materials, the composite roof with polystyrene expanded padding (insulation) placed on the outer side and middle plane of the roof proved to be the most optimal roof based on its lowest decrease factor of 0.130. The roof that made of composite materials, which includes resin-bonded mineral wool insulation positioned at the centre plane and inner side of the roof, was determined to be the most energy efficient based on its highest time lag point of view, which is 9.33 hours. The optimal thicknesses for fabric energy

storage were computed for several materials such as cement plaster, rock wool, expanded polystyrene, foam glass, rice husk, and resin-bound mineral wool. According to the findings, among the seven examined building roof materials, rock wool has the lowest ideal fabric energy storage thickness (0.114 m). Ghedas (Benzarti Ghedas, 2017) uses the REVIT program for residential construction simulation in Tunisia and to optimize the contemporary housing model in their work. After validating the acquired data in REVIT and comparing them to TRNSYS and ASHRAE Spreadsheet, we have used them to evaluate both house types (contemporary and traditional). Using REVIT, the assessment findings indicate that traditional dwelling is more energy efficient than modern housing, especially during the summer. Then, we optimize the contemporary models by using the passive tactics of traditional bioclimatic design and the enhancement techniques uncovered in earlier research. Numerous REVIT software-based experiments have been conducted to assess different modern dwelling types that can be incorporated into the Mediterranean climate. In reality, these experiments demonstrate that REVIT's thermal modelling of residential structures is based on the RTS approach. A qualitative analysis based on image/comment reveals that historic homes are more energy efficient throughout the heating and cooling seasons than modern homes. Quantitative analysis of thermal quality efficiency using REVIT reveals that traditional home B is more efficient than modern house E during the cooling period, although the latter contributes less to the heating load during the heating season.

A study by Kumar (Kumar et al.)demonstrated that optimal wall insulation thickness (OIT) was calculated using a life cycle cost analysis. The heat losses through the building wall were computed using the heating-degree technique. This study investigated the performance of fifteen distinct wall-building materials, utilized electricity as the energy source, and employed rock wool as an insulating material. An Engineering Equation Solver was utilized to simulate a suitable mathematical model in order to determine the return period for initial investments and cost savings. The results indicate that light concrete materials have negligible life cycle expenses, averaging just under $2 per square meter per year, and a return period that varies between 6 and 47 years. In contrast, it was determined that heavy concrete materials, laterite bricks, and concrete blocks exhibited the highest cost-effectiveness, with savings ranging from $12 to $16 per square meter per year and a minimum return period of three years. As a result, it was deduced that the utilization of fire bricks and light concrete materials for wall insulation is not economically viable, given the substantial return on investment required for

insulation. On the other hand, it is advisable to insulate walls made of massive concrete blocks, laterite bricks, and concrete blocks. For optimal performance, the recommended thickness of insulation lies between 54 and 98 mm, as this material exhibited the least rate of return.

2.3. Cooling Load Calculations

Zedan (Zedan & Mujahid, 1993) derived and equation for transient heat transfer in composite walls that subjected to explicit solar radiation and sinusoidal fluctuations in ambient temperature and a fluid with a constant temperature. In order to convert the closed-form solution from the Laplace s-domain back into the time domain, a series formula was used. The approach yielded a transitory response that gradually converges into a constant periodic response. Test instances demonstrated that the approach was precise, resilient, and quantitatively effective for transient and stable periodic responses. Case examples were provided to illustrate the technique's usefulness, which offers an effective alternative to solely numerical treatment. The study of Rees (Rees et al., 2000) providing a qualitative evaluation of three modern cooling load estimation techniques used in the USA and Britain. The general structure of the approaches (HBM, RTS, and AM) was tested and compared. Additionally, an analysis was conducted regarding input data processing and equations that needed to be solved to provide the values of the 24-hour cooling loads. The assumptions utilized by the overmentioned computation techniques to describe some of the main heat transmission pathways were specifically compared. In comparison to the predictions of the Heat Balance Method, conclusions were formed on the capacity of the simpler approaches to accurately anticipate peak-cooling loads. It was also mentioned that comparable methods for calculating cooling demand could emerge in the U.K. and North America. Ansari et al. (Ansari et al., 2005) presented a study that focuses on the creation and validation of digital tools for calculating the cooling load of buildings. Compared to other commercially available, outrageously expensive, and widely used software, this program was easier to use, required fewer input data, and was more adaptable. It was simple to analyse the impacts of important construction elements like orientation, window glass shade type, amount of glass panes utilized, wall insulation, roof type, and floor type. The effects of all these factors have been examined for a typical building block to make an informed choice. It cannot be done

as easily with any other program or technique. All of the aforementioned benefits were achieved without compromising precision and dependability.

Yumrutaş (Yumrutaş et al., 2007) developed a theoretical approach for calculating the Total Equivalent Temperature Differential (TETD) for multilayer flat roofs and building walls. The TETD values determine based on time lag and decrement factor using recorded air temperature and the amount of sunlight falling on a flat surface per hour. A periodic solution to a one-dimensional transient heat transfer problem for building structures is used numerically to compute the time lag and decrement factor. The problem is first formulated as a differential equation with initial and boundary conditions, which is then transformed to a dimensionless form and solved by use of a complex finite Fourier transform (CFFT). Finding the maximum and minimum temperatures at the interior and outside surfaces of roofs and walls, as well as the time periods involved in reaching these temperatures, as well as the hourly temperature fluctuation inside the structure, were all accomplished using the method. TETD values for the structures were computed using collected data on directional sol-air temperatures, time lag, and decrement factor. The study Kaşka (Kaşka & Yumrutaş, 2008) presented compares practical and theoretical findings on transient temperature differences in multilayered building walls and flat roofs, as well as heat transport across the building systems. Experimental and theoretical models were given to determine the transient temperature fluctuations in these structures and heat flow through these components, which rely on the interior surface and room air temperatures. The experimental model, which included two rooms, cooling units, measurement equipment, and computers, was used to measure the surface temperatures of each wall and roof layer as well as the instantaneous interior and outside air temperatures. Computer software was created using the theoretical model as a foundation to carry out numerical computations. Using the hourly measured ambient air temperatures and solar radiation flux on a horizontal surface for the city of Gaziantep (37.11N), Turkey, as well as the thermophysical characteristics of the structures, hourly temperature variations of the nodal points, were computed numerically over a period of 24 h. In this work, the theoretical model's validity was confirmed by comparing the results from the experimental and theoretical models. Calculations for a variety of multilayer construction walls made of briquette, brick, blokbims, and Autoclaved Aerated Concrete (AAC), which were all frequently used in Turkey, were repeated. The results were compared in order to choose the best wall material. AAC and blokbims were identified as more suitable wall materials due to their higher heat conductivity in comparison to briquettes and brick.

Bansal (Bansal et al., 2008) developed a one-dimensional, transient heat transfer model for estimating the difference in building cooling load temperature (CLTD). The governing partial differential equation was solved using the finite difference technique with appropriate starting and boundary conditions. Using a newly developed ambient temperature model for estimating a model of sky radiation and the local dry bulb temperatures and that accounts for the influence of local relative humidity, CLTD values for various roof and wall types were calculated. There have been comparisons between the calculated and ASHRAE CLTD values. Comparing calculated and ASHRAE CLTD values for roofs and walls under the circumstances given in ASHRAE handbooks, a reasonable degree of concordance was observed. However, there are minor to substantial discrepancies between the calculated and the values of CLTD ASHRAE when computations are performed for Kolkata, India. MATLAB software was used to compute CLTD values for various walls and roofs in 40 degrees north latitude and in Kolkata, India. The CLTD values computed for 4 N (standard circumstances) are comparable to those provided by ASHRAE, showing the model's validity. The CLTD values of various roofs for non-standard circumstances in Kolkata's building correspond quite well with the values derived from ASHRAE tables with modifications for latitude, range, etc. In the case of walls, nevertheless, there may be a small difference between the computed and calculated numbers. This may be ascribed to the adoption of more contemporary and accurate ambient temperature and solar radiation models for estimating CLTD values, as well as ASHRAE's possible grouping of various wall types into a single category. Consequently, it may be argued that the CLTD values supplied by ASHRAE for various kinds of walls are not as accurate for places other than those for which they were calculated, particularly when considering local weather fluctuations. In addition to the roofs and walls specified in the ASHRAE tables, this model may be used to determine the cooling load due to additional roofs and walls. In reality, if thermal standards for local building materials are given, it is possible to calculate the cooling load of structures in the area with better precision. They stated that this model does not account for the thermal capacity of the items inside the conditioned area and assumes a constant room temperature. To compute the instantaneous heat transfer rates and the temperature of the conditioned space, if the precise specifications of the objects inside the conditioned area are known, it is possible to adapt the model to account for these impacts as well. Cui (Cui & Chen, 2009) develops a novel approach based on the Radiant Time Series (RTS). The novel technique requires just one additional step following the present RTS design

process, using the estimated overall periodic transfer coefficients. The higher cooling loads created by the new technique correspond well with the outcomes of simulations conducted using Energy Plus. The findings of the analysis also indicate that the extra peak cooling loads vary significantly on building types, orientations, window sizes, and operating durations. The initial section of the updated RTS technique was identical in theory to the existing RTS system, but the computation mechanism was simplified. Utilizing the periodic transfer coefficients derived in the preceding section, an estimation will be made for the increase in peak cooling load resulting from the shift from continuous to intermittent operation. The sum of the peak cooling demand in continuous operation and the extra peak cooling load determined in the second step yields the total peak cooling load in intermittent operation. Kulkarni (Kulkarni et al., 2011) chose a 16 m by 8.4 m by 3.6 m lecture hall situated in Roorkee (28.58N, 77.42E) in the northern area of India to calculate the monthly and yearly cooling load (kWh) and cooling capacity of an air conditioning system using a computer simulation. In addition, the report includes the findings of research examining the impact of various glazing systems on windows and the decrease of building cooling load. The cooling load was computed using computer simulation using 'Design Builder' software. The objective of this study was to examine how modifying the U-values of different types of glazing, insulating the ceiling, implementing cool roofs, applying both exterior and interior insulation on walls, and replacing conventional fluorescent tube lamps (FTL) with energy-efficient compact fluorescent lamps (CFL) can reduce thermal gains and cooling load demands. Implementing a false ceiling, wall insulation, different types of glass, and lighting systems proves to be economically advantageous, leading to annual savings that range from 17 percent to 19.8 percent. In addition, the research emphasized the possibility of lowering CO_2 emissions and earning carbon credits. Retrofitting methods significantly impact energy savings, although the average payback time was about eight years. Barrios (Barrios et al., 2012) investigated numerically the thermal performance of six wall/roof designs in an intermittently air-conditioned room in a location where the outside temperature or sole-air temperature variation exceeds the thermal comfort zone. The intermittent air conditioning system functions as either a heating or cooling system. When working for cooling, it was activated when the indoor temperature exceeded the upper comfort temperature, and when operating for heating, it was activated when the indoor temperature fell below the lower comfort temperature. Consideration was given to a one-dimensional heat transfer model with periodic outside circumstances. The energy for the

on-periods and a thermal index for the off-periods were utilized to assess the designs. For comparative reasons, the wall/roof combinations were also assessed in a room with continuous temperature control and air conditioning. The findings indicated that the thermal assessment of a wall/roof must take into consideration the air conditioning system's operating state.

The Cooling Load Temperature Difference (CLTD) figures found in the literature are only applicable to spaces with constant ambient temperature. However, Ruivo (Ruivo et al., 2013) conducted a study that expands the use of this simplified technique to estimate cooling and heating loads in rooms with daily and weekend temperature setbacks and set thermostats. This study introduced the term Thermal Load Temperature Difference (TLTD). A transient heat transfer model and the accompanying computational tools have been created to forecast the thermal behaviour of multilayered walls and flat roofs in order to yield TLTD values. The notion of sol-air temperature was used. The room's thermal capacity was thought to be minimal. The study developed the TLTD evolutions for high-mass walls and roofs that have thermostats for both winter and summer settings. The times in which the room is empty have been properly accounted for. The TLTD evolutions permitted the estimate of the inner surface energy transfer and the maximum thermal load. Under summertime conditions, the compared scenarios show a relative difference of about 20% in the energy transferred via the sunny envelope, wall, or roof when technique A is replaced with technique B for temperature control.

Periodic solutions of unsteady heat transfer problems for building walls and flat roofs were utilized to get the CLTD values for various building components, as described in Omer Adil's (Zainal & Yumrutaş, 2015) paper. Applying the 'Complex Finite Fourier Transform (CFFT)' approach yields the answer. The periodic character of the solution is a unique use of the CFFT method for estimating the values of the CLTD for these components. A computation technique based on the periodic solution was constructed, and MATLAB software for numerical computations was created. ASHRAE handbooks' values were compared to the CLTD values. For the specified walls and roofs, there was a substantial correlation between calculated findings and CLTD values published in ASHRAE handbooks. It was determined that the disparities in CLTD values for Roof 2, Roof 13, and Wall 3 are varying from 0 to 2.42°C, 0 to 0.94°C, and 1.8 to 4.3°C, respectively, for principal directions. The variances between predicted heat gain figures and RTS measurements vary between 0 and 5W/m^2. Using ASHRAE standard data, the numerical computations are verified. Huang (Huang et al., 2015) presented a technique

for calculating the radiant cooling load of a floor based on the radiant time series (RTS) approach: Radiant cooling demand may be computed from radiant heat gain using radiant time factors. By analysing the measurement results for total heat gain and total cooling loads collected over a 24-hour period, it is possible to calculate the radiant heat gain of the floor. This can be done using the radiation and convection dividing method, along with utilizing a software to generate the PRF/RTF to determine the radiant time factor of the floor. Additionally, the determined radiant cooling load of the floor may be compared to the measured values for further analysis.

The findings for the five testing settings indicate that the radiant cooling load of the floor maximum error is lower than 2.3 percent when compared to the value estimated using the radiant time series approach and that the average error is less than 3.2%. The relative mean absolute errors are 1.2% and 1.7%. The results of the experimental investigation showed that using the heat balancing approach, the convective heat that is isolated from the radiation and convection of the inner surface without heat transfer may be defined as a radiant cooling burden. The total of the convective heat that separates the room from the wall, excluding the heating surface, and the room cooling load. The maximum peak and mean errors for room radiant load are 4.7% and 6.1%, respectively. The five circumstances combined average error is 2.6% and 3.1%, respectively.

Hashim (Hashim et al., 2018) discuss different cooling load estimation approaches in their work. The numerical calculations were made for a particular two-story structure in Basra situated at 47.78° longitude and 32° latitude. The heating and cooling load calculations necessary to properly size your HVAC equipment were not complex but time-consuming and required patience. Suppose you opt to do the calculations on your own. In that case, you'll need to perform particular calculations for each zone, including determining the space's size and insulation level and predicting air infiltration. Despite the fact that the size of HVAC equipment was based on scientific principles, it is an imprecise science. Due to the multitude of variables that contribute to each resident's unique heating and cooling climate, the HVAC system needs will vary greatly. Cooling and heating load estimates were a crucial aspect of the sizing equation - one that has been meticulously crafted to identify the optimal system for your requirements. They attempted to consolidate these ideas and provide a numerical estimate of heat characteristics for a structure in Basra as an example. The study of Mao (Mao et al., 2019) gives the findings of an exhaustive analysis of calculating the maximum cooling load methodologies of a building, emphasizing the sensible building envelope cooling loads. The most accurate

method was determined to be the Heat Balance Method (HBM), with the Radiant Time Series method (RTS) following closely. The Transfer Function Method (TFM), Time Averaging/Total Equivalent Temperature Difference (TA/TETD) method, and the Solar Cooling Load/Cooling Load Factor/Cooling Load Temperature Difference (SCL/CLF/CLTD) method were subsequently ranked in decreasing order of accuracy.

2.4. Summary

The initial survey may be summed up with the following points below:

1. The energy consumption of buildings in developed nations accounts for 20–40% of overall energy consumption. This was higher than the estimates for industry and transportation in the E.U. and the U.S. It was crucial to make accessible complete building energy data in order to provide appropriate analysis and effectively plan future energy strategies.
2. The CO_2 graphs for the computer room reveal that, under identical circumstances, the concentrations were higher near the room's entry than in other areas.
3. The ground-source heat offered the most significant energy savings and best comfort pumps GSHPs with the energy recovery ventilator ERV and specialized dehumidification, but they were also the costliest. ERV (or heat recovery ventilator HRV) and the air-source heat pump ASHP with specialized dehumidification offered reasonable payback periods.
4. The impact of the external layer hue on the regular heat transfer across the roof diminishes as the thermal resistance of the concrete roof increases (>15 cm).. Therefore, if building designers properly use thermal inertia, then the tension between picking a colour for eye-catching and ensuring the energy efficiency of opaque building components in hot regions may be reduced.
5. The contribution of plant-covered wall sections is essential for enhancing the thermal performance of the building envelope.
6. The optimal insulation thickness ranges from 0.2 centimetres and 18.6 centimetres. Energy savings can range from 0.038 $\$/m^2$ to 250.415 $\$/m^2$, while return on investment can range from 0.714 to 9.104 years. These variations depend on factors such as the city, type of wall, insulating material, and fuel costs.

7. The optimal thicknesses for fabric energy storage were computed for several materials including strengthened concrete, expanded Styrofoam, glass foam, woolly rocks, husk insulation, resin-bound mineral wool, and plaster of cement. According to the findings, among the seven examined building roof materials, rock wool has the lowest ideal fabric energy storage thickness (0.114 m).
8. Using wall insulation, different kinds of glass, false ceiling, and illumination systems may result to significant cost reductions. These measures can result in average yearly savings between seventeen percent to 19.8 percent.
9. The findings indicated that the thermal assessment of a wall/roof must take into consideration the air conditioning system's operating state.
10. The results from the five testing settings show that the maximum discrepancy in the floor radiant cooling load is lower than 2.3 percent when compared with the value calculated using the radiant time series method. Additionally, the average discrepancy is less than 3.2 percent.
11. Cooling and heating load estimates were a crucial aspect of the sizing equation - one that has been meticulously crafted to identify the optimal system for your requirements. They attempted to consolidate these ideas and provide a numerical estimate of heat characteristics for a structure in Basra as an example.
12. It was found that the Heat Balance Method (HBM) was the most accurate. The Radiant Time Series method (RTS) came in close behind. The Transfer Function Method (TFM), the Time Averaging/Total Equivalent Temperature Difference (TA/TETD) method, and the Solar Cooling Load/Cooling Load Factor/Cooling Load Temperature Difference (SCL/CLF/CLTD) method were then put in order of how accurate they were.

2.5. Present Work Scope

The study focuses on the performance of various configurations of these building elements (typical walls and roofs) and evaluates their effectiveness in reducing cooling loads. The anticipated outcomes of this investigation are projected to provide a valuable contribution to the field. development of more energy-efficient building designs and help address the challenges of sustainable building practices. A financial analysis may be

conducted to determine the cost while using the appropriate layers and comparing it with energy cost for the typical construction.

3. MATERIAL AND METHOD

Most serious research and investigations must contain an empirical study since experiments, and practical testing are essential for obtaining acknowledged scientific proofs and evidence. Moreover, calculation of design cooling and heating loads stands as a pivotal step in HVAC system design, with organizations like ASHRAE taking a longstanding interest in this matter. Their manuals provide techniques for determining these loads. Each community historically approached the estimation of cooling loads in slightly varied ways. The increasing globalization of the construction business has led to more organizations based in the US and Canada operating within the European continent, and vice versa, with both regions competing for contracts in places like the Far East. Adopting standardized procedures for critical design calculations is essential for enhancing the efficiency and credibility of the global HVAC business in the long term (Yang et al., 2014).

This section will cover the materials utilized to construct the room, the construction process, and the technique employed to carry out the cooling load. In addition to that it shows the theory behind residential cooling and heating load calculations and outlines the research inquiry techniques. Includes general principles, modelling, and numerical procedures.

3.1. Methodology

In order to achieve the thesis objective, the following methodology has been obtained:

1. The first stage is to thoroughly comprehend the study's objectives and their significance to society.

2. Collecting, summarizing, and choosing the most important papers and publications related to energy savings via heat gain reduction, subsequently, an analysis of the primary findings will be presented.

3. Based on the findings and recommendations from the stage above, design and construct the test rig taking into account cost, effectiveness, and material costs. A model of a small room, 1.15 cubic meter outside surfaces, is to be implemented (Figure 3.1). This model structured from different wall materials and layers. The walls will take names such as wall-A, Wall-B …etc. The roof is to be made of concrete and gypsum as well. An AC unit will be implemented to maintain the heat

inside. Thermocouples (type K) are to be adjusted between the wall, window, roof and floor layers, inside and outside the room to measure the temperatures along with time.

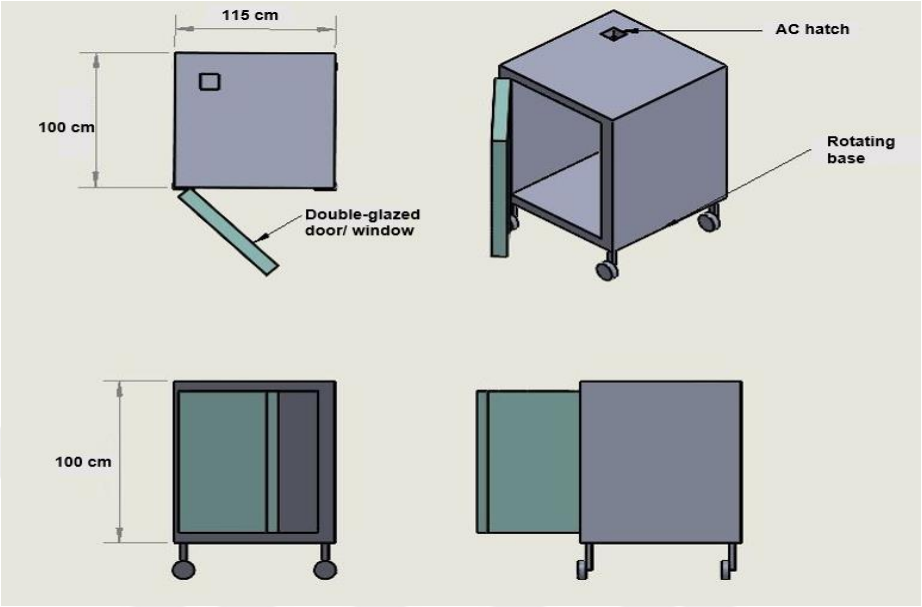

Figure 3.1. Room model

4. Analysing, quantifying, and testing the heat gain and cooling requirements of various building and insulation materials.

5. Compile the results of the performed tests and discuss them, as well as define the key paragraphs and conclusions, identify the benefits and drawbacks as well as preventative measures.

3.2. Materials

Different materials have been used in the experiments. The room model made of several building materials and they are from the local marketplaces. In the coming paragraphs, there will be a brief explanation of each item.

Gypsum: The inner surfaces of walls and roof are covered with a layer of a soft sulphate mineral known as gypsum, having the chemical formula $CaSO_4.2H_2O$, is made up of calcium sulphate dihydrate, as shown in Figure 3.2. It is extensively mined and used as fertilizer, the primary ingredient in many types of plaster, sidewalk, or blackboard chalk, and drywall, and it is also widely utilized as a building material (Hurlbut & Klein, 1977) used to cover the inside walls of the room with a thickness if 20 mm, as in Figure 3.3.

Figure 3.2. Gypsum (Egypt, 2022)

Figure 3.3. The inside walls are covered with Gypsum plastering.

Cement plaster: The outer surfaces of all walls (as is typically done) are covered with Cement plaster (Figure 3.4.). It is a mixture of appropriate plaster, sand, cement, and water commonly used to make a smooth surface on brick interiors and exteriors. It is often put in a single coat with a thickness of 12 mm, 15 mm, or 20 mm, depending on the type of structure being plastered (Spychał & Dachowski, 2021).

Figure 3.4. Cement powder used as mortar and for plastering

Cement plastering was used to cover the exterior walls of the room with a thickness of 25 mm, as shown in Figure 3.5.

Figure 3.5. The exterior walls are covered with Cement plastering

Clay Bricks: The main component of the of two walls of the room (wall A, and wall B) is the Clay Bricks. Its main material is heavy clay, its shape is either a square of a large

size or a rectangle of a small size used in the construction of the floor and in the arching of the ceilings of buildings. The standard dimensions of the bricks are (24, 11.5, 7.5) cm. The bricks are of different types according to the temperature at which they are burned, including (Malomo et al., 2019):

1. Extracted or solid bricks: - One of their properties is that it has few pores, solid with high density, and does not appear on their surface salts and is usually used in the work of foundations for buildings because of their strength and lack of moisture transfer as in Figure 3.6a. The solid bricks were employed in one of the walls in this work case, wall A.
2. White and yellow hollow bricks: They are used in the facades of buildings and internal buildings (Figure 3.6b). The hollow bricks were used in one of the walls of this work case, wall C.
3. Red bricks: It is slightly burnt clay, and their durability is less than other types and is used in constructing interior walls and domes.

(a) (b)

Figure 3.6 (a) Solid Bricks (*Bricks PNG 7 - PNG All*) . (**b)** White and Yellow Hollow Bricks.(Ltd, 2024)

Concrete blocks: The other wall (Wall B) made from Concrete blocks. It is a rectangular mold with a regular dimension used in building construction. Because concrete bricks may be used for many manifestations, they are one of the most adaptable and readily accessible construction materials (Croft, 2004).

Cast concrete is used to create concrete blocks (bricks) (i.e., Portland cement, aggregates, fine sand, and gravel are usually used to produce high-density bricks).

Low-density bricks may include aggregates made of industrial waste, such as fly ash or bottom ash. Bricks are often made from recycled resources, including discarded glass or recovered aggregates (Croft, 2004). The concrete bricks were employed in one of the walls in this work case, wall B (Figure 3.7.).

Figure 3.7. Concrete Blocks

The schematic Figure 3.8. showing the room walls, type of material and wall thickness, indicating the orientation of the room, the A/C unit and hot air discharge. In the table below, the dimensions of the materials used in the construction of the room (Table 3.1) and showing their dimensions:

Table 3.1. Dimensions of the material used in model construction

Material	Thickness (mm)	Width (mm)	Length (mm)
Hollow Brick	115	75	235
Solid fire clay bricks	115	75	235
Hollow concrete block	115	200	400
Concrete roof	170	1200	1200

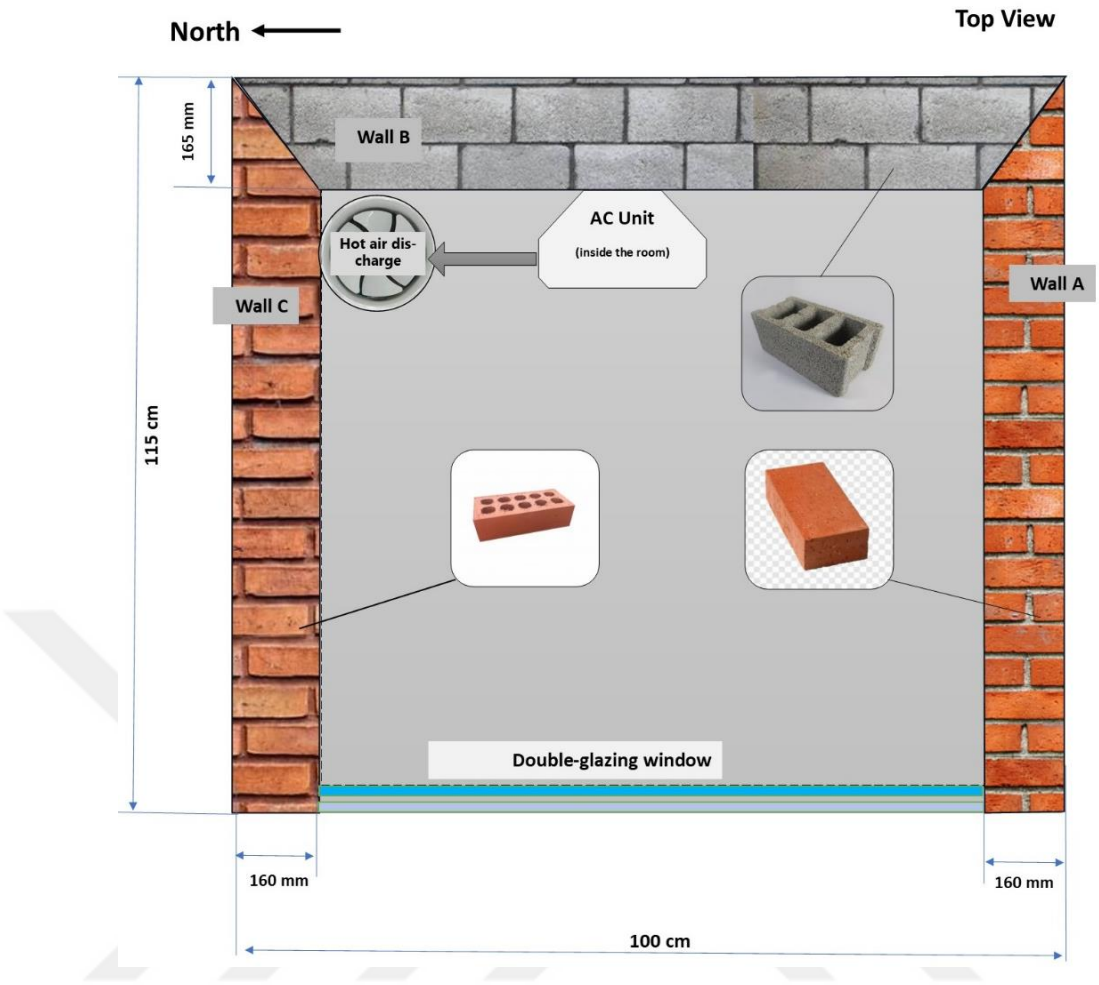

Figure 3.8. Room schematic showing each wall components

3.3. Measurement Equipment

This section outlines the tools and equipment that used in this work mentioned one by one in the next paragraphs.

Thermocouple: Any temperature sensor with Chromel and Alumel (Chromega®Nickel-Chromium Ni-Cr, Alomega®Nickel-Aluminum Ni-AI) conductors that satisfy the output ad meets specifications of the American Society for Testing and Materials ASTM E230/E230M-17 standards is called a K-type thermocouple (Figure 3.9.). They can be employed for measuring the temperature, ranging between −270° C to 1370° C, with errors within 0.5 to 2° C (Kadir & Kako, 2022). This type of sensors has a sensitivity that is approximately 41 microvolts per ° C. This might be a wire, a surface sensor, an immersion sensor, or another kind of sensor or cable (Leonidas et al., 2022). The K-type thermocouple was employed in this work to measure the temperature of wall layers.

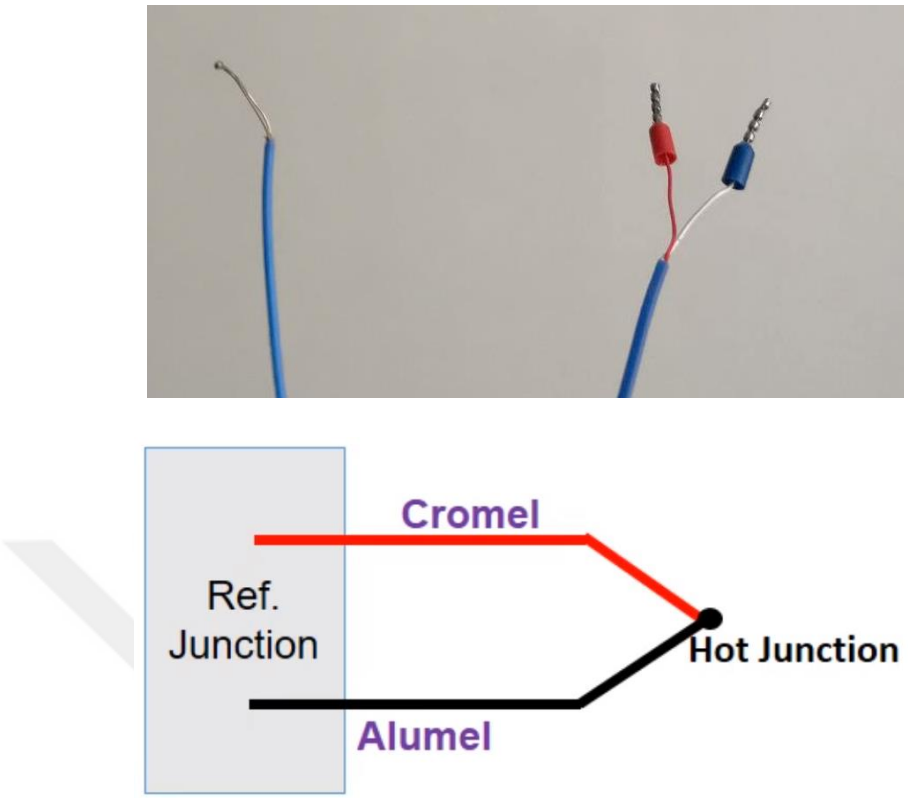

Figure 3.9. K-Type Thermocouple

Temperature Sensor: A wet bulb thermometer measures (Figure 3.10.) the amount of surface cooling that occurs when moisture evaporates (evaporative cooling). The temperature of the wet bulb is always lower than the (Zheng et al., 2016) dry bulb, unless the relative humidity is 100 % Both relative humidity and dry bulb temperature were measured using a sensor type AM2302 (wired DHT22). This sensor is good for 0-100% humidity readings with 2-5% accuracy, and good for -40 to 80°C temperature readings with ±0.5°C accuracy.

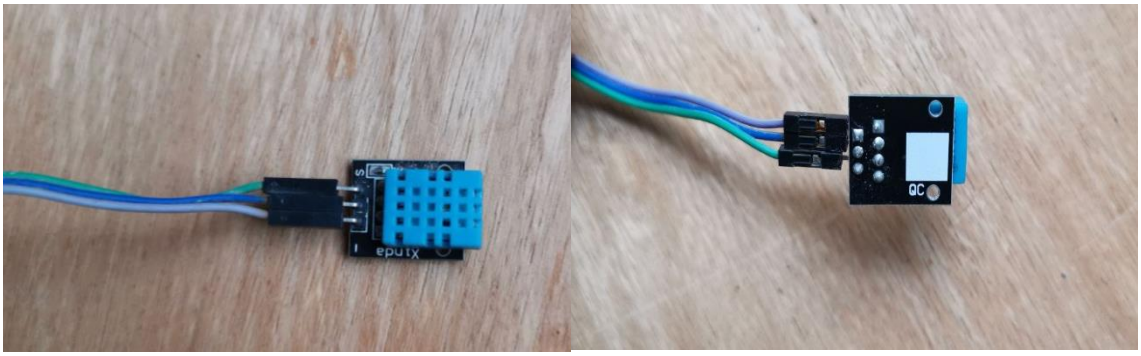

Figure 3.10. Temperature Sensor.

Data Logger: A comprehensive data collection system was implemented using various sensors and modules. Subsequently, the Arduino efficiently stored all the gathered data onto an SD card for comprehensive analysis. K-type thermocouples, responsible for temperature measurements, transmitted data to the MAX 6675 module, which then relayed it to a microprocessor (Arduino). The AM2302 sensor monitored relative humidity, sending the data streams to the Arduino. collect the data from the sensors (thermocouples) every 10 seconds. This data logger, represented by Figure 3.11., operated continuously, capturing information on relative humidity, and temperatures at different locations throughout the day.

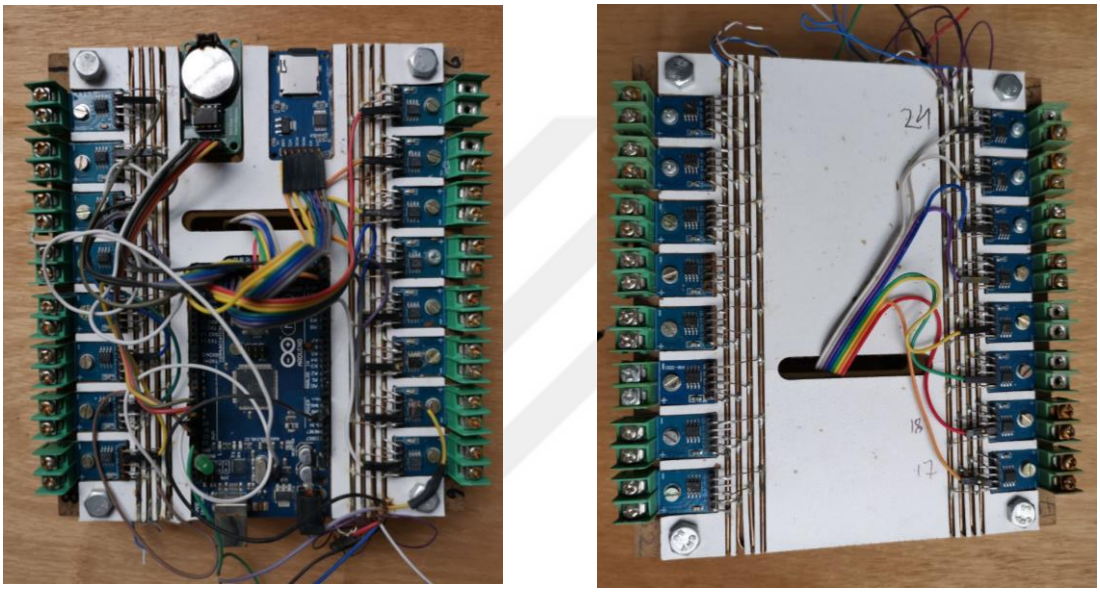

Figure 3.11. Data Logger

Power supply: To ensure that the data logger continues working even when the electricity is cut out, a DC UPS power supply (Figure 3.12.) of the " Gold Vision, Mini–DC UPs " company was used It has a capacity of 10200 mAh with USB output used for supply the power

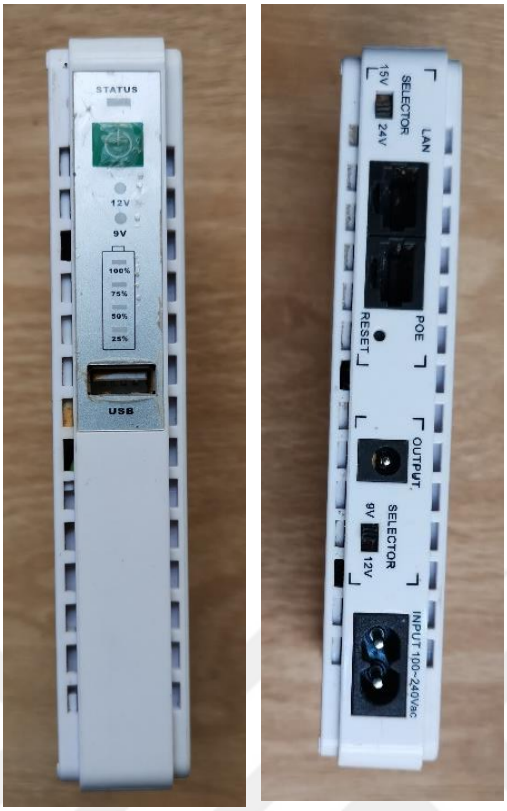

Figure 3.12. UPS power supply

3.4. Case Study

The experimental tests conducted to analyse the impact of using different layers on the thermal behaviour of the walls and its consequences on energy consumption and cost effectiveness by using the RTS method. In order to accomplish this, a model of a small room with dimensions 1.15 x 1 x 1 m, exterior surface which have various wall materials and layers was constructed in Daquq, (35.3235724, 33.322831), Kirkuk, Iraq. The walls were named wall-A, wall-B, etc. To regulate the temperature inside the space, an air conditioner was installed. Between the wall layers, inside and outside the room, thermocouples were adjusted (and numbered from 1 to 20) to measure the temperatures. The room was built over a cubic iron structure made of metal V-shaped right-angle bar mild steel. The thickness of each bar is 7 mm to make it strong enough to carry the room. The ground face is supported by a metallic sheet of mild steel that covers the lower face and makes the floor of the room. The room constructed on a rotating foundation that will enable the researcher to observe the impact of room orientation (sun direction) on the heat gain. The room component was as follows:

Wall A: This wall consists of three layers and as following order from the inside to the outside; 20 mm of gypsum plastering, solid bricks of 115 mm thickness, and 25 mm of cement plastering on the outer surface (Figure 3.13.).

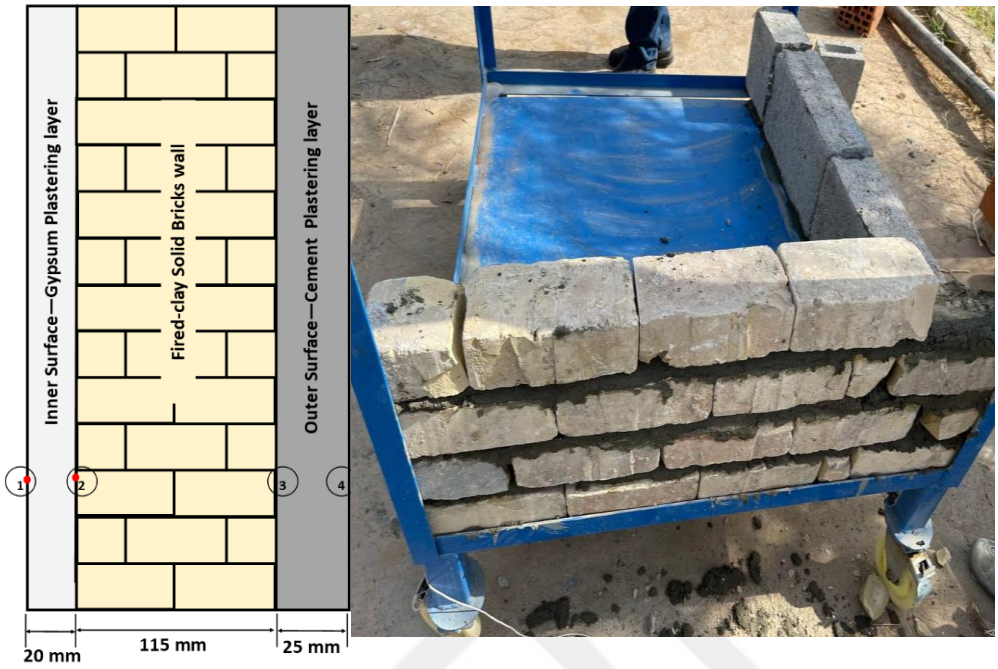

(a) (b)

Figure 3.13. Wall A: (a) section in the wall, (b) wall under construction

Wall B: This wall consists of three layers and as following order from the inside to the outside; 20 mm of gypsum plastering, concrete blocks of 120 mm thickness, and 25 mm of cement plastering on the outer surface (Figure 3.14.).

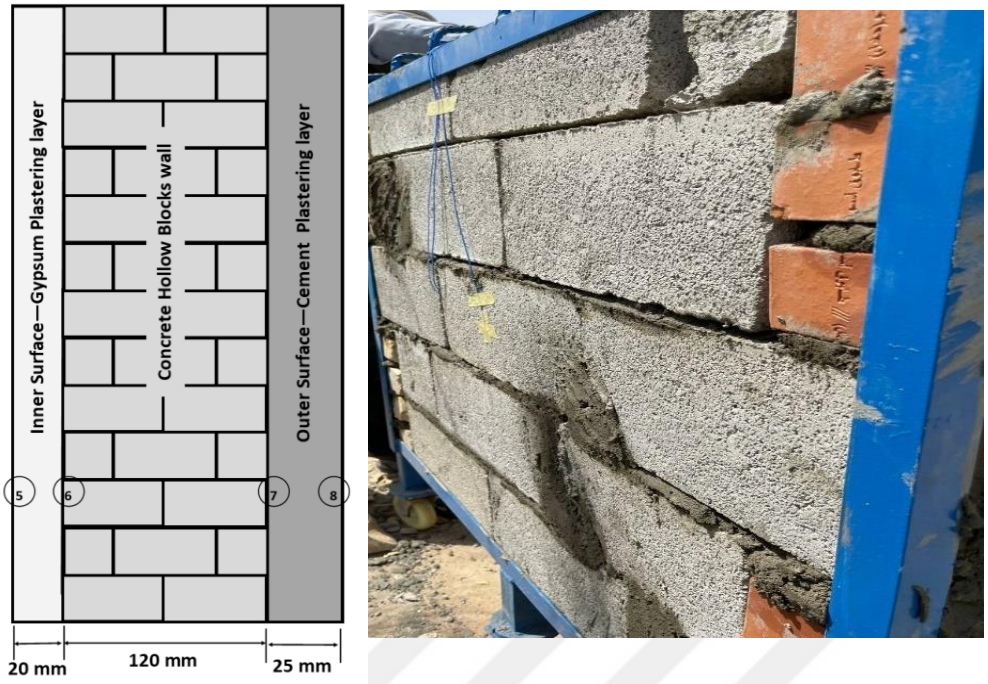

(a) (b)

Figure 3.14. Wall B: (a) section in the wall, (b) wall under construction

Wall C: This wall consists of three layers and as following order from the inside to the outside; 20 mm of gypsum plastering then concrete blocks 120 mm thickness, and 25 mm of cement plastering on the outer surface (Figure 3.15.).

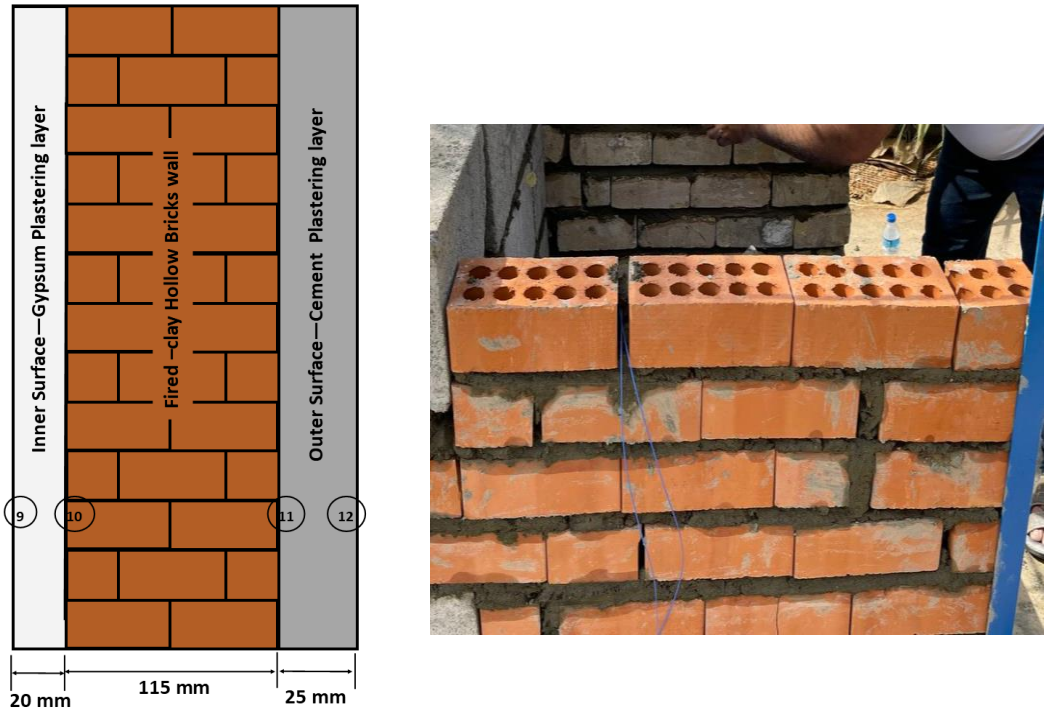

(a) (b)

Figure 3.15. Wall C: (a) section in the wall, (b) wall under construction

Double- glazed door/window: This door -unlike traditional single-glazed windows- consist of two separate pieces of glass. These glass panes are divided by an airtight sealed space, serving as a form of insulation. The thickness of each glass layer is 3 mm and the spacing between them is 6 mm (Figure 3.16.).

Figure 3.16. Double-glazed door. (*Ecosafe - TPRS*)

Roof: The inner face of the roof is covered by a false ceiling layer locally made of Gypsum with thickness of 8 mm then a concrete pile of 15 cm thickness as shown in figure 3.17.

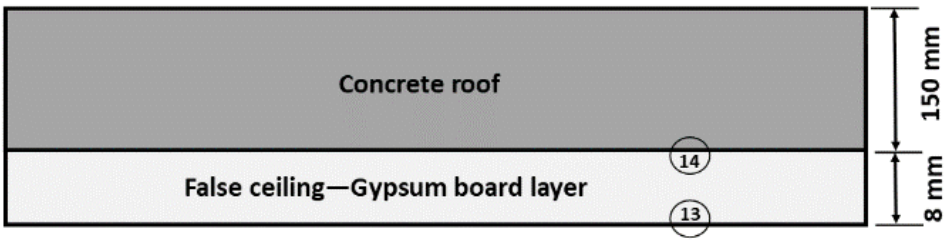

(a)

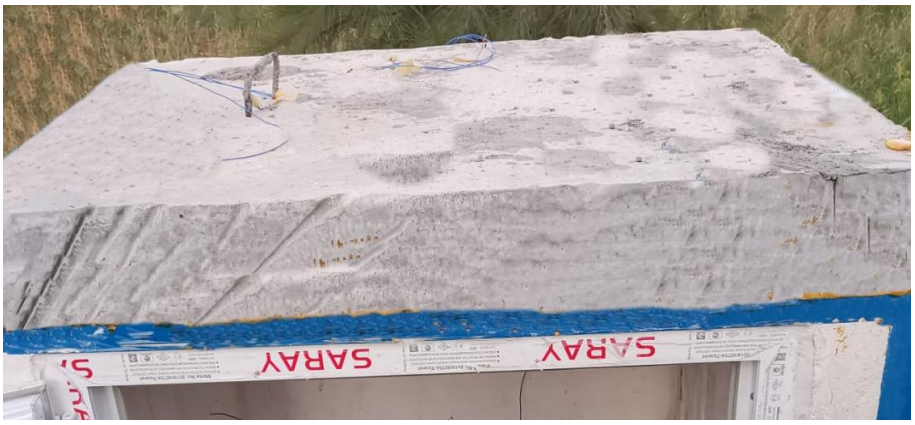

(b)

Figure 3.17. Concrete roof: (a) section showing the layers (14, 15 are thermocouples), (b) roof under construction.

Floor: The floor of the room was constructed from 40 mm layer of 'Loam', which is a soil composed mostly of sand, silt, and a smaller amount of clay, and ceramic piles with thickness of 9 mm as seen in Figure.18.

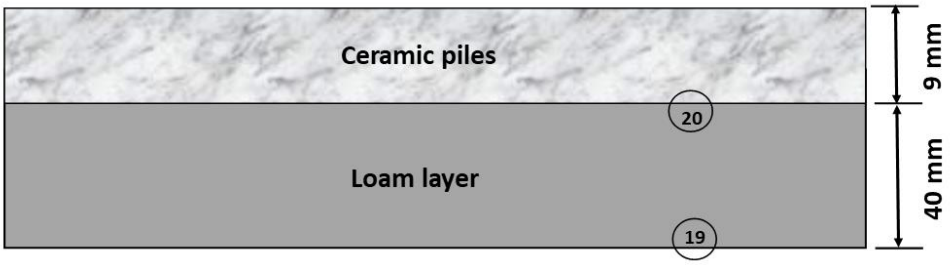

Figure 3.18. Section in the floor layers.

The model was constructed on the rotatable base as shown in Figure 3.19a. The three types of bricks/blocks were built on the base as in Figure 3.19b, and thermocouples were installed as in Figure 3.19c and 3.19d on each type of wall. The cement plastering was added to the outer side of walls and the gypsum plastering also added to the inner side of walls as in Figure 3.19e and 3.19f. The roof made of concrete poured into a cast then it was fixed on the room (Figure 3.19g, h), was added to the roof. The properties of the materials used to in the construction are all listed in Table 3.2.

(a)

(b)

(c)

(d)

(e)

(f)

(g)

(h)

Figure 3.19. Model Construction Steps.

Table 3.2. Thermophysical properties of walls and roof materials used in Iraq (Yang et al., 2014)

Building Materials	Thickness, t	Density, ρ	Thermal conductivity, k	Specific heat, c	Thermal diffusivity, α
	(mm)	(kg/m^3)	(W/m·K)	(kJ/kg·K)	·10^{-7} (m^2/s)
Cement Plastering layer	25	2020	0.99	0.840	5.83
Gypsum Plastering layer	20	1200	0.57	0.840	5.65
Hollow Brick	115	1100	0.5	0.840	5.41
Hollow concrete block	120	1440	0.72	0.840	5.95
Fired clay bricks layer	115	1200	0.54	0.840	5.36
Concrete roof	150	2300	1.49	0.880	7.50

3.5. Implementing RTS Method to Calculate the Heat Gains

3.5.1. Data collection

In the first stage of the RTS approach, all internal heat gains are calculated. The procedure is identical to that of the HBM. All gains that are not affected by temperatures of the surface of the area may thus be estimated and recorded as hourly values at the beginning of the simulation. These include gains from solar rays passing through the glass, infiltration (assuming a constant temperature in the tested space), and the internal heat gains, which are derived from the 24-hour schedule.

The interior dry bulb temperature and the sol-air temperature can be found by calculating the periodic response factors. The room ambient temperature and the sol-air temperature hourly data are known at the start of the computation. Calculating the conduction heat gains via each surface individually is the first stage. The next crucial step is to separate the gains into radiant and convective components. For each form of heat gain, this is accomplished using predetermined radiative and convective divides (Domínguez-Muñoz et al., 2010). To contribute to the load at the air node, all heat gains are converted into contributions in the second step of the RTS calculation process. The cooling load is instantaneously contributed to by the convective components of the gains, while the radiant time factors allow the heat gain part that came from the radiation to be transformed into cooling loads (RTF). The 24-hourly radiant heat gains and the RTF are used to assess the periodic (hourly) amounts of the radiative portion of the heat gain and convert it to cooling load. The radiant time factors, a zone dynamic response feature that depends on the zone's overall dynamic thermal storage characteristics, describe how the

radiant gain at one hour is dispersed over time to contribute to the cooling load at later hours. To calculate the hourly cooling load, the hourly convective gains are simply added to the contributions made by the past and present radiant gains. The RTS approach, in terms of processing the input data and procedures to determine the 24-hourly cooling loads, is detailed below, and Figure 3.20. depicts the calculation flowchart.

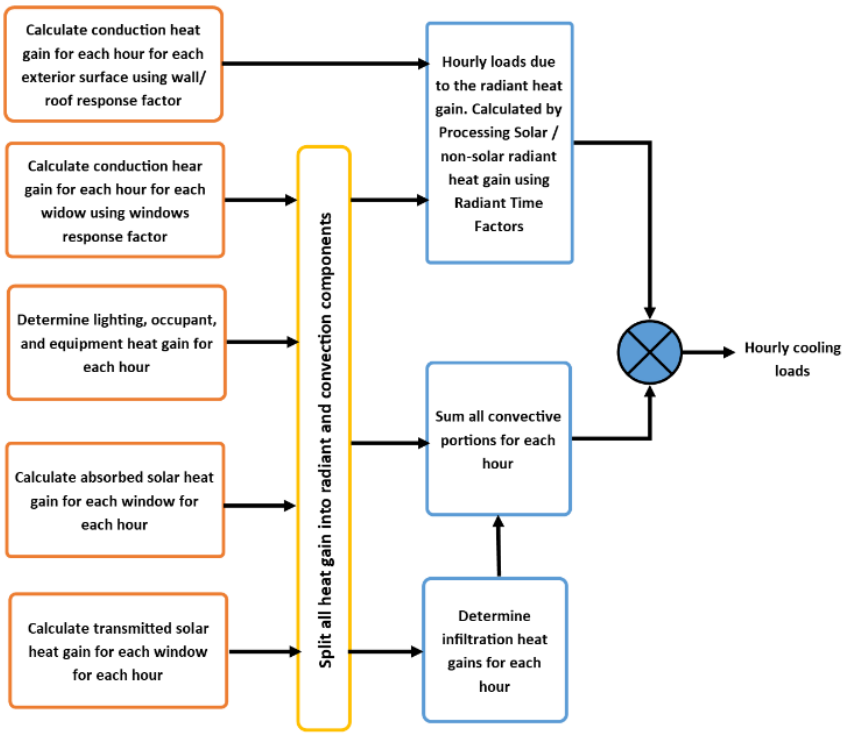

Figure 3.20. The flow diagram for the original RTSM cooling load calculation technique (Rees et al., 2000)

3.5.1.1. Sol-air temperature

The sol-air temperature concept was proposed as the temperature at which a surface is equal to a convective and radiative environment was proposed as T_{sa} (Olofsson et al., 2017). Solar radiation is included in this concept. T_{sa} is frequently represented as (Joudi & Hussien, 2015) state:

$$T_{san} = T_{on} + \frac{\mu}{h_o} I_{t-n} - \frac{\varepsilon \Delta R}{h_o} \quad 3.1$$

Where:

T_{san}: sol-air temperature for n time.

T_{on}: outdoor temperature for n time.

μ: absorberity.

h_o: outside heat transfer coefficient, W/m^{2}K.

$\varepsilon\Delta R$: discrepancy (at a given ambient temperature) between radiation (long-wave) that falls on the ground from the sky, and the radiation that a black body emits.

3.5.1.2. Conductive heat gains calculation

Twenty-four response variables are used to compute the conduction part of the heat gain for each kind of roofs and/or walls. The transient, one-dimensional conductive heat transfer issue has a time series solution provided by the response factor formulation. According to Equation 3.2., for each hour, θ, the conductive component of the heat gain for the surface, q_θ, is determined by adding the response factors and dividing the temperature difference over the surface (Spitler et al., 1997).

$$q_\theta = A\sum_{j=0}^{23} Y_{Pj}\left(t_{e,\theta-j\delta} - t_{rc}\right) \qquad 3.2$$

Where:

q_θ: hourly conductive heat gain, Btu/h (W), for the surface;

A: surface area, ft^2 (m^2);

Y_{Pj}: response factor;

$t_{e,\theta-j\delta}$: sol-air temperature, °F (°C), j hours ago; and

t_{rc}: presumed constant room air temperature, °F (°C).

3.5.1.3. Convective heat gains calculation

The radiative exchange that occurs among surfaces, partitions, furniture and other object in the studied space complicates the calculation of convective heat gains. Radiant heat transfer adds a time dependence to the process that is difficult to quantify. Heat balancing techniques use surface temperatures and emissivity to compute the radiant exchange between surfaces. Instead of simultaneously solving for the instantaneous convective and radiative heat transfer from each surface, the radiant time series procedure divides the conduction part of the heat gain into radiation and convection shares, along with the internal gains comes from the device, individuals, and illumination inside the space to simplify the heat balance procedure (Spitler et al., 1997).

The RTS approach states that after dividing every portion of heat gains into heat gains from radiation and convection, the heat gains may be transformed into cooling loads. The thermal mass in the zone absorbs the radiative component, which is subsequently transferred by convection into space. An impact of dampening and temporal lag is produced by this procedure. Contrarily, the convective part is expected to quickly become a cooling load, therefore calculating its contribution to the hourly cooling load merely requires adding it up. The next sections go through the process of converting the radiative component to cooling loads (Nigusse, 2007).

3.5.1.4. Changing the radiation heat gains to cooling loads

Using radiant time series coefficients, the radiant time series technique translates the radiant part of hourly heat gains to hourly cooling loads. Radiant time factors, like reaction factors, determine the cooling load for the current hour based on present and historical heat gains. An area's periodic response to a time-dependent radiation pulse can be represented by RTS. The series depict the fraction of radiant pulse/hour which is transferred towards the interior space by convection. Hence, r_0 denotes the proportion of the radiant pulse transferred (by convection) to the zone air in the current hour, r1 in the previous hour, etc. Using equation 3.2., the resulting radiant time series is utilized to convert the radiant part of hourly heat gains to hourly cooling loads (Spitler et al., 1997).

$$Q_\theta = r_0 q_\theta + r_1 q_{\theta-\delta} + r_2 q_{\theta-2\delta} + r_3 q_{\theta-3\delta} + \cdots + r_{23} q_{\theta-23\delta} \qquad 3.3$$

Q_θ = cooling load (Q) for the current hour (θ)
q_θ = heat gain for the current hour,
$q_{\theta-n\delta}$ = heat gain n hours ago, and
r_0, r_1, etc. = radiant time factors.

A thermal balance-based method is the most practical for generating radiant time factors. Various series of RTFs is needed for every particular area and radiant energy distribution function. For transmitted solar heat gain, one series of radiant time factors is used (radiant energy is considered to be interchanged solely to the floor), and for all other forms of heat gains, a second series is used (radiant energy is assumed to be spread evenly across all inside surfaces). The process for producing radiant time factors is covered in the section titled "Implementing the RTS Technique." The cooling loads may all be estimated directly at this point in the analysis since the heat gains are all known, hence there is no requirement for an iterative solution for the cooling loads (Rees et al., 2000).

3.5.1.5. Wall and roof response factor generation procedure

To calculate conductive heat gain for walls and roofs using the above-described approach, it is needed to find a set of response factors for each wall and roof used in the building of interest. The response factors may be generated in a variety of methods; the approach presented employs a traditional approach (Hittle & Bishop, 1983) to compute a set of one hundred and twenty response factors per each pulse. A group of response factors per pulse could lessened to a group of twenty-four response factors adequate to constant hourly input. They will be referred to as periodic response factors.

The initial step to develop the PRFs of heat gain's conductive portion is the representation of the classic response factor across the tested wall (Spitler et al., 1997):

$$q''_{\theta} = -\sum_{j=0}^{n} Z_j T_{i,t-j\delta} + \sum_{j=0}^{n} Y_j T_{o,t-j\delta} \qquad 3.4$$

Where:

q''_{θ}: heat flux at the inside surface of the wall at the current hour,

n: large number dependent on the construction of the wall,

Z_j, Y_j : response factors,

$T_{i,t-j\delta}$: inside surface temperature j hour's ago, and

$T_{o,t-j\delta}$: outside surface temperature j hours ago.

Rearranging the summations in the manner described below is useful if the boundary conditions are stable periodic throughout 24 hours:

$$\begin{aligned} q_{\theta}^{N} = &-\sum_{j=0}^{23} Z_j T_{i,t-j\delta} + \sum_{j=0}^{23} Y_j T_{o,t-j\delta} \\ &-\sum_{47}^{63} Z_j T_{i,t-j\delta} + \sum_{j=24} Y_j T_{o,t-j\delta} \\ &-\sum_{j=48} Z_j T_{i,t-j\delta} + \sum_{j=48} Y_j T_{o,t-j\delta} + \cdots \end{aligned} \qquad 3.5$$

If the first term of the Z summations is isolated from the remainder, the following results are obtained:

$$q''_\theta = -Z_0 T_{i,t} - \sum_{j=1} Z_j T_{i,t-j\delta} + \sum_{j=0}^{23} Y_j T_{o,t-j\delta} - Z_{24} T_{i,t-24} - \sum_{j=25}^{47} Z_j T_{i,t-j\delta} + \sum_{j=24}^{47} Y_j T_{o,t-j\delta} - Z_{48} T_{i,t-48} + \sum_{j=49}^{63} Z_j T_{i,t-j\delta} + \sum_{j=48}^{63} Y_j T_{o,t-j\delta} + \cdots \quad 3.6$$

With a constant periodic forcing function, $T_{i,t}$, $T_{i,t-24}$, $T_{i,t-48}$, etc. are all identical. Combining the coefficients of these temperatures yields a new set of periodic response factors (Z_{pj} and Y_{pj}):

$$Y_{P1} = Y_0 + Y_{24} + Y_{48} + \cdots \quad 3.7$$

Similarly,

$$Y_{P2} = Y_0 + Y_{25} + Y_{49} + \cdots \quad 3.8$$

and so on.

As a result, the normally high number of response factors may be replaced by 24 periodic response factors for the exceptional case of a stable periodic forcing function, and the heat flow can be written in terms of periodic response factors as:

$$q''_\theta = -\sum_{j=0}^{23} Z_{Pj} T_{i,t-j\delta} + \sum_{j=0}^{23} Y_{Pj} T_{o,t-j\delta} \quad 3.9$$

Depending on the temperature by which they are multiplied, the wall heat gain coefficients are referred to as either inside coefficients (z) or cross-coefficients (y).

Equation 3.9 may be simplified as follows the interior temperature is considered to remain constant when computing design loads and the total of the Y_{Pj} coefficients equal the sum of the Z_{Pj} coefficients:

$$q''_\theta = \sum_{j=0}^{23} Y_{Pj}\left(t_{e,\theta-j\delta} - t_{rc}\right) \quad 3.10$$

3.5.2. Applying RTS method

Before employing the RTS technique, compute two sets of response factors (walls and roofs), two sets of radiant time factors (internal loads and solar), sol-air temperatures, and solar heat gains. The information provided in the next section guides the computational process, and we discuss the assumptions and improvements of the procedure here.

The computational process of producing wall and roof response factors that was discussed above can be summarized as below:

1- Determine conductive heat gains per hour using response variables: Equation 3.2. is employed to determine the hourly conductive heat gains for each exterior wall and roof. To achieve this, the algorithm utilizes response factors for the wall and roof, together with hourly sol-air temperatures, as illustrated in the following pseudo-code in Figure 3.21.
2- Divide the total wall heat gain into convective and radiative components: The response factor for the conductive heat gain for each hour is calculated by multiplying it by the appropriate sol-air zone temperature difference. By adding the fractional heat gains, the surface's total hourly heat gain is calculated. Radiative and convective components make up the entire conductive heat gain. The Radiant Time Series method integrates the radiative portion of conductive heat gain alongside internal heat gains, transforming this information into hourly cooling loads. The cooling load is increased by the convective component.
3- Determine the hourly solar heat gains using the accepted ASHRAE method.
4- Divide the radiative and convective components of the hourly internal heat gains.

Per every external wall

Per each hour within a 24-hour period

For every one of the 24 wall response variables,

Determine the fractional heat gains

= the wall area x the response factor x (sol-air temperature - the zone temperature)

Calculate the subsequent Response Factor using the past Sol-air Temperature.

Combine all fractional heat gains to get the hourly heat gain for this wall.

Combine all heat gains from the walls to calculate the overall heat gain from this walls.

Figure 3.21. Pseudo-Code for Determine Conductive Heat Gains per hour using response variables.

5- Using radiant time factors, convert the radiative fraction of internal heat gains to hourly cooling loads.

6- Use radiant time factors to translate solar heat gains to hourly cooling demands. Equation 3.2 describes how heat gains are converted into cooling loads. The following pseudo-code (Figure 3.22.) displays the fractional cooling load for each hour by multiplying each of the 24 radiant time factors by the appropriate hourly solar heat gain. A total hourly cooling load due to solar heat gains is calculated by adding the fractional cooling loads.

7- Combine the convective component of internal and conductive heat increases with the hourly cooling load from radiative and solar heat gains.

Per each hour within a 24-hour period

For each one of the 24 Radiant Time Factors

Compute the fractional cooling load by multiplying the Solar Radiant Time Factor with the Hourly Solar Heat Gain.

The next Radiant Time Factor with past solar heat gain.

Combine all fractional cooling load to get the hourly cooling load resulting from internal heat gains and the radiative component of conduction.

Figure 3.22. Pseudo-Code of Converting Heat gains to cooling loads.

In a similar way the coefficients of the interior heat gain, which are represented by the radiant time series, affect both the radiant and conductive components of heat gains, as well as the diffuse portion of the solar heat gain. various coefficients are used to calculate the hourly fractional cooling loads from various sources (Figure 3.23.).

Per each hour within a 24-hour period

For each one of the 24 Radiant Time Factors

Compute the fractional cooling load.

Radiant Time Factor= the radiant component of the internal and conductive heat gains + solar heat gain that is spread out or diffused

Calculate the subsequent Radiant Time Factor by considering the prior heat gain.

Combine all fractional cooling load to get cooling load per hour resulting from internal heat gains and the radiative part of conduction.

Figure 3.23. Pseudo code of generating hourly fractional cooling loads.

T The last stage of the process involves adding up all the convective components of the hourly heat gains and transforming the radiative components using the radiant time series into hourly cooling loads, as seen in Figure 3.24.

Per each hour within a 24-hour period

Calculate the total of all contributions to the cooling load

= Heat gain generated by convection inside a system

+ The convective component of conductive heat gains.

+ solar heat gains transformed to cooling load.

+ Internal; diffusive, conductive and radiative.

Conversion of solar heat gains into cooling load.

Combine the fractional cooling load to get the hourly cooling load resulting from internal heat gains and the radiative component of conduction. the fractional cooling load to get the hourly cooling load resulting from internal heat gains and the radiative component of conduction.

Figure 3.24. Pseudo Code for Summing all Portions.

3.5.3. RTS method MATLAB code modelling

The Radiant Time Series (RTS) method is a widely-used approach for calculating cooling loads in buildings, which involves analysing the heat transfer through building elements over time to determine the total cooling load required to maintain a comfortable indoor temperature. While the RTS method can be implemented using manual calculations or spreadsheet tools, the use of a programming language such as MATLAB can provide a more efficient and flexible solution. Several studies have employed MATLAB to implement the RTS method and analyse building cooling loads. For instance, in a study by Mendes (Mendes et al., 2003), the authors developed a MATLAB program to calculate the cooling loads of a residential building in different climate zones, taking into account the effect of shading devices and ventilation systems. The program was found to provide accurate and efficient results and was used to optimize the design of the building's cooling system. Similarly, in a study by Xie et al. (2020, the authors used MATLAB to develop a numerical model for simulating the thermal performance of a building under different environmental conditions. The model was based on the RTS method and incorporated various building components, such as walls, roofs, and windows. The authors demonstrated the effectiveness of the model in predicting the

cooling load of the building and optimizing the performance of the cooling system. The use of MATLAB to implement the RTS method offers several advantages, such as the ability to easily modify and extend the code, and the availability of built-in functions and toolboxes for numerical simulation and optimization. MATLAB's powerful computing capabilities can also enable faster and more accurate analysis of building cooling loads.

In conclusion, the use of MATLAB to implement the RTS method provides a powerful and flexible tool for designers and engineers to accurately calculate cooling loads, optimize energy efficiency, and improve indoor comfort. Appendix A shows the MATLAB code used in this work based on the above pseudo codes.

3.6. ASHRAE RTS Procedure Spreadsheet

The spreadsheet that calculates cooling loads for a zone using the ASHRAE RTS (Radiant Time Series) Procedure is a valuable design and energy analysis instrument for buildings. The RTS Procedure was developed by the American Society of Heating, Refrigerating, and Air-Conditioning Engineers (ASHRAE) to provide a comprehensive procedure for calculating building cooling loads. Using this method, the spreadsheet precisely estimates the cooling requirements of a particular zone within a building. The spreadsheet created for calculating cooling loads using the ASHRAE RTS Procedure is a user-friendly and efficient tool that simplifies the complex calculations required to determine cooling loads. It incorporates the key ASHRAE principles and methodologies, allowing engineers, architects, and energy analysts to accurately assess the cooling requirements of a zone.

Typically, the spreadsheet includes several input fields where users can enter parameters such as zone dimensions, building orientation, window properties, occupancy schedules, internal heat gains, ventilation rates, and weather data as shown in Figure 3.25. These inputs provide the information necessary to evaluate the cooling load for the zone in question, where the needed inputs are highlighted in yellow

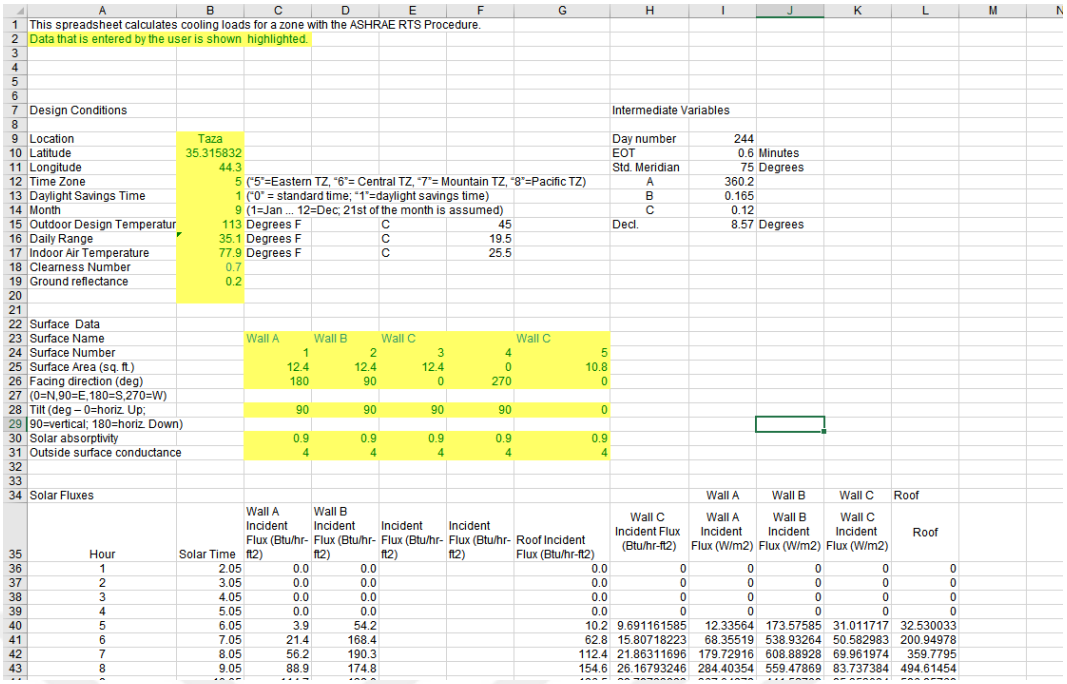

This spreadsheet calculates cooling loads for a zone with the ASHRAE RTS Procedure.
Data that is entered by the user is shown highlighted.

Design Conditions							Intermediate Variables		
Location	Taza						Day number	244	
Latitude	35.315832						EOT	0.6	Minutes
Longitude	44.3						Std. Meridian	75	Degrees
Time Zone	5	("5"=Eastern TZ, "6"= Central TZ, "7"= Mountain TZ, "8"=Pacific TZ)					A	360.2	
Daylight Savings Time	1	("0" = standard time; "1"=daylight savings time)					B	0.165	
Month	9	(1=Jan ... 12=Dec; 21st of the month is assumed)					C	0.12	
Outdoor Design Temperatur	113	Degrees F		C	45		Decl.	8.57	Degrees
Daily Range	35.1	Degrees F		C	19.5				
Indoor Air Temperature	77.9	Degrees F		C	25.5				
Clearness Number	0.7								
Ground reflectance	0.2								

Surface Data						
Surface Name		Wall A	Wall B	Wall C		Wall C
Surface Number		1	2	3	4	5
Surface Area (sq. ft.)		12.4	12.4	12.4	0	10.8
Facing direction (deg)		180	90	0	270	0
(0=N,90=E,180=S,270=W)						
Tilt (deg – 0=horiz. Up;		90	90	90	90	0
90=vertical; 180=horiz. Down)						
Solar absorptivity		0.9	0.9	0.9	0.9	0.9
Outside surface conductance		4	4	4	4	4

Solar Fluxes								Wall A	Wall B	Wall C	Roof
Hour	Solar Time	Wall A Incident Flux (Btu/hr-ft2)	Wall B Incident Flux (Btu/hr-ft2)	Incident Flux (Btu/hr-ft2)	Incident Flux (Btu/hr-ft2)	Roof Incident Flux (Btu/hr-ft2)	Wall C Incident Flux (Btu/hr-ft2)	Wall A Incident Flux (W/m2)	Wall B Incident Flux (W/m2)	Wall C Incident Flux (W/m2)	Roof
1	2.05	0.0	0.0			0.0	0	0	0	0	0
2	3.05	0.0	0.0			0.0	0	0	0	0	0
3	4.05	0.0	0.0			0.0	0	0	0	0	0
4	5.05	0.0	0.0			0.0	0	0	0	0	0
5	6.05	3.9	54.2			10.2	9.691161585	12.33564	173.57585	31.011717	32.530033
6	7.05	21.4	168.4			62.8	15.80718223	68.35519	538.93264	50.582983	200.94978
7	8.05	56.2	190.3			112.4	21.86311696	179.72916	608.88928	69.961974	359.7795
8	9.05	88.9	174.8			154.6	26.16793246	284.40354	559.47869	83.737384	494.61454

Figure 3.25. ASHRAE RTS Procedure Spreadsheet (Spitler et al., 1997).

Once the inputs are provided, the spreadsheet uses the ASHRAE RTS Procedure to calculate the cooling load, taking into account radiant heat transfer, convective heat transfer, and solar heat gains. To create a comprehensive analysis, the procedure incorporates factors such as the thermal properties of building materials, solar radiation, internal heat sources, and thermal storage effects. More snaps from the sheet are presented in Appendix B.

The spreadsheet generates outputs that include cooling load profiles for different time intervals (e.g., hourly, and daily), peak cooling load values, and total cooling load values based on the inputs and calculations. These outputs facilitate the design of suitable cooling systems, the selection of equipment capacities, and the optimization of the zone's energy efficiency. Using the ASHRAE RTS Procedure spreadsheet streamlines the cooling load calculation process, eliminates human error, and yields consistent and reliable results. It is a valuable resource for professionals involved in building design, energy analysis, and HVAC system sizing, allowing them to make well-informed decisions that create comfortable and energy-efficient indoor environments.

4. RESULTS AND DISCUSSION

This section provides a comprehensive analysis of the data collected during the experiment, including the various parameters and factors that affect the cooling load. The results are presented clearly and concisely to facilitate the understanding of the effectiveness of the different types of multilayered walls and flat roofs in reducing cooling loads. The section concludes with a discussion of the implications of the findings and their potential applications in building design and construction.

The findings of this study were analysed through two distinct approaches. The first approach involved utilizing the ASHRAE RTS Procedure spreadsheet, as outlined in reference (Spitler et al., 1997). The second approach, on the other hand, was developed through the implementation of MATLAB code, as introduced in this study.

4.1. Results of ASHRAE RTS Procedure Spreadsheet

The Radiant Time Series Method has been implemented in this spreadsheet for a basic building, with modifications made to the model room for the purposes of this study. The periodic response factors (PRF) and radiant time factors (RTF) for walls were ascertained utilizing the PRF-RTF Generator, which is available for download at no cost from the website of the OSU Building and Environmental Thermal Systems Research Group. The data from Table 3.1 were used as input for this software to get PRF and RTF as shown in Figure 4.1. In Appendix C, more steps are shown to clarify how the interface works and where the layers' specification are entered.

By following the aforementioned methodology, a collection of 24 periodic response factors and radiant time factors was generated, as depicted in Figure 4.2.

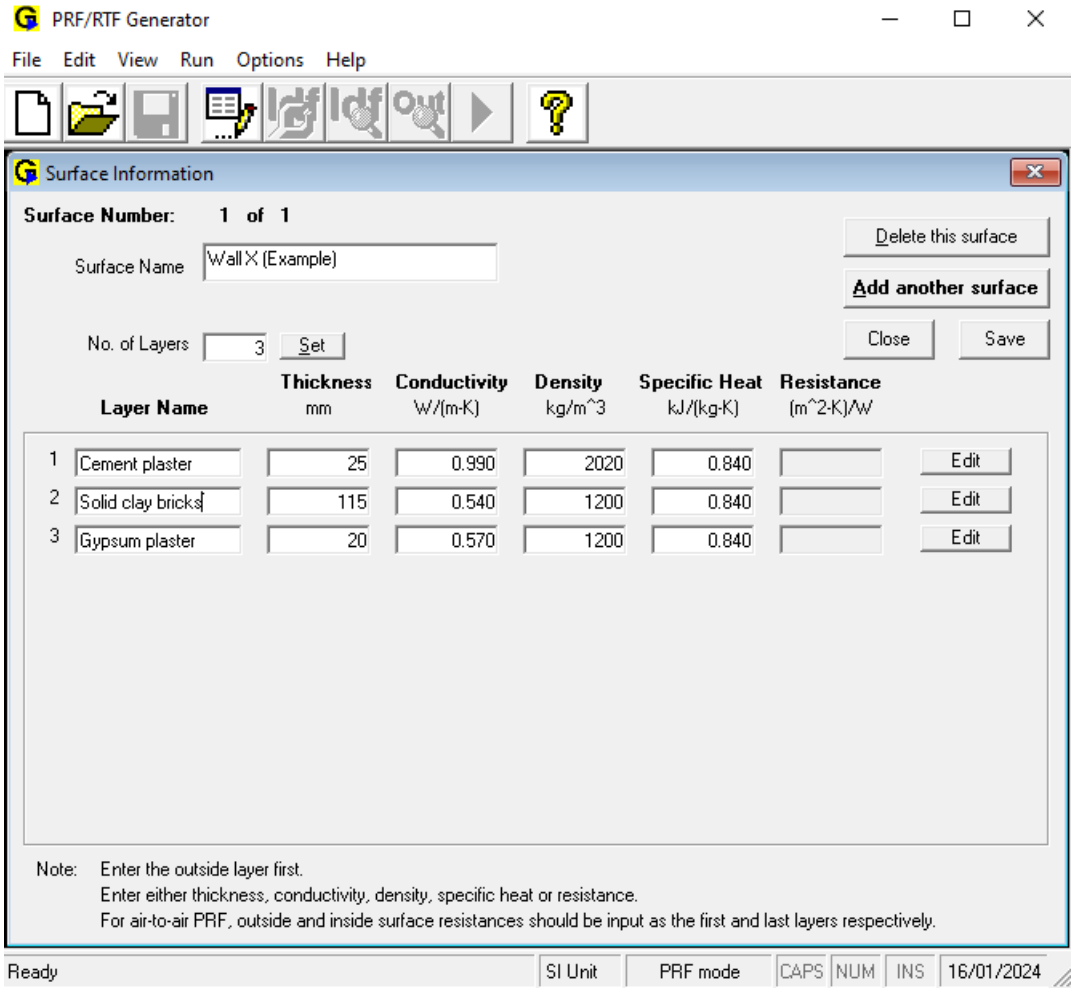

Figure 4.1. Program interface to generate PRF/RTFs.

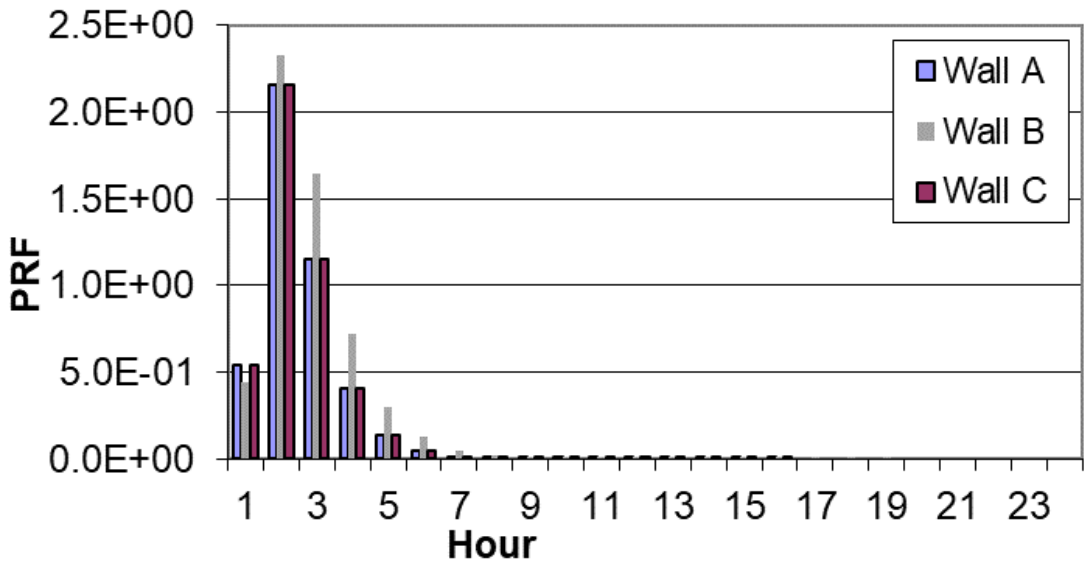

Figure 4.2. Periodic Response Factors.

4.1.1. Incident solar flux

The objective of this investigation was to assess and quantify the solar flux incident on diverse room walls, Wall A, Wall B, and Wall C. The solar flux incident quantified in W/m^2 offers significant insights into the quantity of solar radiation that directly affects the walls' surfaces. Through an analysis of the solar flux data, valuable information can be obtained regarding the building's solar heat gain and the associated cooling load. The aforementioned findings were obtained through the utilization of the ASHRAE RTS Procedure spreadsheet.

The solar flux values for each hour of the day, along with the corresponding solar time, are presented in Figure 4.3. The incident flux values in W/m^2 units have been furnished for Wall A, Wall B, Wall C, and the roof. The findings offer a comprehensive comprehension of the solar radiation exposure encountered by each wall over the course of the day.

Based on the findings, The incident flux for Wall A remains at 0 W/m^2 during the range 01:00-04:00 and 16:00-12:00. From hour 5 onwards, it starts to receive solar radiation, with the flux gradually increasing until it reaches a peak of 436 W/m^2 at hour 11. After hour 11, the incident flux gradually decreases, reaching 0 W/m^2 again by hour 17. This pattern indicates that Wall A receives significant solar radiation during the day, peaking around midday.

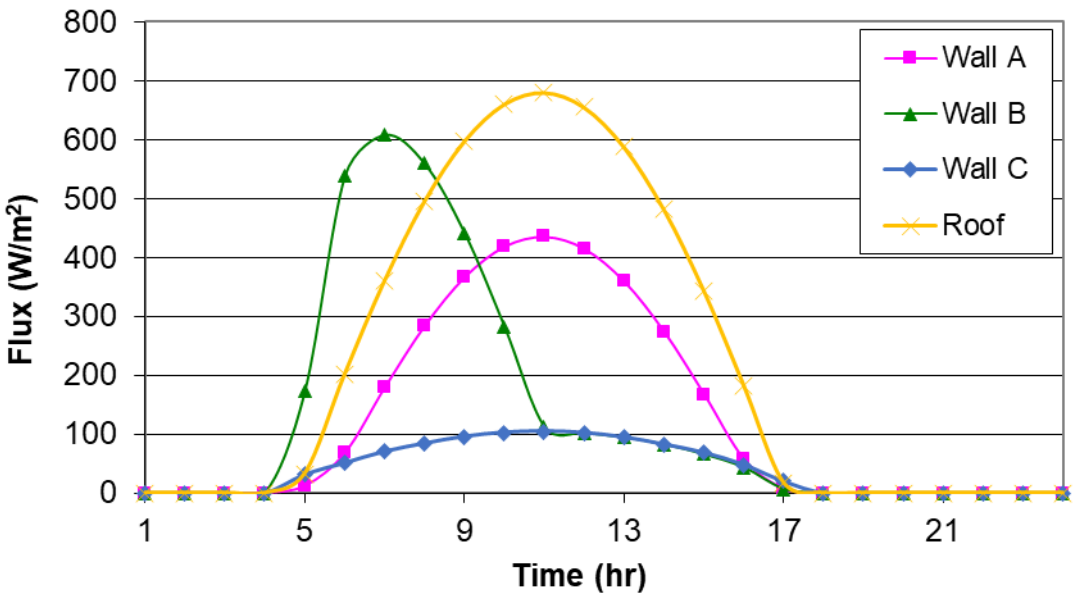

Figure 4.3. Incident Solar Irradiation.

Similar to Wall A, the incident flux for Wall B remains at 0 W/m² during the same range. However, it experiences a more substantial increase in flux starting at hour 5, reaching a peak of 609 W/m² at hour 7. Afterward, the incident flux decreases, but it remains relatively higher compared to Wall A, reaching 0 W/m² by hour 17. This indicates that Wall B receives even higher solar radiation throughout the day compared to Wall A since Wall B is facing the east direction.

The incident flux for Wall C follows a similar pattern to Wall A and Wall B. It starts at 0 W/m² during the same range, and from hour 5 onwards, it gradually increases. The flux peaks at 105 W/m² at hour 11 and then decreases, reaching 0 W/m² by hour 17. The incident flux for Wall C is generally lower than Wall B but higher than Wall A, indicating moderate solar radiation exposure.

The incident flux for the roof starts to increase from hour 5, reaching a peak of 680 W/m² at hour 11. Afterward, the incident flux gradually decreases, reaching 0 W/m² by hour 17. The roof receives significant solar radiation throughout the day, reflecting its exposure to direct sunlight.

The following deductions are concluded based on the analysis of the incident solar flux throughout the day using a comparative evaluation of the outcomes of Wall A, Wall B, and Wall C:

- Wall B receives the highest incident flux among all surfaces, indicating its higher exposure to direct sunlight.
- Wall A and Wall C receive moderate levels of incident flux, suggesting they have comparable solar radiation exposure.
- The incident flux for the roof is the highest, indicating that it also receives significant solar radiation.
- The magnitude of incident solar flux was evaluated among three walls, and it was found that Wall B consistently received the highest values of incident solar flux throughout the day since it was facing the east (sunrise). The findings suggest that Wall B is subject to a higher degree of solar radiation and consequent thermal absorption in contrast to Wall A and Wall C.
- Variation in Solar Flux: While all three walls exhibit a similar trend of increasing incident solar flux during the morning hours, Wall C experiences the least variation in solar flux. Its values remain relatively lower throughout the day compared to Wall A and Wall B. On the other hand, Wall B exhibits the highest variation in solar flux,

with significantly higher values during peak hours and a steeper decline towards the evening.

- Time of Peak Solar Flux: The peak incident solar flux occurs at different hours for each wall. Wall A reaches its highest value (435 W/m^2) at hour 11, while Wall B reaches its peak (609 W/m^2) at hour 7. Wall C, with the lowest incident solar flux, reaches its peak (104 W/m^2) at hour 11. The observed dissimilarities imply variances in the positioning and level of solar irradiation on the walls.

4.1.2. Air temperature and sol-air temperatures

Based on the ASHRAE RTS Procedure spreadsheet the sol-air temperatures for each wall were conducted using the air temperature of the day. Figure 4.4. illustrates the results of the sol-air temperatures. Upon analysing the results of the sol-air temperature, the following observations can be made:

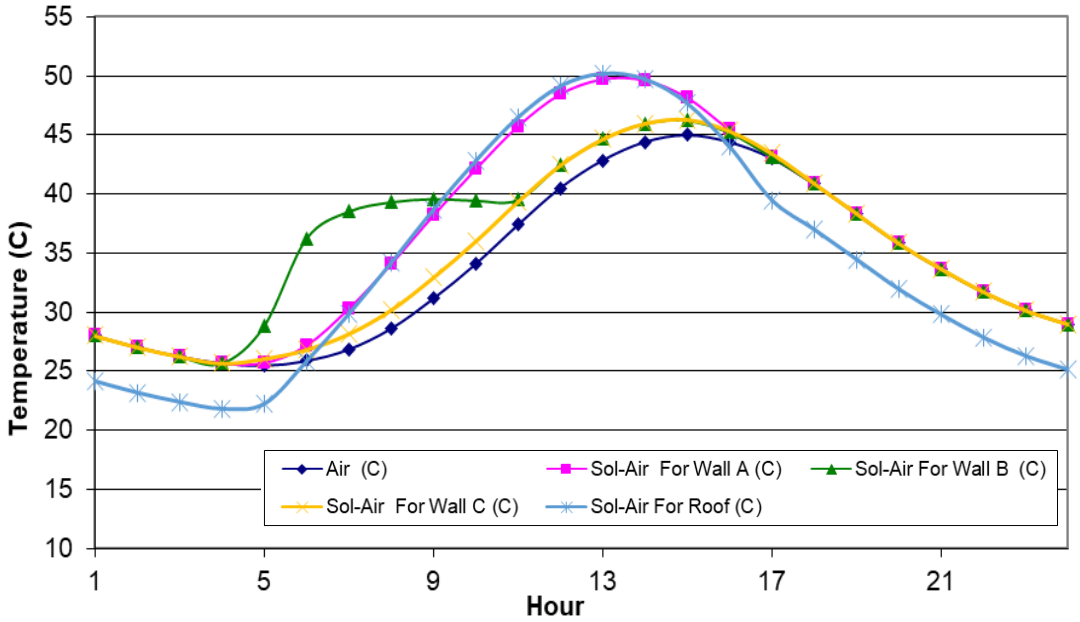

Figure 4.4. Air and Sol-Air Temperatures.

- Wall A exhibits a stable sol-air temperature throughout the diurnal cycle, with values ranging from 26°C to 50°C. The temperature initiates at 28°C and progressively ascends until it culminates at hour 12, attaining a value of 57°C. Subsequently, there is a gradual decrease in temperature to 29°C at the end of the 24th hour. Based on the observed temperatures, it can be inferred that Wall A undergoes a process of diurnal thermal cycling, whereby it absorbs thermal energy

from the surrounding environment during the daytime and subsequently dissipates it throughout the night.

- The sol-air temperature for Wall B exhibits a comparable trend to that of Wall A, fluctuating between 26°C and 48°C. Nevertheless, there is a discernible peak at the ninth hour, reaching 39°C, and it sustains a comparatively elevated level until the fourteenth hour. Subsequently, there is a gradual decline in temperature, ultimately attaining a value of 29°C at the 24th hour. The observed fluctuations suggest that Wall B exhibits a higher capacity for heat absorption during specific time intervals, plausibly attributable to its particular orientation or solar radiation exposure.
- The sol-air temperature for Wall C exhibits a relatively stable pattern, fluctuating within the range of 26°C to 48°C. The temperature commences at 28°C and progressively ascends until it culminates at hour 14, attaining a maximum value of 48°C. Subsequently, the temperature is sustained at this level until the 19th hour, following which it gradually diminishes to 29°C by the 24th hour. The temperature pattern of sol-air for Wall C exhibits a resemblance to that of Wall A, indicating a parallel thermal performance.
- The temperature of the roof's sol-air varies between 22°C and 50.5°C. The initial temperature of the system was recorded at 24°C, which then exhibited a gradual rise over time until it reached its maximum value of 50.5°C at the 12th hour. The temperature of the roof exhibits greater variability in comparison to that of the walls, which can be attributed to its direct exposure to solar radiation. The temperature exhibits a gradual decline post the 12th hour, ultimately stabilizing at 25°C at the 24th hour.
- Upon comparing the sol-air temperatures of walls A, B, and C, it can be observed that they demonstrate analogous patterns and magnitudes, thereby suggesting a comparable thermal performance. Throughout the day, it can be observed that the sol-air temperatures of the walls are comparatively higher than the sol-air temperature of the roof, indicating a greater absorption of heat by the walls from the surrounding environment.
- In conclusion, the sol-air temperature results provide insights into the heat absorption and release patterns of the walls and roof.

4.1.3. Conduction heat gains

The most valuable results of the ASHRAE RTS Procedure spreadsheet are the conduction heat gain results (Figure 4.5.), which give a great picture and comparison between the multi-layer walls. Analysing the conduction heat gain (W) results for wall A, wall B, and wall C at each hour of the day, we can observe the following overview, comparisons, and conclusions:

- Wall A: The conduction heat gain values for Wall A are relatively consistent throughout the day, ranging from 5 to 102 W. Hour 15 exhibits the maximum heat gain, while hour 6 demonstrates the minimum. The data suggest that wall A makes a substantial contribution to the total heat gain of the room, particularly during daylight hours.
- Wall B: The conduction heat gain values for wall B exhibit a similar pattern to wall A, ranging from 3 to 102 W. Hour 17 exhibits the maximum heat gain, while hour 5 demonstrates the minimum. Wall B experiences moderate heat gain, indicating that it is relatively well-insulated but still conducts some heat from the outside to the inside.

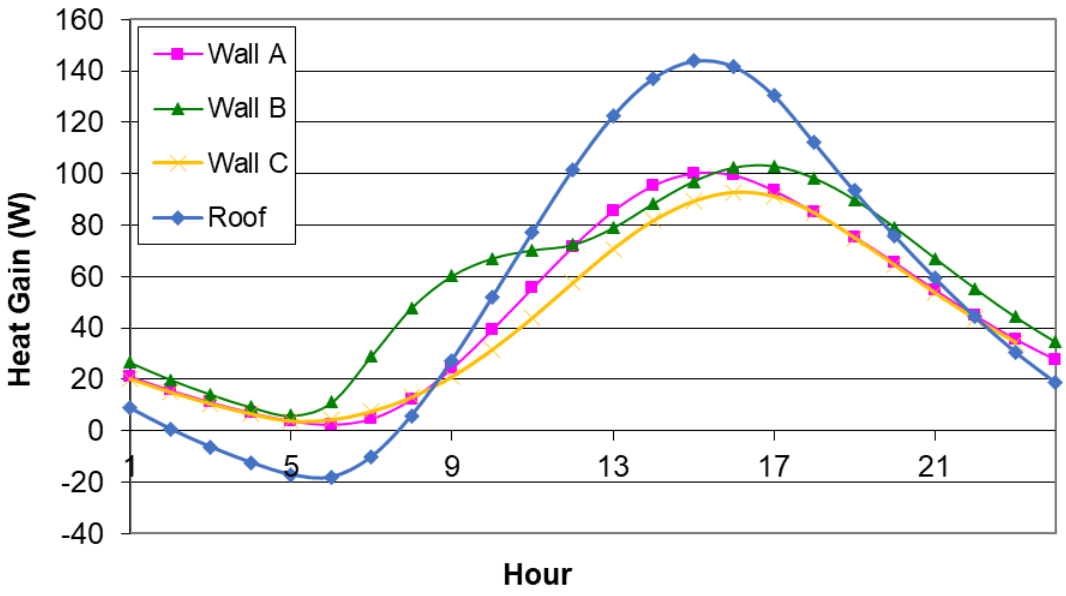

Figure 4.5. Conduction Heat Gains

- Wall C: The heat gain values for wall C exhibit similarities with those of walls A and B, with a range of 3 to 93 W. The highest heat gain occurs at hour 16, and the

lowest is at hour 5. Similar to walls A and B, wall C significantly contributes to the least heat gain. The values are lower compared to wall A and wall B.

- Roof: The conduction heat gain values for the roof show a different pattern compared to the walls. The values range from -18 to 143 W. Negative values indicate a heat loss from the room through the roof. The highest heat gain occurs at hour 15, while the highest heat loss occurs at hour 6. The roof's heat gain/loss is generally higher compared to the walls.
- The negative conduction heat gain values for the roof during certain hours indicate that the roof acts as a heat sink, absorbing excess heat from the room and dissipating it to the surroundings.
- The findings regarding conduction heat gain emphasize the importance of wall components (A, B, and C) in their contribution to the total heat gain within the enclosed space. To sum up, these results demonstrate the significance of these wall elements in the overall thermal performance of the room. In contrast, the roof exhibits distinct heat transfer characteristics, serving as a dual-purpose element that can either facilitate heat gain or heat loss contingent upon the diurnal cycle.

4.1.4. Window solar heat gain

SHRAE RTS Procedure spreadsheet also calculates the room window solar heat gain as shown in Figure 4.6. with transmitted and absorbed heat gain based on the type, direction, and dimensions of the window. It is obvious that the transmitted heat gain reached the maximum value of 277 W at hour 11, while the absorbed heat gain reached the maximum value of 6 W at the same hour.

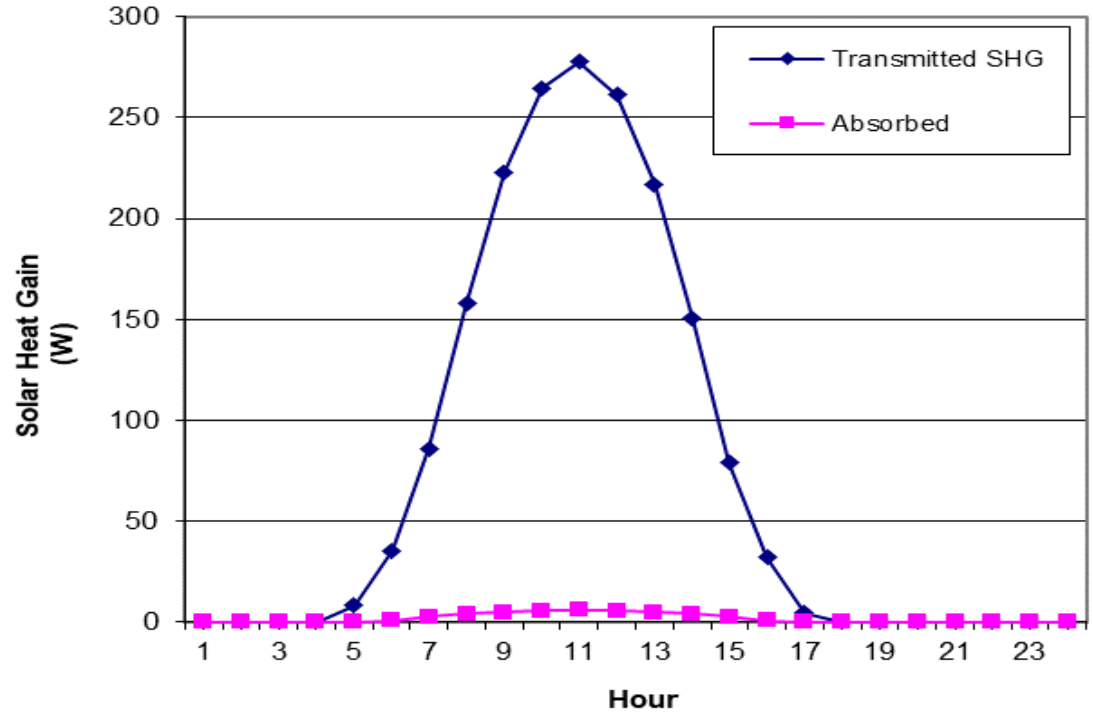

Figure 4.6. Solar Heat Gain

4.2. Results of the Developed MATLAB Code

Using MATLAB, a code was developed to measure the heat gain for each of the three types of walls with multiple layers using the RTS method. The purpose of this study is to compare any types of wall materials that have a higher thermal insulation capacity and require less cooling load, thus achieving the objective of this investigation. The general equation for heat gain through a multilayered wall using the radiant time series method is:

$$Q = \sum(Fij * \Delta Tij * A) \qquad 4.1$$

where: Q = total heat gain Fij = radiant heat transfer coefficient between layers i and j ΔTij = temperature difference between layers i and j A = area of the wall

This equation calculates the radiant heat flux at each interface between the wall layers by multiplying the radiant heat transfer coefficient (Fij) by the temperature difference (ΔTij) between the two adjacent layers. The total heat gain is then obtained by summing up the radiant heat flux across all interfaces.

Wall A: The results of sol-air temperature for wall A are presented in Figure 4.7., where the results starting in first hour at almost 32 °C, then a slight decrease for the range (01:00-06:00) till reach near 30 °C. the values starting to increase till reach the maximum at hour (13:00), then the values decrease gradually.

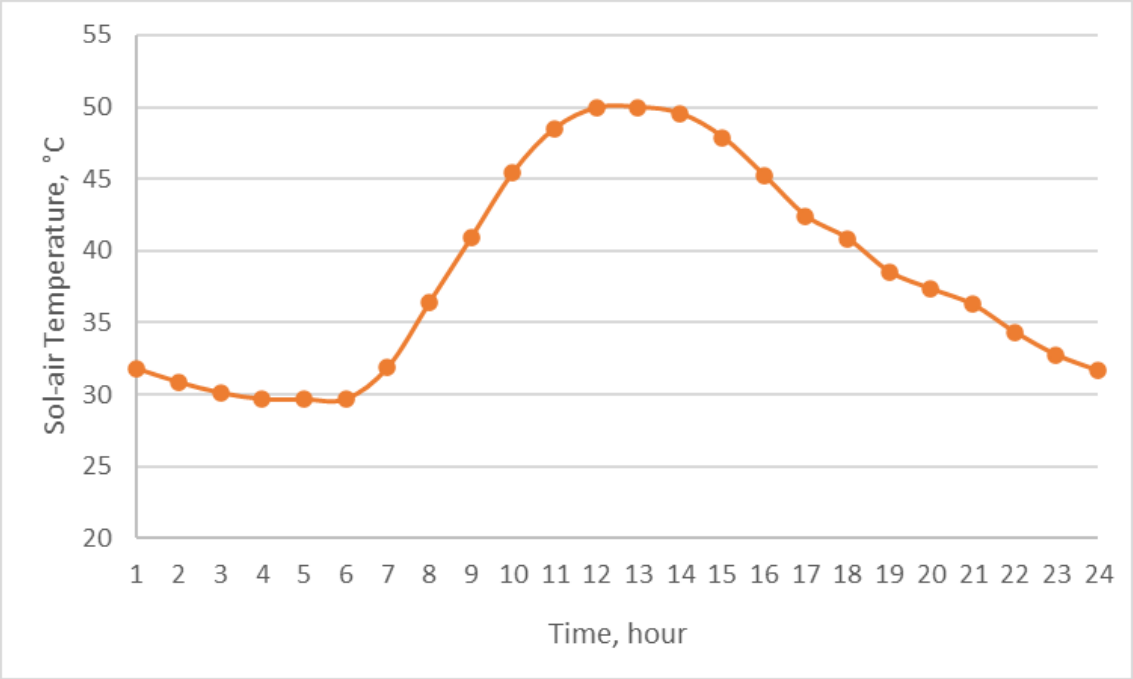

Figure 4.7. Sol-air Temperature Results for Wall A.

Figure 4.8. shows the results of the heat gain for each layer of wall A. The given heat gain results represent the heat gain/loss the three layers of wall A over 24 hours.

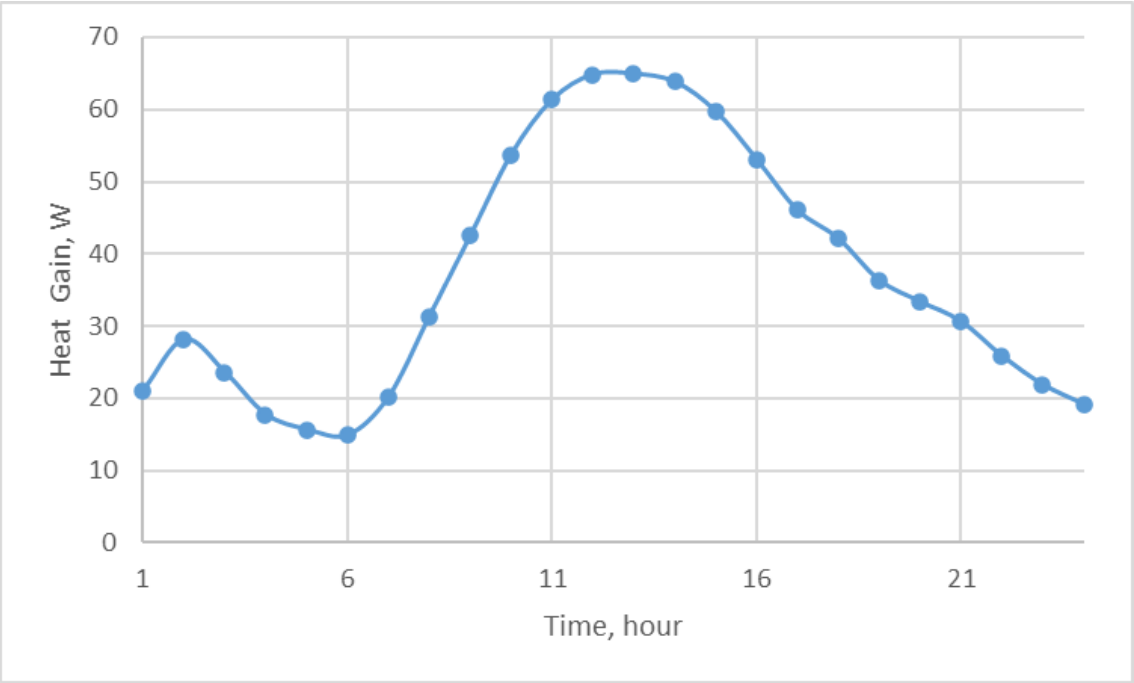

Figure 4.8. Heat gain results for wall A layers.

The values are starting at 20 W, then a slide increase in the first hour, and after that the heat gain are decrease during the range (2:00 - 6:00), where the indoor temperature was higher than the outdoor. The values then continue to increase, with a sharp rise around the midpoint of the measurements, before gradually decreasing again towards the end.

Wall B: Sol-air temperature results are shown in Figure 4.9., where at about 32 °C the starting value, then a slight decrease for the range (01:00-04:00). An increase in the temperature for range (04:00-08:00), then another slight decrease for the range (08:00-11:00) followed by slight increase for the range (11:00-15:00) where reaching the maximum value (45 °C). the gradually decrease starting till the last day hour.

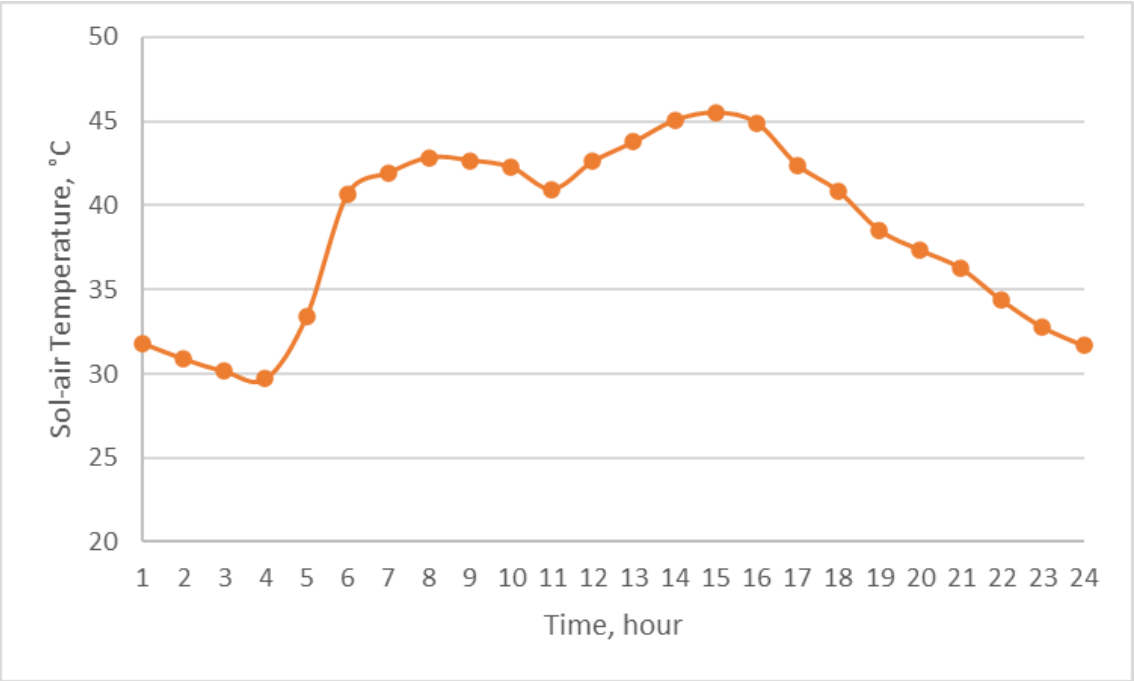

Figure 4.9. Sol-air Temperature Results for Wall B.

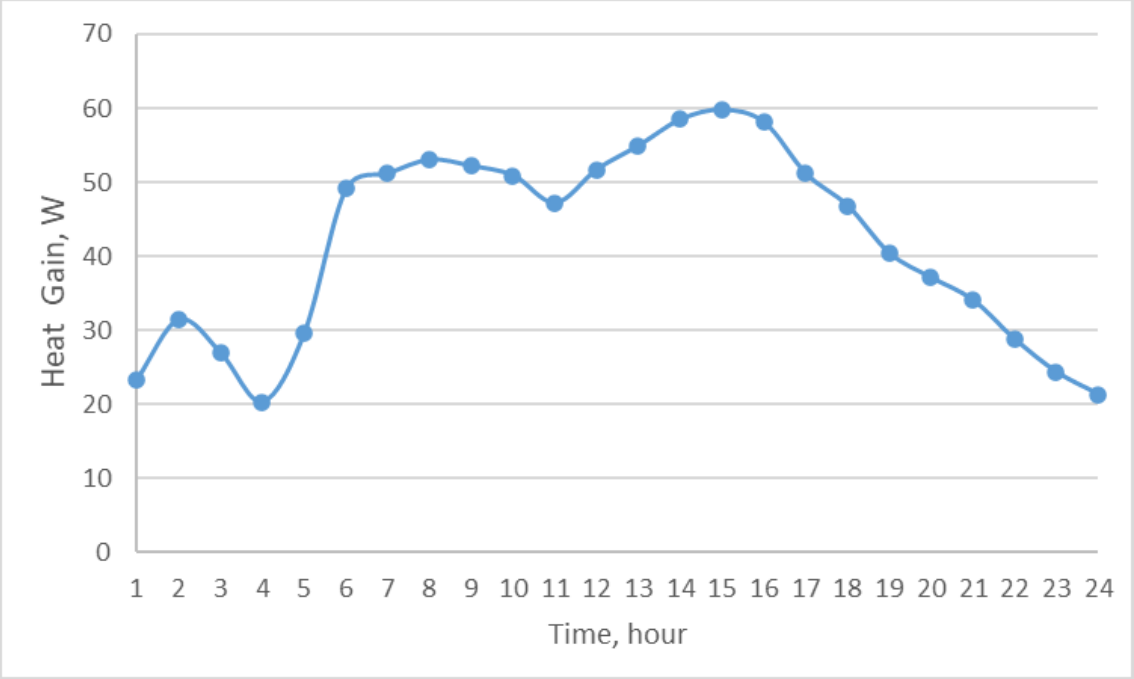

Figure 4.10. Heat Gain Results of Wall B Layers.

From the given results of wall B (Figure 4.9. and 4.10.), the following notes can obtain:

1. The results of heat gain of wall B starting with over 20 W, then a fluctuation for the range of time (01:00-04:00).

2. The values of heat gain started to increase for the range (04:00-08:00) reaching to about 55 W at hour (08:00).
3. A fluctuation for the range (08:00-11:00) reaching the maximum value about 60 W at hour (15:00).
4. A gradual decrease for the rest hours of the day.

Wall C: The results provided (Figure 4.11.) represent the sol-air temperature for wall, whereas the other walls the values started with about 32 C, then a slight decrease for the range of (01:00-07:00). The values started to increase for the range (08:00- 15:00) where the maximum value about 45 C at hour 15:00, the gradual decrease then appeared till the last hours of the day.

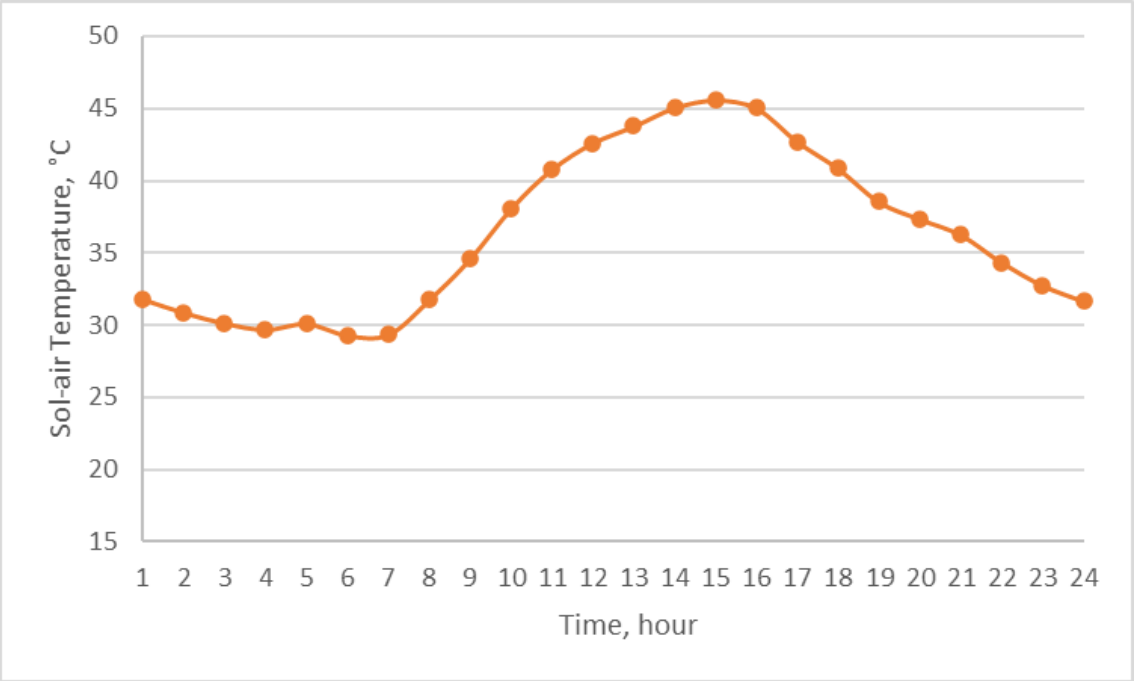

Figure 4.11. Sol-air Temperature Results for Wall C

The heat gain results of wall C are shown in Figure 4.12., where it can be seen that the maximum value reached about 52 W at hour 15:00, and it was started at 20 W then decreased till reached to about 12 W at hour 07:00.

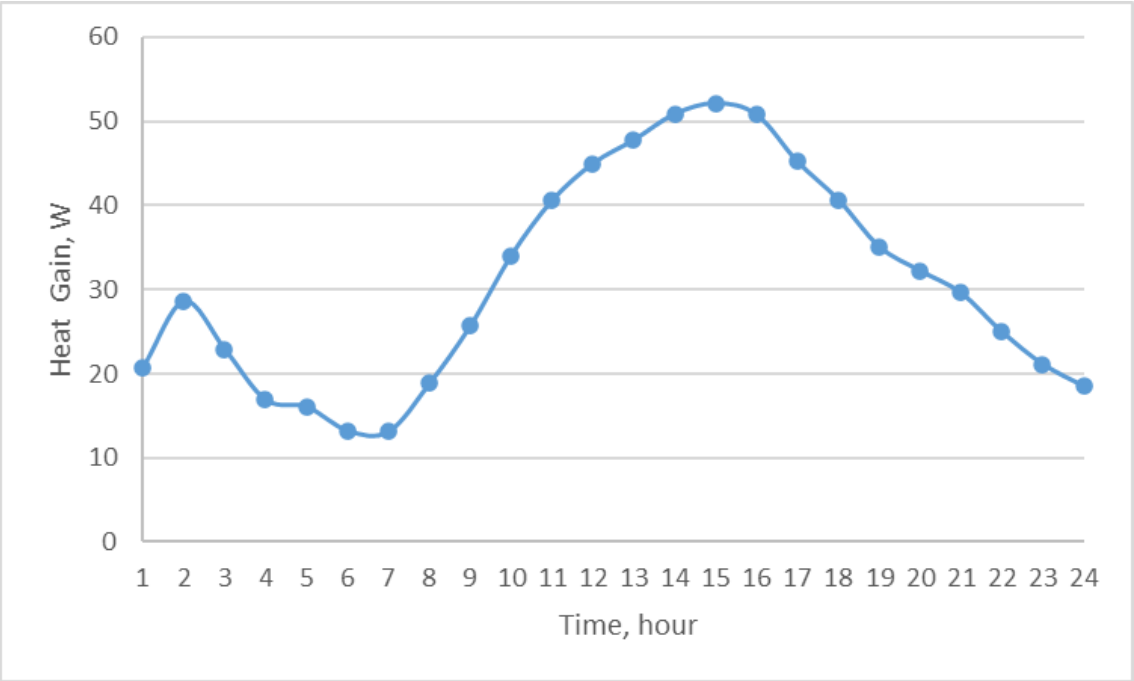

Figure 4.12. Heat Gain Results of Wall C Layers.

Roof: By examining the data (Figure 4.13.), we can make the following observations:

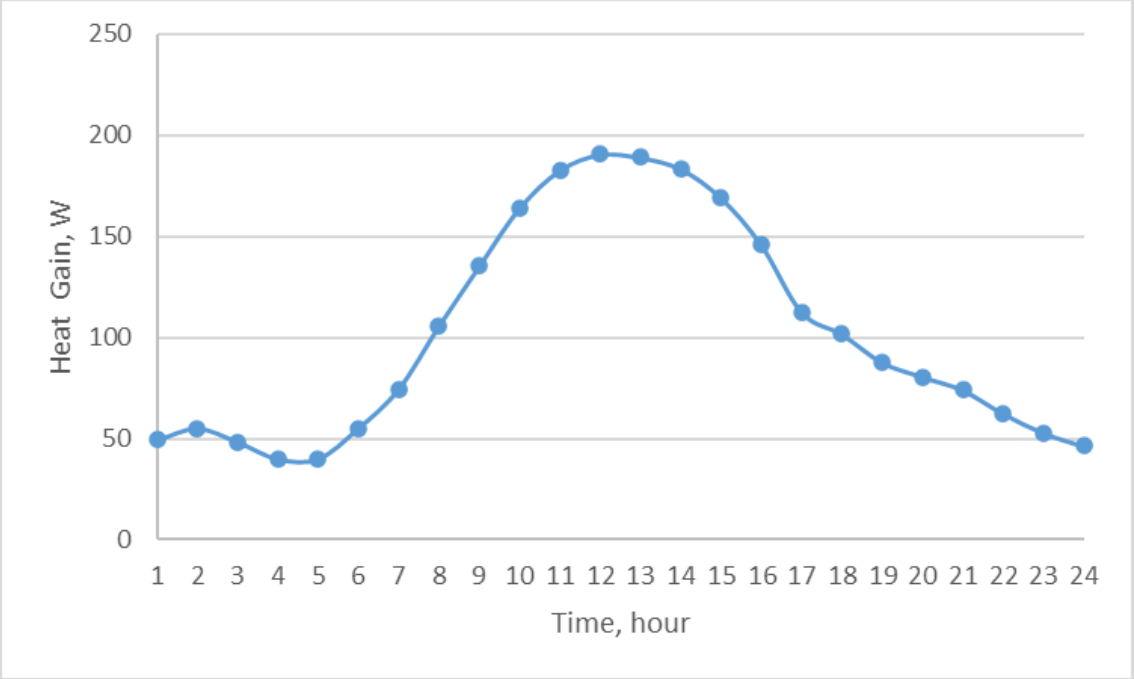

Figure 4.13.. Heat Gain Results for Roof.

1. Unlike the walls, the heat gain results for the roof started with 50 W at hour 01:00.
2. A fluctuation for the range of time (01:00-05:00) with a minimum value about 40 W at hour 05:00.
3. An increase for the range of hours (05:00-12:00) with a maximum value of near 200 W at hour 12:00.
4. A decrease in the heat gain for the rest hours of the day.

4.3. Walls Results in Comparison

Figure 4.14. shows the total heat gain for each wall of the room for each hour of the day. Based on that, the following observations can be drawn:

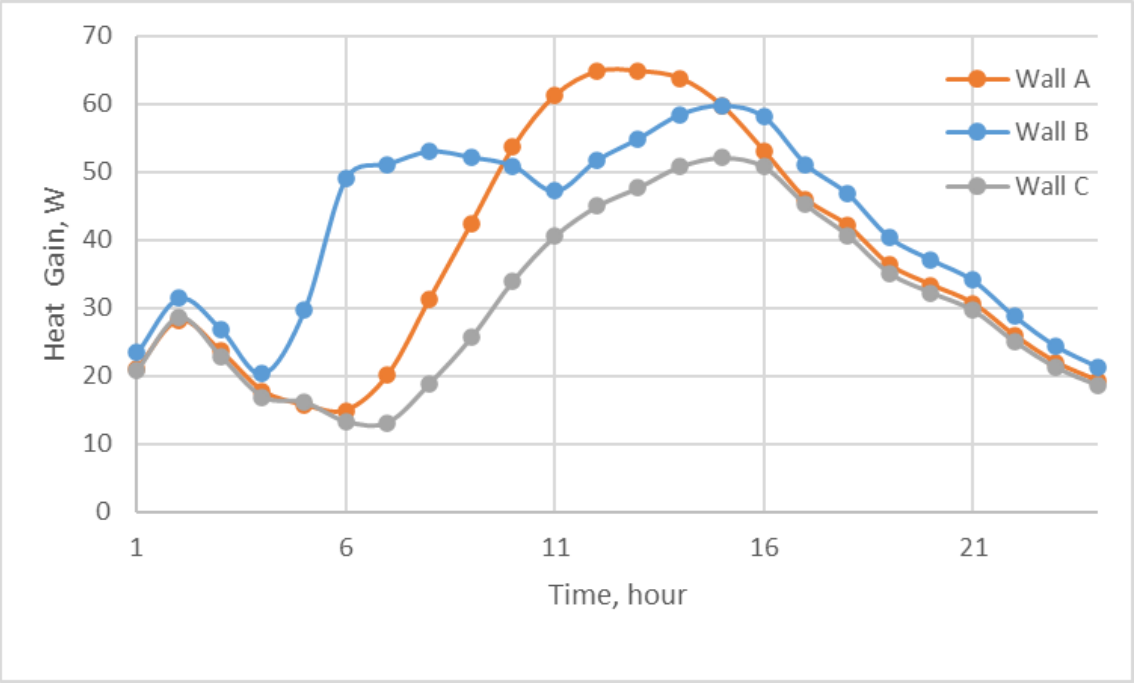

Figure 4.14. Total Heat Gain Results.

1. The hourly heat gain results for all components (Wall A, Wall B, and Wall C) indicate varying levels of heat transfer throughout the day.
2. Wall A exhibits the highest heat gains, where it reached about 65 W maximum.
3. Wall B exhibits moderate heat gains, where it reached about 60 W maximum.
4. Wall C exhibits the minimum heat gains, where it reached about 52 W maximum.
5. Comparing the magnitudes of heat gain, the Roof typically has greater values than the walls, indicating that it contributes significantly to the room's overall heat gain.

4.4. Results Validation

While the current results depend fully on the RTS method, basic comparison is implemented to validate the developed RTS code with the CLTD method code results. The analysis showed some variations between the two, and the peak error percentage reached 12.87 % as presented in Table 4.1.

Table 4.1. Error Percentages Results of Heat gain.

Method	Wall	Heat gain
CLTD	Wall A	22.39
	Wall B	26.86
	Wall C	23.70
RTS	Wall A	21.09
	Wall B	23.40
	Wall C	20.78
% Error	Wall A	5.81%
	Wall B	12.87%
	Wall C	12.31%

4.5. Orientation Effect

The wall orientation effect was investigated by using the MATLAB code together with ASHRAE spreadsheet to get the heat gain results, where the solar flux regarding each orientation was taken from the ASHRAE spreadsheet and used in the present MATLAB code. Figure 4.15. shows the results of heat gain regarding each direction for wall A, where it appears that when wall A faces south, the greatest amount of heat gain is achieved with about 65 W at hour 12:00. The minimum heat gain is acquired for the other three directions with a maximum of 52 W at 14:30.

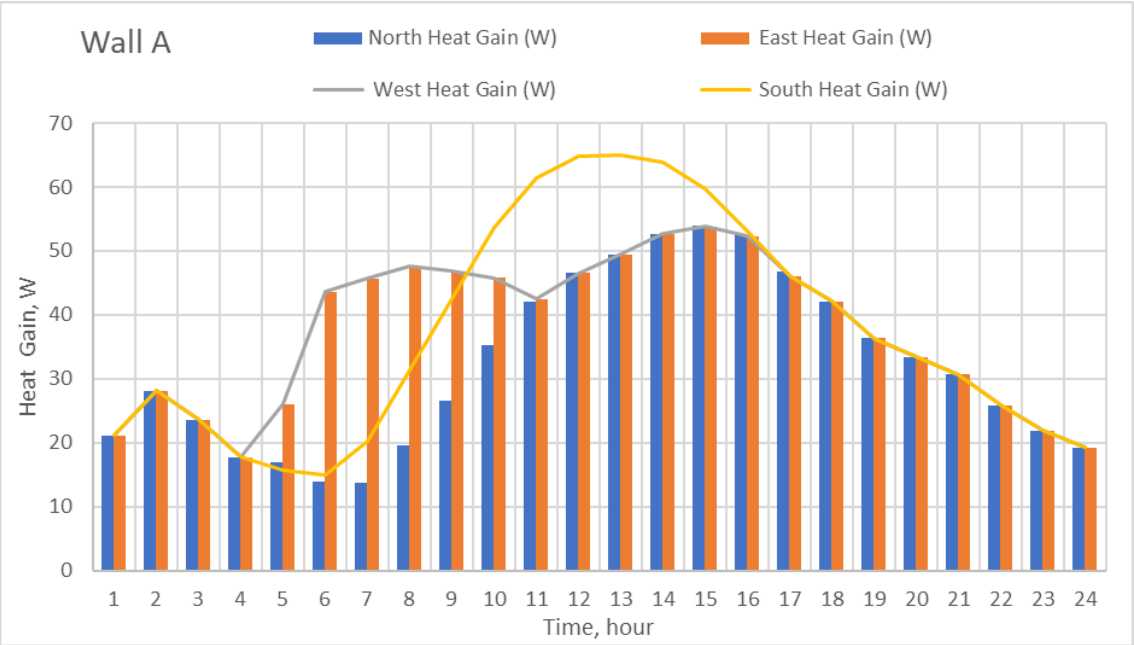

Figure 4.15. Heat gain for each orientation of wall A.

The orientation effect for wall B is presented in Figure 4.16., where it reaches the maximum heat gain when facing the west with about 95 W at hour 14:30. The minimum heat gain is acquired for both east and north directions with a 60 W maximum at hour 14:30.

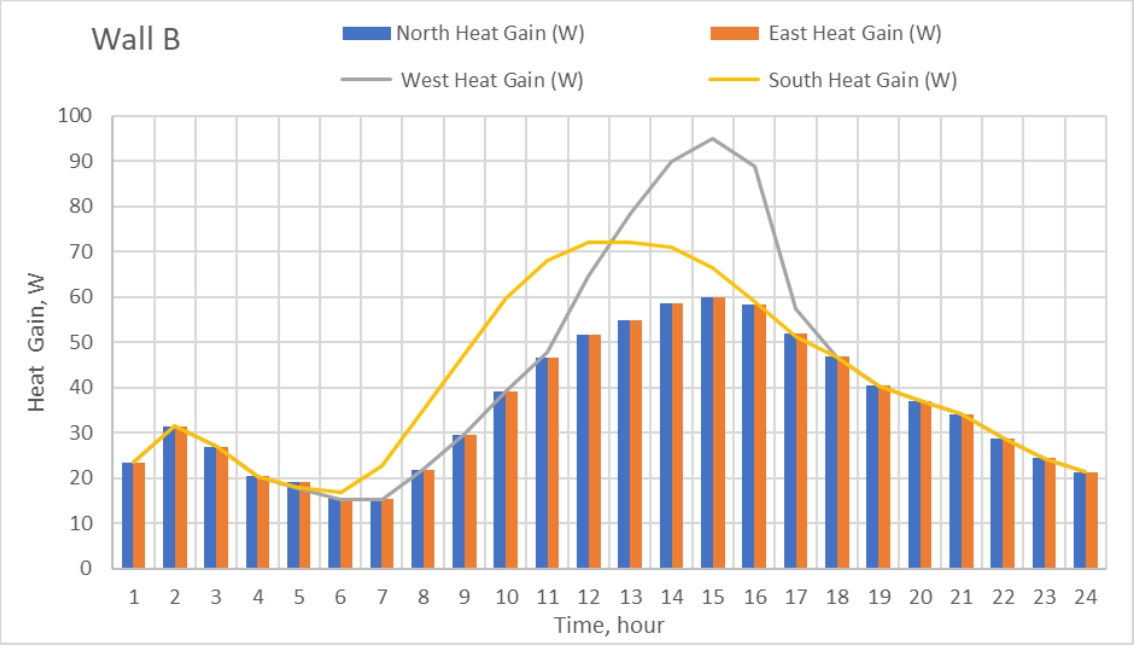

Figure 4.16. Heat gain for each orientation of wall B.

Figure 4.17. illustrates the effect of orientation on wall C, where the maximum heat gain appeared for the west direction with about 82 W at hour 14:30, while the minimum heat gain appeared for both east and north directions again with 52 W at 14:30.

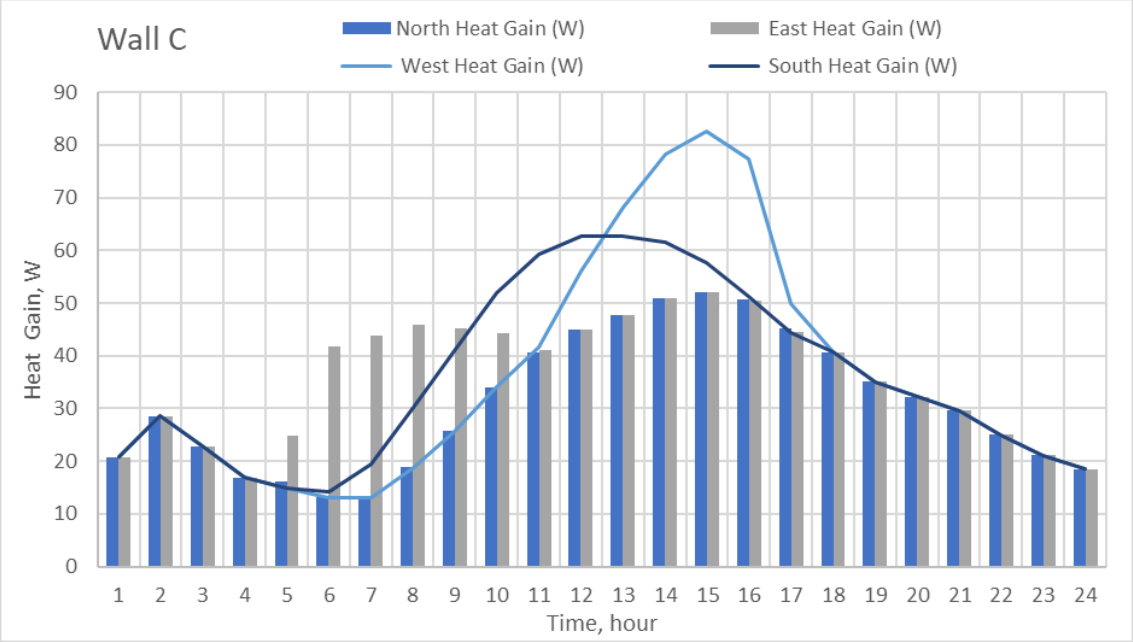

Figure 4.17. Heat gain for each orientation of wall C.

4.6. Cost Analysis Results

The cost of each wall of the model room is presented in the table below (Table 4.2.), where the total room cost is 241,345 IQD. The result of the calculation made can be presented visually in Figure 4.18.

Table 4.2. Costs of the wall's material

Wall Type	Material	Unit	Qty	unit cost in IQD	total	Cost IQD
Wall A	Solid fire clay bricks	m^3	0.184	150,000	27,600	50,750
	Gypsum plastering layer	m^2	0.935	10,000	9,350	
	Cement plastering layer	m^2	1.15	12,000	13,800	
Wall B	Hollow concrete block	m^3	0.165	85,000	14,025	32,825
	Gypsum plastering layer	m^2	0.68	10,000	6,800	
	Cement plastering layer	m^2	1	12,000	12,000	
Wall C	Hollow Brick	m^3	0.184	140,000	25,760	48,910
	Gypsum plastering layer	m^2	0.935	10,000	9,350	
	Cement plastering layer	m^2	1.15	12,000	13,800	
Roof	Roof	m^2	1.15	90,000	103,500	108,860
	False ceiling (Gypsum)	m^2	0.67	8,000	5,360	

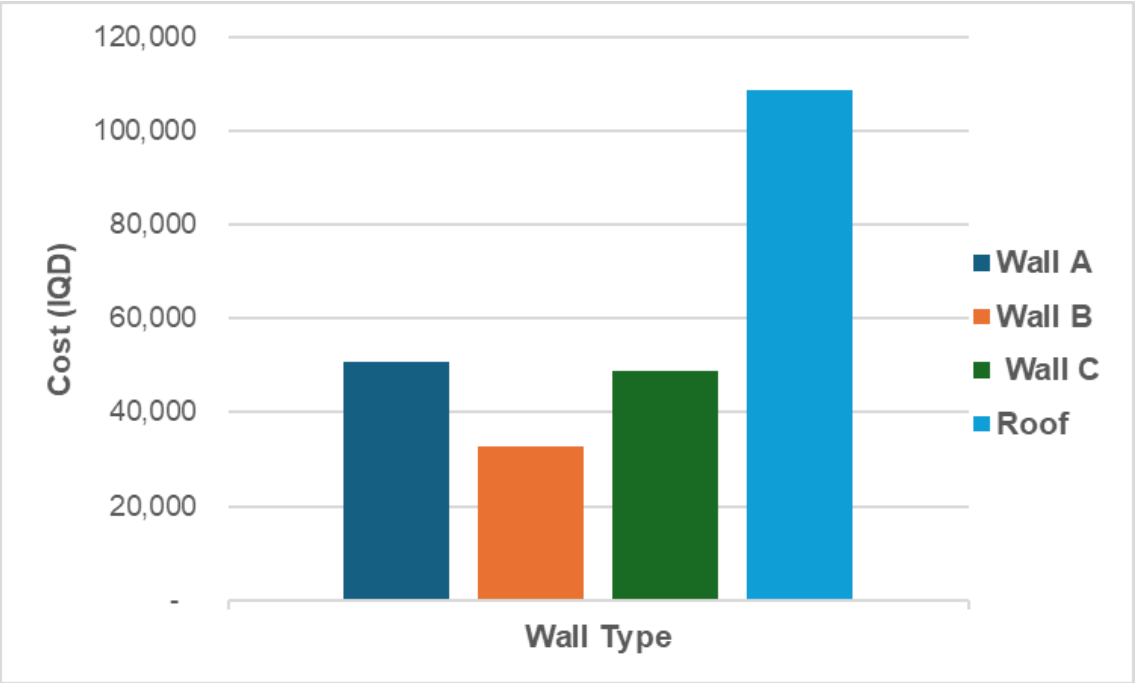

Figure 4.18. Walls and Roof Cost.

4.7. Monthly Energy Cost

In this study, a comparison was made between several rooms consisting of the walls mentioned previously, while keeping the same ceiling and door for the purpose of calculating the amount of heat gain and then calculating the energy needed to cool the rooms in order to calculate the total monthly energy cost. The average global electricity price until 2023 is US$0.156 kWh for households and US$0.153 kWh for businesses (Aliehyaei et al., 2024).

Figure 4.19. depicts the cooling load required to maintain an indoor temperature of 24 degree centigrade, for three-room models, where room A consisted of three walls of type A constructed from solid bricks, room B of three walls of type B constructed from concrete bricks, and room C of hollow bricks. Room B appears to have had the highest cooling load, requiring around 7500 W per day, followed by room A, which required approximately 7340 W per day, and room C, which required approximately 7270 W per day. The monthly electrical energy cost for each of the aforementioned rooms may be computed using the cooling load above, as shown in Figure 4.20., where the lowest cost

is for room C, amounting to $34 per month, and the highest cost is for room B, amounting to $35 per month.

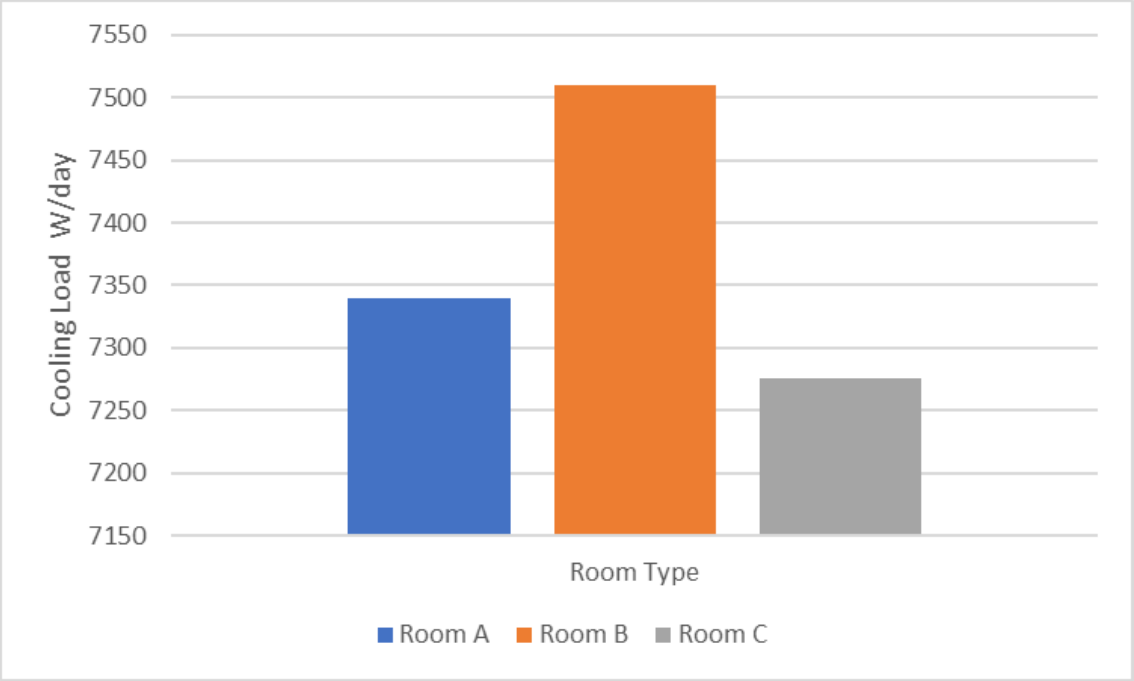

Figure 4.19. Cooling Loads for each room.

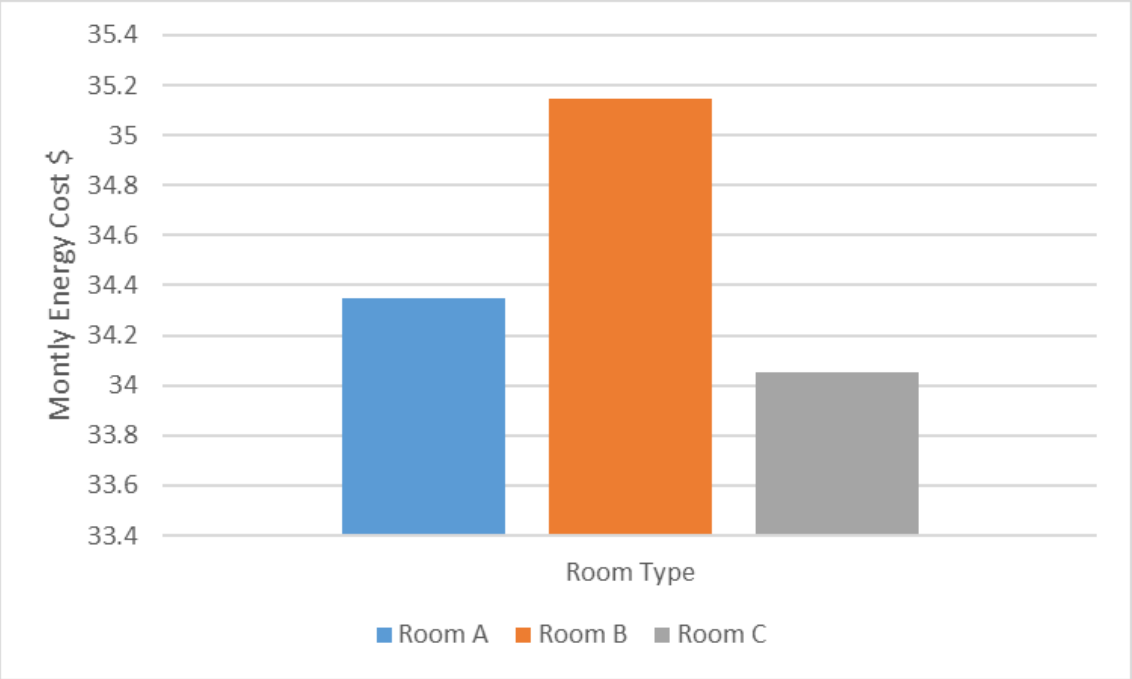

Figure 4.20. Monthly Energy Cost for each room

5. CONCLUSIONS AND RECOMMENDATIONS

The final Section of the work presents the conclusions and suggestions drawn from the conducted research. Based on the previous discussions, this section provides a summary of the findings and insight into future directions in the field of RTS-based heat gain calculations for multilayered walls.

5.1. Conclusions

This thesis's research centred on the application of the RTS method to the calculation of heat gain in multilayered walls. Combining theoretical analysis with experimental research, the following conclusions have been reached:

1. The RTS method is effective: It was proved to be a dependable and precise method for estimating heat gain in multilayered walls.
2. Material characteristics affect heat gain: The thermal properties of the materials used to construct the multilayered walls have a significant impact on heat gain. The conductivity, density, and specific heat of the materials have an impact on the overall heat transfer and must be accounted for in the calculations.
3. Solar radiation influence: Solar radiation incident on walls has a significant impact on heat gain. Understanding the solar exposure patterns in the area and incorporating this information into the RTS method increases the precision of heat gain forecasts.
4. Wall construction and design are significant: Heat gain is significantly affected by the arrangement and composition of layers in multilayered walls. Different wall configurations may result in varying heat transfer characteristics, emphasizing the importance of factoring in the specific construction details when calculating heat gain.
5. Solar flux incident on various walls (Wall A, Wall B, Wall C, and the roof) provides valuable insight into solar radiation exposure and heat gain. Wall B receives the highest incident flux, indicating its greater exposure to direct sunlight. Wall C experiences the least variation in solar flux during peak hours, whereas Wall B experiences the greatest variation. The peak incident solar flux occurs at different times for each wall, indicating differences in wall orientation and solar irradiance.
6. The conduction heat gain results illustrate the contribution of each wall to the total heat gain of the room. Walls B and the roof significantly contribute to the heat gain, whereas Wall C and Wall A experiences a moderate heat gain

7. The cooling load exhibits diurnal variation, with a peak in the afternoon and a gradual decline throughout the evening and early morning. The cooling demand is affected by the ambient temperature and the amount of solar radiation, with the peak cooling demand occurring in the late evening.
8. Overall, the heat gain results show that the composition of walls plays a significant role in controlling heat gain, and that using hollow clay bricks in construction can be an effective way to reduce heat gain.
9. From the given data, Wall C is the best one based on the minimum heat gain. It has the least amount of heat gain throughout the 24-hour period, which means that it is better at controlling heat gain than walls A and B. The reasons for this could be due to the empty (hollow) space in the bricks of Wall C which would act as insulation and helps to reduce heat transfer through the wall.

5.2. Recommendations

The recommendations below aim to provide a more nuanced and comprehensive approach to addressing the challenges and opportunities identified in the study. These recommendations cover various aspects, from design considerations and material innovation to community education and holistic building assessments, providing a comprehensive guide for optimizing energy efficiency and thermal comfort in buildings.

1. **Optimized Wall Components and Building Materials:**
    - Findings stress the importance of wall components for overall thermal performance.
    - Designers and decision-makers should prioritize suitable wall layers and building materials to achieve better heat gain control.
    - Consider the use of building materials with hollow spaces to limit heat transfer.

2. **Building and Wall Orientation:**
    - Plan and consider building and wall orientation strategically to optimize solar radiation exposure and minimize heat gain.
3. **Surface Treatment and Reflective Materials:**
    - Implement surface treatments with reflective materials to mitigate solar heat gain.

- Incorporate multiple layers in the roof to minimize heat transfer.

4. **Window Design and Cooling Systems:**
    - Exercise careful consideration in window selection and design to limit solar heat gain while ensuring adequate daylighting.
    - Implement energy-efficient cooling systems based on cooling load analysis.
5. **Natural Cooling Utilization:**
    - Utilize the decreasing trend of the cooling load throughout the night for natural cooling during cooler hours, reducing reliance on mechanical systems and energy consumption.
6. **Material Innovation:**
    - Encourage research and development in building materials tailored for the Iraqi climate.
    - Investigate innovative materials with enhanced thermal properties (conductivity, density, and specific heat) to optimize heat gain reduction.
7. **Holistic Building Assessments:**
    - Propose comprehensive building assessments considering external shading devices, thermal mass, HVAC system efficiency, and other factors.
    - Ensure a holistic approach for a thorough understanding of overall building dynamics.
8. **Community Education Programs:**
    - Recommend educational initiatives to raise awareness among architects, builders, and homeowners about the impact of building design on energy efficiency.
    - Promote understanding of the significance of wall components and solar exposure for informed construction decisions.
9. **Additional Parameters and Research:**
    - Investigate the effect of heat gain from the floor for accurate calculations.
    - Conduct further research on additional parameters and variables like external shading devices, thermal mass, and HVAC system efficiency for a more comprehensive understanding of multilayered wall thermal performance.

REFERENCES

Ali, S., & Thummakul, P. (2011). Mapping and analyzing Ventilation system in University building. In.

Aliehyaei, M., Tofighi, A., Rosen, M., Afshari, H., Gheisari, S., & Safari, A. (2024). Development a policy for the production of Bitcoins with renewable energy sources. *Future Energy*, *3*(2), 16-23.

Almalki, A. E. (2020). *Energy Consumption Analysis of a Residential Unit for Varying Structural Scenarios* Southern Illinois University at Edwardsville].

Ansari, F., Mokhtar, A., Abbas, K., & Adam, N. (2005). A simple approach for building cooling load estimation. *American Journal of Environmental Sciences*, *1*(3), 209-212.

Bansal, K., Chowdhury, S., & Gopal, M. R. (2008). Development of CLTD values for buildings located in Kolkata, India. *Applied Thermal Engineering*, *28*(10), 1127-1137.

Barrios, G., Huelsz, G., & Rojas, J. (2012). Thermal performance of envelope wall/roofs of intermittent air-conditioned rooms. *Applied Thermal Engineering*, *40*, 1-7.

Benzarti Ghedas, H. (2017). Modeling and thermal optimization of residential buildings using BIM and based on RTS method: application to traditional and standard house in Sousse city.

Bhatia, A. (2001). Cooling load calculations and principles. *Continuing Education and Development, Inc. New York*, *877*, 39.

Bricks PNG 7 - PNG All. Retrieved January 20, 2024 from https://www.pngall.com/bricks-png/download/390

Costa, A. (2010). Cooling load calculation by the radiant time series method-effect of solar radiation models.

Croft, C. (2004). *Concrete architecture*. Laurence King Publishing.

Cui, M., & Chen, T. (2009). A revised radiant time series (RTS) method for intermittent cooling load calculation.

Domínguez-Muñoz, F., Cejudo-López, J. M., & Carrillo-Andrés, A. (2010). Uncertainty in peak cooling load calculations. *Energy and Buildings*, *42*(7), 1010-1018.

Ecosafe - TPRS. (Octuber 18, 2023). Retrieved January 20, 2024 from https://tprsglass.com/ecosafe/

Egypt, C. S. (2022). *Gypsum Powder*. https://cpimg.tistatic.com/07660506/b/4/Gypsum-Powder.jpeg

Ekici, B. B., Gulten, A. A., & Aksoy, U. T. (2012). A study on the optimum insulation thicknesses of various types of external walls with respect to different materials, fuels and climate zones in Turkey. *Applied Energy*, *92*, 211-217.

Eumorfopoulou, E., & Kontoleon, K. (2009). Experimental approach to the contribution of plant-covered walls to the thermal behaviour of building envelopes. *Building and Environment*, *44*(5), 1024-1038.

Global, A. (2020). Global status report for buildings and construction. *Global Alliance for Buildings and Construction*.

Granja, A., & Labaki, L. (2003). Influence of external surface colour on the periodic heat flow through a flat solid roof with variable thermal resistance. *International Journal of Energy Research*, *27*(8), 771-779.

Handbook, A. (2013). Nonresidential cooling and heating load calculations. *Atlanta, GA: American Society of Heating, Refrigerating and Air-Conditioning Engineers, Atlanta, Georgia*.

Handbook, A. F. (1997). ASHRAE Fundamentals Handbook. In: Inc.

Hashim, H., Sokolova, E., Derevianko, O., & Solovev, D. (2018). Cooling load calculations. IOP Conference Series: Materials Science and Engineering,

Hittle, D. C., & Bishop, R. (1983). An improved root-finding procedure for use in calculating transient heat flow through multilayered slabs. *International Journal of Heat and Mass Transfer*, *26*(11), 1685-1693.

Huang, C., Bai, T., Cai, J., Lv, L., Chen, J., & Li, L. (2015). Experimental study on the radiant cooling load of floor based on the radiant time series method. *Procedia Engineering*, *121*, 45-51.

Hurlbut, C. S., & Klein, C. (1977). *Manual of mineralogy (after James D. Dana)*. Wiley.

Joudi, K. A., & Hussien, A. N. (2015). Cooling Load Calculations For Typical Iraqi Roof And Wall Constructions Using Ashrae's RTS Method. *Journal of Engineering*, *21*(5), 98-114.

Kadir, A. M., & Kako, S. A. (2022). Comparative Investigation on the Quality of Sensitivity of Six Different Types of Thermocouples. *Al-Rafidain Engineering Journal (AREJ)*, *27*(2), 117-126.

Kaşka, Ö., & Yumrutaş, R. (2008). Comparison of experimental and theoretical results for the transient heat flow through multilayer walls and flat roofs. *Energy*, *33*(12), 1816-1823.

Kulkarni, K., Sahoo, P. K., & Mishra, M. (2011). Optimization of cooling load for a lecture theatre in a composite climate in India. *Energy and Buildings*, *43*(7), 1573-1579.

Kumar, D., Zou, P. X., Alam, M. M., & Sanjayan, J. G. Impact of Construction Materials on Building Wall's Thermal Optimization.

Kusiak, A., Li, M., & Tang, F. (2010). Modeling and optimization of HVAC energy consumption. *Applied Energy*, *87*(10), 3092-3102.

Leonidas, E., Ayvar-Soberanis, S., Laalej, H., Fitzpatrick, S., & Willmott, J. R. (2022). A comparative review of thermocouple and infrared radiation temperature measurement methods during the machining of metals. *Sensors*, *22*(13), 4693.

Ltd, A.-B. (2024). *Solid Brick buy in Tbilisi*. Retrieved January 20, 2024 from https://ge.all.biz/solid-brick-g11489

Malomo, D., Pinho, R., & Penna, A. (2019). Applied element modelling of the dynamic response of a full-scale clay brick masonry building specimen with flexible diaphragms. *International Journal of Architectural Heritage*.

Mao, C., Baltazar, J.-C., & Haberl, J. S. (2019). Comparison of ASHRAE peak cooling load calculation methods. *Science and Technology for the Built Environment*, *25*(2), 189-208.

Mendes, N., Oliveira, G. H. d. C., Araújo, H. D., & Coelho, L. (2003). A Matlab-based simulation tool for building thermal performance analysis. Eighth International IBPSA Conference, Eindhoven, Netherlands,

Nigusse, B. A. (2007). *Improvements to the radiant time series method cooling load calculation procedure*. Oklahoma State University.

Olofsson, T., Ohlsson, K. A., & Östin, R. (2017). Measurement of the environmental temperature using the sol-air thermometer. *Energy Procedia*, *132*, 357-362.

Olu-Ajayi, R., Alaka, H., Sulaimon, I., Sunmola, F., & Ajayi, S. (2022). Building energy consumption prediction for residential buildings using deep learning and other machine learning techniques. *Journal of Building Engineering*, *45*, 103406.

Pérez-Lombard, L., Ortiz, J., & Pout, C. (2008). A review on buildings energy consumption information. *Energy and buildings*, *40*(3), 394-398.

Reddy, T., Kreider, J. F., Curtiss, P. S., & Rabl, A. (2016). *Heating and cooling of buildings: principles and practice of energy efficient design*. CRC press.

Rees, S. J., Spitler, J. D., Davies, M. G., & Haves, P. (2000). Qualitative comparison of North American and UK cooling load calculation methods. *Hvac&R Research*, *6*(1), 75-99.

Risk, C. W. (2022). *Rivers are Running Dry Today*. China Water Risk. https://chinawaterrisk.org/resources/analysis-reviews/rivers-are-running-dry-today/

Ruivo, C. R., Ferreira, P. M., & Vaz, D. C. (2013). Prediction of thermal load temperature difference values for the external envelope of rooms with setback and setup thermostats. *Applied thermal engineering*, *51*(1-2), 980-987.

Shaik, S., & Talanki, A. B. P. S. (2016). Optimizing the position of insulating materials in flat roofs exposed to sunshine to gain minimum heat into buildings under periodic heat transfer conditions. *Environmental Science and Pollution Research*, *23*, 9334-9344.

Skelly, L. (2021). *Analysis of Energy Efficiency, Alternative Energy Sources, and the Carbon Footprint of a Campus Building Using BIM* Southern Illinois University at Edwardsville].

Spitler, J. D., Fisher, D. E., & Pedersen, C. O. (1997). *The radiant time series cooling load calculation procedure* (0001-2505).

Spychał, E., & Dachowski, R. (2021). The influence of hydrated lime and cellulose ether admixture on water retention, rheology and application properties of cement plastering mortars. *Materials*, *14*(19), 5487.

Šujanová, P., Rychtáriková, M., Sotto Mayor, T., & Hyder, A. (2019). A healthy, energy-efficient and comfortable indoor environment, a review. *Energies*, *12*(8), 1414.

Wu, W., Skye, H. M., & Domanski, P. A. (2018). Selecting HVAC systems to achieve comfortable and cost-effective residential net-zero energy buildings. *Applied Energy*, *212*, 577-591.

Yang, L., Yan, H., & Lam, J. C. (2014). Thermal comfort and building energy consumption implications–a review. *Applied energy*, *115*, 164-173.

Yumrutaş, R., Kaşka, Ö., & Yıldırım, E. (2007). Estimation of total equivalent temperature difference values for multilayer walls and flat roofs by using periodic solution. *Building and Environment*, *42*(5), 1878-1885.

Zainal, O. A., & Yumrutaş, R. (2015). Validation of periodic solution for computing CLTD (cooling load temperature difference) values for building walls and flat roofs. *Energy*, *82*, 758-768.

Zedan, M., & Mujahid, A. (1993). An efficient solution for heat transfer in composite walls with periodic ambient temperature and solar radiation. *International journal of ambient energy*, *14*(2), 83-98.

Zheng, K., Watt, J., Wang, C., & Cho, Y. K. (2016). Development and implementation of a virtual outside air wet-bulb temperature sensor for improving water-cooled chiller plant energy efficiency. *Sustainable Cities and Society*, *23*, 11-15.

APPENDIX A

A.1. Code for the first Pseudo Code

```
      % Define inputs
A_of_Wall= 100; % in square meters
Temperature|sol-air= [10 12 14 ...]; % in degrees Celsius, 24 hourly values
Temperature|zone= 20; % in degrees Celsius
resp_fact(RF)= [0.1 0.2 0.3 ...]; % 24 response factors

% Initialize variables
hourly_heat_gains = zeros(1, 24);
total_heat_gain = 0;

% Loop over each exterior wall
for wall = 1:num_walls
    % Loop over each hour of the day
    for hour = 1:24
        % Loop over each wall response factor
        for rf = 1:length(response_factors)
            % Calculate fractional heat gain.
            frac_HG = A_of_Wall * resp_fact(RF) * (Temperature|sol-air(hour)
– Temperature|zone);

            % Add to hourly heat gains for this wall
            hourly_heat_gains(hour) = hourly_heat_gains(hour) +
fractional_heat_gain;

            % Update sol-air temperature for use in the next iteration
            sol_air_temp(hour) = sol_air_temp(hour) + fractional_heat_gain /
wall_area;
        end
    end

    % Add wall's hourly heat gains to total heat gain
    total_heat_gain = total_heat_gain + sum(hourly_heat_gains);
end

% Display results
disp(['Overall Layer’s heat gain: ' num2str(total_heat_gain) ' W']);
```

A.2. Code for the Second Pseudo Code

```
% Define how long your test take in hours on that date
hours = 24;

% Define the hourly solar heat gain as a vector of length "hours"
H_SHG = [insert your data here];

% Define the 24 Radiant Time Factors as a vector
RTF = [insert your data here];
```

```
% Initialize the previous solar heat gain
prev_SHG = 0;

% Initialize the hourly cooling load as a vector of length "hours"
hourly_cool_load = zeros(hours, 1);

% Loop through each hour in the day
for hour = 1:hours

    % Initialize the previous Radiant Time Factor
    prev_RTF = 0;

    % Loop through each of the 24 Radiant Time Factors
    for i = 1:24

        % Compute the fractional cooling load for the current RTF
        frac_cool_load = RTF(i) * (H-SHG(hour) - prev_SHG);

        % Add the fractional cooling load to the hourly cooling load
        hourly_cool_load(hour) = hourly_cool_load(hour) + frac_cool_load;

        % Set the current solar heat gain as the previous solar heat gain for
the next iteration
        prev_solar_heat_gain = hourly_solar_heat_gain(hour);

        % Set the current Radiant Time Factor as the previous Radiant Time
Factor for the next iteration
        prev_RTF = RTF(i);

        % Add the conductive cooling load to the hourly cooling load
        hourly_cool_load(hour) = hourly_cool_load(hour) + [insert your
conductive cooling load calculation here];
    end
end

% Sum the hourly cooling load to obtain the total cooling load
total_cool_load = sum(hourly_cool_load);
```

A.3. Code for the Third Pseudo Code.

```
% Define how long your test take in hours on that date
hours = 24;

% Define the Radiant Time Factors as a vector
radiant_time_factors = [insert your data here];

% Define Radiation component of inside and Conduction HGs as a vector of
length "hours"
radiant_portion_internal_conductive = [insert your data here];
```

```
% Define the Diffuse Solar Heat Gain as a vector of length 'hours'
diffuse_solar_heat_gain = [insert your data here];

% Initialize the previous heat gain
prev_heat_gain = 0;

% Initialize the hourly cooling load as a vector of length 'hours'
hourly_cool_load = zeros(hours, 1);

% Loop through each hour in the day
for hour = 1:hours

    % Initialize the previous Radiant Time Factor
    prev_rad_time_factor = 0;

    % Loop through each of the 24 Radiant Time Factors
    for i = 1:24
        % Calculate the fractional cooling load for this Radiant Time Factor
        frac_cool_load = radiant_time_factors(i) *
(radiant_portion_internal_conductive(hour) * diffuse_solar_heat_gain(hour) -
prev_heat_gain);

        % Add the fractional cooling load to the hourly cooling load
        hourly_cool_load(hour) = hourly_cool_load(hour) + frac_cool_load;

        % Set the current heat gain as the previous heat gain for the next
iteration
        prev_heat_gain = radiant_portion_internal_conductive(hour) *
diffuse_solar_heat_gain(hour);

        % Set the current Radiant Time Factor as the previous Radiant Time
Factor for the next iteration
        prev_rad_time_factor = radiant_time_factors(i);
    end
end

% Summation of periodic (per hour) cooling loads for obtaining overall
cooling load
total_cool_load = sum(hourly_coo_load);
```

A.4. Code for the Fourth Pseudo Code.

```
      % Define how long your test take in hours on that date
      hours = 24;

      % Define the Convective Component of Internal Heat Gains as a vector of
length "hours"
      convective_component_internally = [insert your data here];

      % Define the Convective Component of Conductive Heat Gains as a vector
of length "hours"
```

```
      convective_component_conductive = [insert your data here];

      % Define the Beam ‘Solar Heat Gains’ that transformed into ‘Cooling Load’
as a vector of length "hours"
      beam_solar_heat_gain = [insert your data here];

      % Define the Radiative Component of Internal and Conductive Heat Gains
as a vector of length "hours"
      radiative_component_internally_conductive = [insert your data here];

      % Define the Diffuse Solar Heat Gain as a vector of length "hours"
      diffuse_solar_heat_gain = [insert your data here];

      % Initialize the hourly cooling load as a vector of length "hours"
      hourly_cool_load = zeros(hours, 1);

      % Loop through each hour in the day

      for hour = 1:hours

% Summation of all component that contribute to cooling load for this hour
convective_cool_load      =      convective_component_internally(hour)      +
convective_component_conductive(hour);
bean_solar_cooling_load= bean_solar_heat_gain(hour);

radiative_cooling_load
=radiant_time_series(radiative_component_internal_conductive(hour),
diffuse_solar_heat_gain(hour));

 % Add all contributions to get cooling load for this hour caused by to
internally gained heat and the radiation component of conduction
          hourly_cool_load(hour)       =       convective_cool_load       +
bean_solar_cool_load + radiative_cool_load;
      end

      % Summation of hourly cooling load to get the total cooling load caused
by to internally gained heat and the radiation component of conduction
      total_cool_load = sum(hourly_cool_load);
```

A.5. RTS Combined MATLAB Code. (example)

```
% Calculate Sol-air Temperature in Celsius and Heat Gain for Wall A

% Define input parameters
outdoorTempInKelvin = [31.80333333 30.87333333 30.13666667 29.706 29.39333333
28.115 27.72833333 29.80333333 32.37666667 35.68833333 38.35333333 40.235
41.57333333 43.13166667 43.98833333 43.90666667 42.25166667 40.84666667
38.53666667 37.35 36.26 34.34833333 32.76166667 31.67666667];
solarAbsCoeff = [0.442 0.442 0.442 0.442 0.442 0.442 0.442 0.442 0.442 0.442
0.442 0.442 0.442 0.442 0.442 0.442 0.442 0.442 0.442 0.442 0.442 0.442 0.442
0.442];
```

```
solarRadInWattsPerSqMeter = [0 0 0 0 173.575849 538.932636 608.88928
559.478686 441.527086 282.158485 112.150908 101.818714 94.3137012 82.2072276
65.5006231 42.8396614 6.56102426 0 0 0 0 0 0 0];
heatTransferCoeffInWattsPerSqMeterKelvin = 25 *
ones(size(outdoorTempInKelvin)); % Constant value for heat transfer
coefficient
tiltAngleInRadians = pi / 6;
PrioResFac = [0.175676703 1.387792945 1.170876026 0.53223139 0.226446196
0.095778801 0.040489521 0.01711571 0.007235116 0.00305841 0.001292844
0.000546508 0.000231018 9.76555E-05 4.12807E-05 1.74501E-05 7.37645E-06
3.11816E-06 1.3181E-06 5.57184E-07 2.35531E-07 9.95632E-08 4.20871E-08
1.7791E-08];
T_in = 24 * ones(size(outdoorTempInKelvin));
WallArea = 1.15; % m2
U = 2.174;

% Pre-calculate constants based on tilt angle
radiationCorrectionInKelvin = 7 * cos(tiltAngleInRadians);

% Calculate sol-air temperature for each hour
solAirTempsInKelvin = zeros(size(outdoorTempInKelvin));
for hour = 1:numel(outdoorTempInKelvin)
    % Calculate radiation correction for the current hour
    currentRadiationCorrection = max(0, radiationCorrectionInKelvin);

    % Calculate sol-air temperature for the current hour
    solAirTempsInKelvin(hour) = outdoorTempInKelvin(hour) +
((solarAbsCoeff(hour) * solarRadInWattsPerSqMeter(hour)) /
(heatTransferCoeffInWattsPerSqMeterKelvin(hour) -
currentRadiationCorrection));
end

% Convert sol-air temperature from Kelvin to Celsius
solAirTempsInCelsius = solAirTempsInKelvin - 273.15;

% Display the sol-air temperature for each hour (Celsius)
fprintf('Sol-air temperature for each hour of the day (Celsius):\n');
for hour = 1:numel(solAirTempsInCelsius)
    fprintf('Hour %d: %.2f °C\n', hour, solAirTempsInCelsius(hour));
end

% Write sol-air temperatures to an Excel file
hourlyData = [1:numel(solAirTempsInCelsius); solAirTempsInCelsius];
headerSolAir = {'Hour', 'Sol-Air Temperature (Celsius)'};
xlRangeSolAir = 'W';
xlswrite('C:\Users\Owner\Desktop\WallA.xlsx', [headerSolAir;
num2cell(hourlyData')], xlRangeSolAir);
disp('Sol-air temperatures written to WallA.xlsx');

% Calculate hourly heat gain
Q_con = PrioResFac .* WallArea .* (solAirTempsInKelvin - T_in);
Q_f = U * WallArea * (solAirTempsInKelvin - T_in);
```

```
Q_t = Q_f + Q_con;

% Write results to an Excel file
headerHeatGain = {'Hour', 'Heat Gain (W)'};
hourlyDataHeatGain = [1:numel(Q_t); Q_t];
xlRangeHeatGain = 'Z';
xlswrite('C:\Users\KHALIL\Desktop\WallA.xlsx', [headerHeatGain;
num2cell(hourlyDataHeatGain')], xlRangeHeatGain);
disp('Hourly Heat Gain (W) for WallA.xlsx');
```

APPENDIX B

In this appendix, screenshots from the ASHRAE Spreadsheet are added to show the interface and the inputs needed.

This spreadsheet calculates cooling loads for a zone with the ASHRAE RTS Procedure.								
Data that is entered by the user is shown highlighted.								
Design Conditions								
Location	Taza, Kirkuk, Iraq							
Latitude	35.315832							
Longitude	44.3							
Time Zone	5	("5"=Eastern TZ, "6"= Central TZ, "7"= Mountain TZ, "8"=Pacific TZ)						
Daylight Savings Time	1	("0" = standard time; "1"=daylight savings				Intermediate Variables		
Month	9	(1=Jan ... 12=Dec; 21st of the month is assumed)						
Outdoor Design Temperature	113	Degrees F		C	45	Day number	244	
Daily Range	35.1	Degrees F		C	19.5	EOT	0.6	Minutes
Indoor Air Temperature	77.9	Degrees F		C	25.5	Std. Meridian	75	Degrees
Clearness Number	0.7					A	360.2	
Ground reflectance	0.2					B	0.165	
						C	0.12	
						Decl.	8.57	Degrees
Surface Data								
Surface Name		Wall A	Wall B	Wall C		Wall C		
Surface Number		1	2	3	4	5		
Surface Area (sq. ft.)		12.4	12.4	12.4	0	12.4		
Facing direction (deg)		180	90	0	270	0		
(0=N,90=E,180=S,270=W)								
Tilt (deg – 0=horiz. Up;		90	90	90	90	90		
90=vertical; 180=horiz. Down)								
Solar absorptivity		0.9	0.9	0.9	0.9	0.9		
Outside surface conductance		4	4	4	4	4		

Figure B.1. ASHRAE Spreadsheet used to calculate the cooling loads

Solar Fluxes							Wall A	Wall B	Wall C		
Hour	Solar Time	Wall A Incident Flux (Btu/hr-ft2)	Wall B Incident Flux (Btu/hr-ft2)	Incident Flux (Btu/hr-ft2)	Incident Flux (Btu/hr-ft2)	Wall C Incident Flux (Btu/hr-ft2)	Wall A Incident Flux (W/m2)	Wall B Incident Flux (W/m2)	Wall C Incident Flux (W/m2)		
1	2.05	0.0	0.0			0.0	0	0	0		
2	3.05	0.0	0.0			0.0	0	0	0		
3	4.05	0.0	0.0			0.0	0	0	0		
… up to 24											
Air and Sol-Air Temperatures											
Hour	Air T (F)	Sol-Air T For Wall A (F)	Sol-Air For Wall B T (F)	Sol-Air T (F)	Sol-Air T (F)	Sol-Air T For Wall C (F)		Air (C)	Sol-Air For Wall A (C)	Sol-Air For Wall B (C)	Sol-Air For Wall C (C)
1	82.5	82.5	82.5			82.5		28.035	28.035	28.035	28.035
2	80.7	80.7	80.7			80.7		27.06	27.06	27.06	27.06
3	79.3	79.3	79.3			79.3		26.28	26.28	26.28	26.28
… up to 24											
Periodic Response Factors		Wall A	Wall B			Wall C					
1		5.4460E-01	4.4471E-01			5.4460E-01					
2		2.1608E+00	2.3308E+00			2.1608E+00					
3		1.1525E+00	1.6441E+00			1.1525E+00					
… up to 24											
							watt				
Conduction Heat Gains, Btu/hr		Wall A	Wall B	Wall C		Wall C	Wall A	Wall B	Wall C		
1		423.0	593.6	211.4		423.0	126.91	178.0948	126.901		
2		309.8	441.0	95.3		309.8	92.9379	132.3113	92.9349		
3		209.1	307.4	-7.9		209.1	62.7337	92.20674	62.7326		
… up to 24											
Window Absorbed Heat Gains, Btu/hr					Window Absorbed Heat Gains, W						
1	2.05	0.0	0.0		0						
2	3.05	0.0	0.0		0						
3	4.05	0.0	0.0		0						
… up to 24											

Cooling Loads														
	Wall Conduction		Roof Conduction		Window Absorption		Window Conduction		Window Transmitted SHG	...	Infiltration	Total	Total	Wall (all)	Roof
	Radiative	Convective	Radiative	Convective	Radiative	Convective	Radiative	Convective	Radiative		Convective				
	Btu/hr	Btu/hr	Btu/hr	Btu/hr	Btu/hr	Btu/hr	Btu/hr	Btu/hr	Btu/hr		Btu/hr	Btu/hr	W	W	W
1	2092.7	454.4	817.4	69.4	0.7	0.0	16.5	3.2	32.2		0.0	3486.5	1045.9447	779.92176	266.02291
2	1862.7	313.1	732.8	50.8	0.6	0.0	14.6	2.0	28.7		0.0	3005.3	901.58064	666.49136	235.08928
3	1642.2	188.2	651.1	34.3	0.6	0.0	12.7	1.0	25.6		0.0	2555.6	766.69059	561.06017	205.63042
… up to 24															

	Wall(all)	Roof	Lights	People	Equip.	Infilt	Total
	Btu/hr	Btu/hr	Btu/hr	Btu/hr	Btu/hr	Btu/hr	Btu/hr
1	2599.7	886.7	0.0	0.0	0.0	0.0	3486.5
2	2221.6	783.6	0.0	0.0	0.0	0.0	3005.3
3	1870.2	685.4	0.0	0.0	0.0	0.0	2555.6
… up to 24							

	BASE window area, Chicago		
	HBM	RTS	%
1	572.7	3486.5	509%
2	409.8	3005.3	633%
3	271.7	2555.6	841%
Peak	10826.5	7964.266229	-26%

Window Conducted Heat Gains, Btu/hr		Note: This now uses air temperature, not Sol-air as in Eq. 8-75	
1		8.8	0.0
2		5.4	0.0
3		2.7	0.0
Sensible Internal Heat Gains, Btu/hr			
Name	Lights	People	Equipment
Fraction radiative	0.7	0.7	0.5
1	0.0	0	0.0
2	0.0	0	0.0
3	0.0	0	0.0
… up to 24			

Heat Gain Summary										
	Wall Conduction		Roof Conduction		Window Absorption		Window Conduction		Window Transmitted SHG	Infiltration
	Radiative	Convective	Radiative	Convective	Radiative	Convective	Radiative	Convective	Radiative	Convective
	Btu/hr	Btu/hr	Btu/hr	Btu/hr	Btu/hr	Btu/hr	Btu/hr	Btu/hr	Btu/hr	Btu/hr
1	773.7	454.4	355.3	69.4	0.0	0.0	5.5	3.2	0.0	0.0
2	533.1	313.1	260.2	50.8	0.0	0.0	3.4	2.0	0.0	0.0
3	320.4	188.2	175.7	34.3	0.0	0.0	1.7	1.0	0.0	0.0
4	139.4	81.9	104.0	20.3	0.0	0.0	0.4	0.2	0.0	0.0
… up to 24										
Radiant Time Factors	Non-solar		Non-solar		Non-solar		Non-solar		Solar	
1	0.24463710		0.24463710		#######		#######		0.4209561	
2	0.12226960		0.12226960		#######		#######		0.1384633	
3	0.08985554		0.08985554		#######		#######		0.0731338	
… up to 24										

Figure B.1. (continue)

APPENDIX C

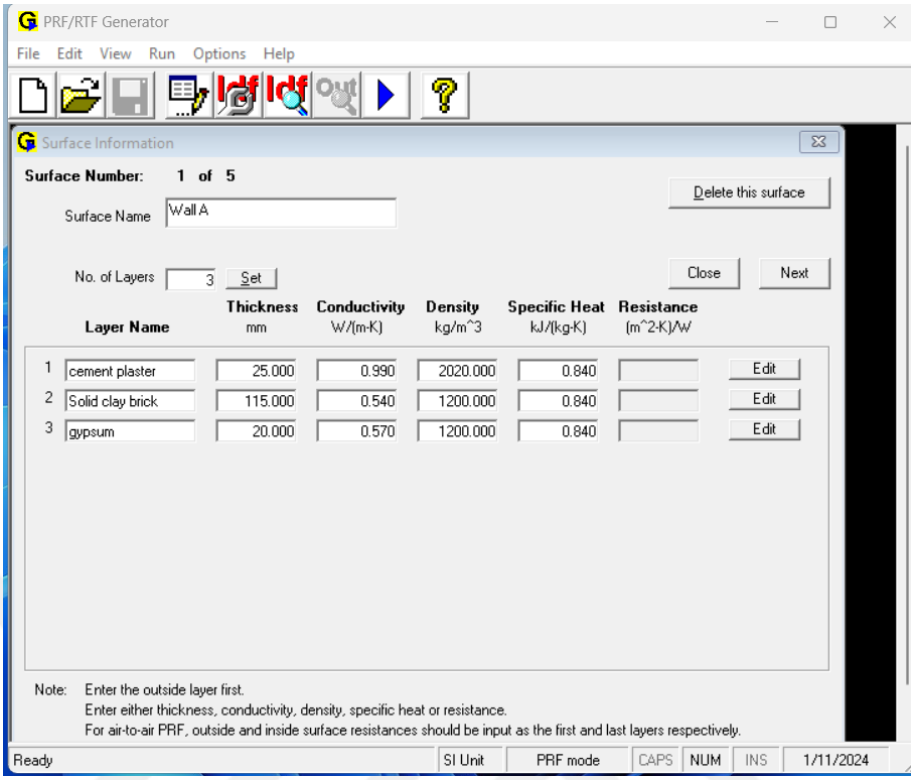

Figure C.1. Wall A layers and specifications.

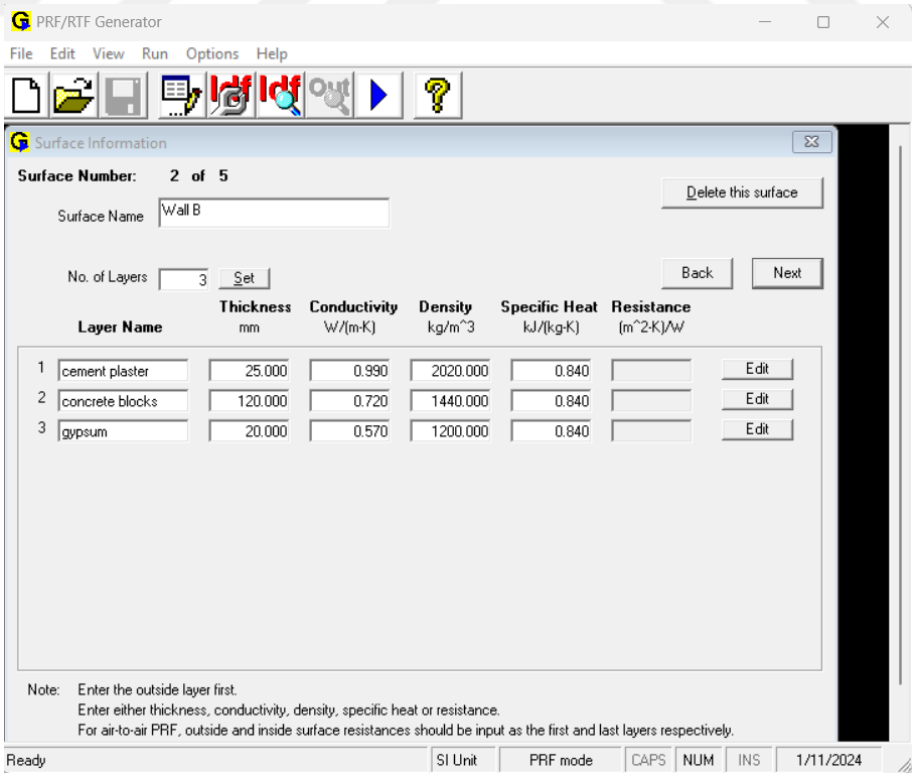

Figure C.2. Wall B layers and specifications.

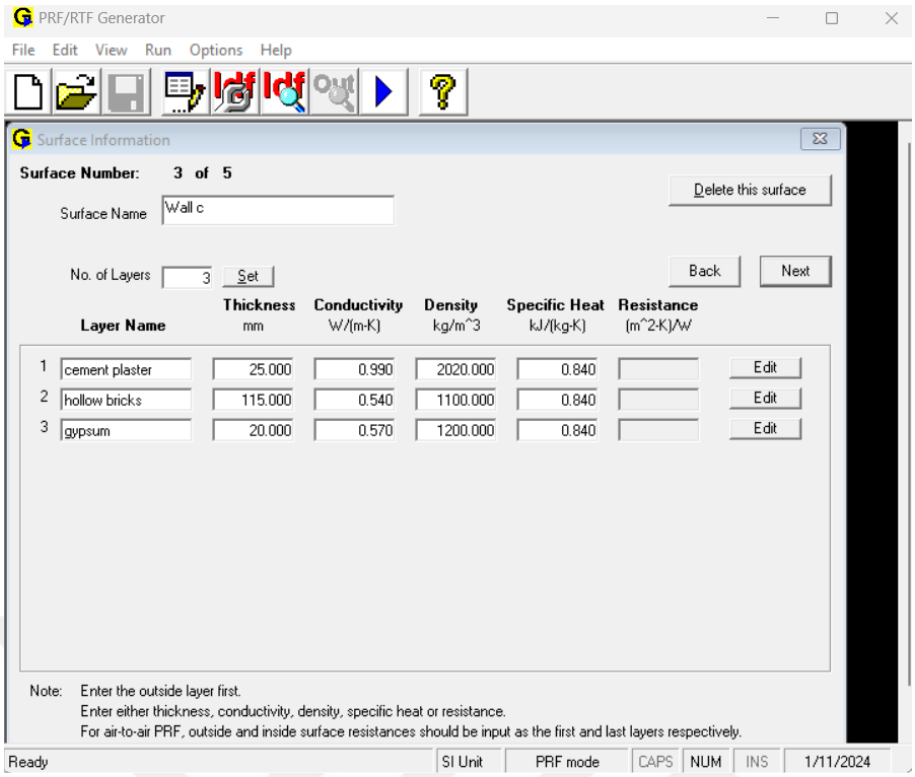

Figure C.3. Wall C layers and specifications.

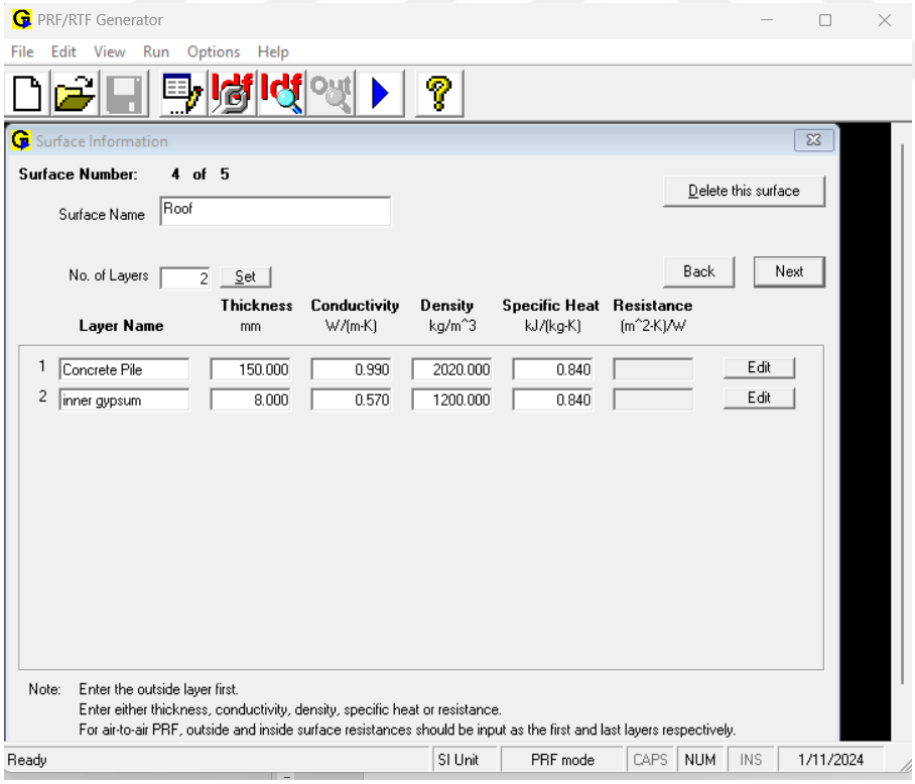

Figure C.4. Roof layers and specifications.

CURRICULUM VITAE

Student Information	
Name/Surname:	KHALIL HASSAN KHALIL
Nationality:	IRAQI
ORCID No:	0000-0002-1599-7064

School Information	
Undergraduate Study	
University	UNİVERSİTY OF KİRKUK
Faculty	COLLEGE OF ENGİNEERİNG
Department	MECHANİCAL ENGİNEERİNG DEPARTMENT
Graduation Year	2016
Graduate Study	
University	KIRŞEHİR AHİ EVRAN UNIVERSİTY
Institute	INSTITUTE OF NATURAL AND APPLIED SCIENCES
Department	DEPARTMENT OF MECHANİCAL ENGİNEERİNG
Graduation Year	2024

Articles and Papers Produced from the Thesis

Articles in International Refereed Journals

Khalil, H. K., Danismaz, M., & Al-Bayati, O. A. Z. Experimental investigation of RTS method to calculate heat gain on walls and flat roof. *Pollack Periodica, AKJournals,* vol 19, 2024

International Conferences and Symposia

International Conference on Design, Research and Development (RDCONF), Dec.2021